ABSTRACT

Title of Document: MECHANISMS OF RESISTANCE TO IONIZING RADIATION IN EXTREMOPHILES

Kimberly Michelle Webb, Master of Science, 2012

Directed by: Dr. Frank T. Robb, Marine Estuarine Environmental Sciences

Extremophiles display an astonishing array of adaptations to harsh environmental conditions. We analyzed the mechanisms of ionizing radiation resistance from a diverse group of extremophilic archaea and bacteria. In *Halobacterium salinarum* IR resistance is conferred by antioxidant Mn^{2+}-complexes, and protein-free cell extracts (ultrafiltrates, UFs) of super-resistant (IR^{+}) isolates of *H. salinarum* had increased concentrations of Mn, PO_4 and amino acids compared to the founder strain. Proteomic analysis determined that IR^{+} isolates with increased Mn had elevated protein expression for central carbon metabolism, suggesting a Mn-stimulated metabolic route to increased IR resistance. We examined the role of mannosylglycerate, di-*myo*-inositol phosphate, and trehalose in the IR resistance of various thermophiles; aerobic thermophiles had UFs which were radioprotective of enzyme activity under aerobic conditions, which is attributed to Mn, PO_4 and trehalose accumulation. In contrast, anaerobic thermophile UFs did not contain significant amounts of Mn, and were radioprotective only under anaerobic conditions; we conclude the anaerobic environment confers their IR resistance.

MECHANISMS OF RESISTANCE TO IONIZING RADIATION IN EXTREMOPHILES

By

Kimberly Michelle Webb

Thesis submitted to the Faculty of the Graduate School of the
University of Maryland, College Park in partial fulfillment
of the requirements for the degree of
Master of Science
2012

Advisory Committee:
Dr. Frank T. Robb, Chair
Dr. Michael Daly
Dr. Jocelyne DiRuggiero
Dr. Kevin R. Sowers

Dedication

This work is dedicated to my entire family, especially my husband Nathan, and my parents Kevyn and Peter, for all your love and support.

Acknowledgements

I would like to thank Dr. Jocelyne DiRuggiero for her support, direction and patience throughout my graduate career. I would also like to thank various members of the DiRuggiero lab for their assistance and/or camaraderie: Shuhong Lu, Michelle Ploch, and especially Courtney Robinson. Thanks also to the members of my committee for their time and insight, Dr. Frank Robb, Dr. Kevin Sowers, and Dr. Michael Daly.

I would like to thank Dr. Noboru Tomiya, for his insight and HPAEC analysis; Dr. Lai-Xi Wang and Jared Orwenyo (UMD School of Medicine) for their help with the compatible solute analysis; and Robert Cole (JHU School of Medicine) for his assistance with the proteomic analysis. I'd also like to acknowledge Jana Mihalic (JHU School of Public Health) for her ICP-MS and ion chromatography analysis, as well as for her morale-boosting discussion and accommodation for fast sample processing.

A special thank you goes to Dr. Michael Daly and all the members of his lab at USUHS, Dr. Vera Matrosova, Dr. Elena Gaidamakova, and Margaret Wear, for their assistance and guidance at USUHS, access to the Co-60 irradiator, as well as their insight and thoughtful discussion.

Lastly, thank you to my family and friends, especially my husband Nathan, and my parents; without your support none of this would have been possible.

Table of Contents

List of Tables

List of Figures

List of Abbreviations

D_{10} – dose of ionizing radiation at which 10% of a microbial population survives
DIP – di-*myo*-inositol phosphate
DSB – double-strand break
ESDSA - extended synthesis-dependent strand annealing
H_2O_2 – hydrogen peroxide
$HO^{\bullet}$ – hydroxyl radical
HR – homologous recombination
IR – ionizing radiation
IR^{+} – super-IR resistant
MG – mannosylglycerate
NHEJ – non-homologous end-joining
$O_2^{\bullet-}$ – superoxide
PCR – polymerase chain reaction
PER – protein expression ratio
ROS – reactive oxygen species
RFA – replication factor protein A
RPA – replication protein A
SASP – small, acid-soluble proteins
SOD – superoxide dismutase
SOR – superoxide reductase
SSA – single strand annealing
SSB – single-strand break
UF – ultrafiltrate

Chapter 1 - Introduction

Earth contains a wide variety of extreme environments, including those characterized by temperature and pH extremes, high pressure, high salinity, and extreme dryness. Members of the Archaea, Bacteria and Eukarya have been found thriving in these hostile environments that were originally considered too harsh to support life [1]. Extreme environments vary greatly from those commonly encountered by humans, but nevertheless are populated by a myriad of extraordinary organisms. These are known collectively as "extremophiles" [2].

Extremophiles have been studied extensively over the last several decades. Initial studies focused mainly on the inhabitants of environments accessible to researchers, such as geothermal vents, the Dead Sea, and abandoned metal mines, with extremes in temperature, salinity and pH [2]. These extreme habitats were generally considered to be populated by prokaryotes [3]. Since then, however, representatives of all three domains of life have been identified in these environments, including fungi (*e.g.*, *Ustilago maydis*) and small animals (*e.g.*, *Adineta vaga*) (Fig. 1-1) [4, 5]. Many extremophiles (*e.g.*, thermophiles) are defined by their optimum growth characteristics and/or requirements, however, within such groups there is an enormous metabolic diversity [6]. By understanding how extremophiles meet the physical and chemical challenges found in hostile environments, we extend our view of biochemistry and metabolism.

A great example is the characterization of thermostable proteins in *Thermus aquaticus* [7]. Before the discovery of hyperthermophiles, it was generally accepted that temperatures > 60°C denature all proteins, but thermophilic proteins maintain their structural integrity at temperatures of 80°C – 100°C [8]. Understanding mechanisms of thermostability has not only led to a greater comprehension of protein function and structure, but also to practical applications such as polymerase chain reaction (PCR). Taq polymerase is a thermophilic DNA polymerase that was isolated from *Thermus aquaticus,* a thermophilic bacterium [7]. This thermostable enzyme has completely revolutionized molecular biology [9].

The physiology and metabolic diversity of extremophiles remains an unexhausted reservoir of potential biotechnological exploration and innovation [6]. Once abundant life was discovered in what were considered extreme environments, our view of the underlying biochemistry supporting those organisms fundamentally changed.

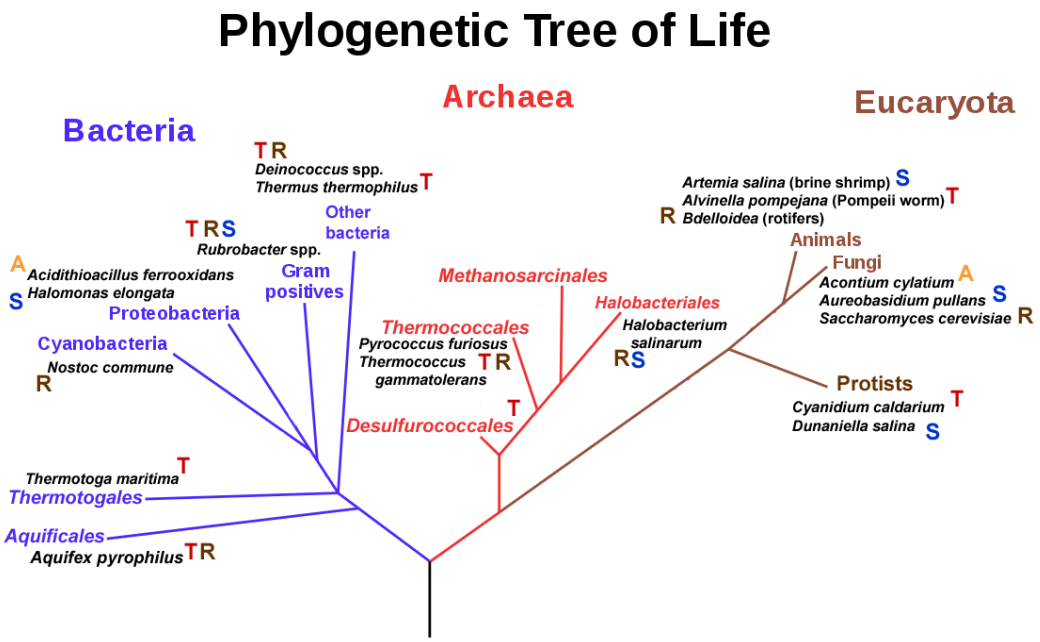

Figure 1-1. Examples of extremophiles in the three domains of life. T denotes thermophilic members; S denotes halotolerant and halophilic members; A denotes acidophilic members; R denotes radiation and desiccation resistant members.

Extremophiles on Earth are typically classified by a singular characteristic that allows existence under a singular extreme condition. However, the archaeon *Halobacterium salinarum*, in addition to being adapted to high salt, also shows a high level of resistance to desiccation, high pressure, UV and ionizing radiation (IR) [10-12]. This "polyextremetism" is quite common among extremophiles as these microorganisms are typically exposed to multiple stresses. For example, bacteria inhabiting salterns are also exposed to high levels of UV [13]. The definition of a polyextremophile also fits the model organism *Deinococcus radiodurans*, a bacterium which displays extreme resistance to a range of damage caused by radiation, desiccation, oxidizing agents, and electrophilic mutagens [14, 15]. In *D. radiodurans*, a system based on small-molecule antioxidants preserves the activity of repair enzymes [14, 16]. There are very few

terrestrial environments characterized by high radiation and it has been suggested that radiation resistance is a fortuitous consequence of a high tolerance to desiccation, as many organisms that are desiccation-resistant are also resistant to IR [17, 18]. Accordingly, IR is used to mimic the damaging effects of desiccation and can be used as a convenient proxy to study desiccation resistance. This chapter will discuss how radiation damages cells and then we will review what we know about radiation resistance, which we have learned from studies of radiation-resistant organisms.

Ionizing Radiation Damage

Ionizing radiation damages cellular components by direct and indirect effects [19]. While direct ionization within the cell results in molecular damage, the vast majority of cellular insults under aqueous conditions are caused by indirect effects, through the actions of reactive oxygen species (ROS) formed from the radiolysis of water (Fig. 1-2) [19]. The radiolysis of water generates hydroxyl radicals ($HO^{\bullet}$), protons, and free electrons (eq. 1).

(1) $H_2O \rightarrow HO^{\bullet} + e^-_{aq} + H^+$

(2) $2HO^{\bullet} \rightarrow H_2O_2$

(3) $O_2 + e^-_{aq} \rightarrow O_2^{\bullet -}$

The hydroxyl radicals react indiscriminately with all macromolecules in the cell or react with each other to form hydrogen peroxide (H_2O_2) (eq. 2), and free electrons react with dissolved oxygen to form superoxide ($O_2^{\bullet -}$) (eq. 3). DNA-associated water molecules that undergo radiolysis become an immediate threat for nucleic acids, as $HO^{\bullet}$ cause base damage, single strand breaks (SSBs), and DSBs [19]. Superoxide and H_2O_2 are

potentially the most deleterious to the cell, mostly from their interaction with iron associated with proteins or DNA [20, 21]. For example, proteins' iron-sulfur clusters (*e.g.*, 4Fe-4S dehydratases) are readily destroyed by $O_2^{\bullet-}$ and H_2O_2, which can perpetuate and amplify ROS generation by the Fenton reaction (eq. 4) and related cascading reactions [20].

(4) $Fe^{2+} + H_2O_2 \rightarrow Fe^{3+} + HO^{\bullet} + OH^-$

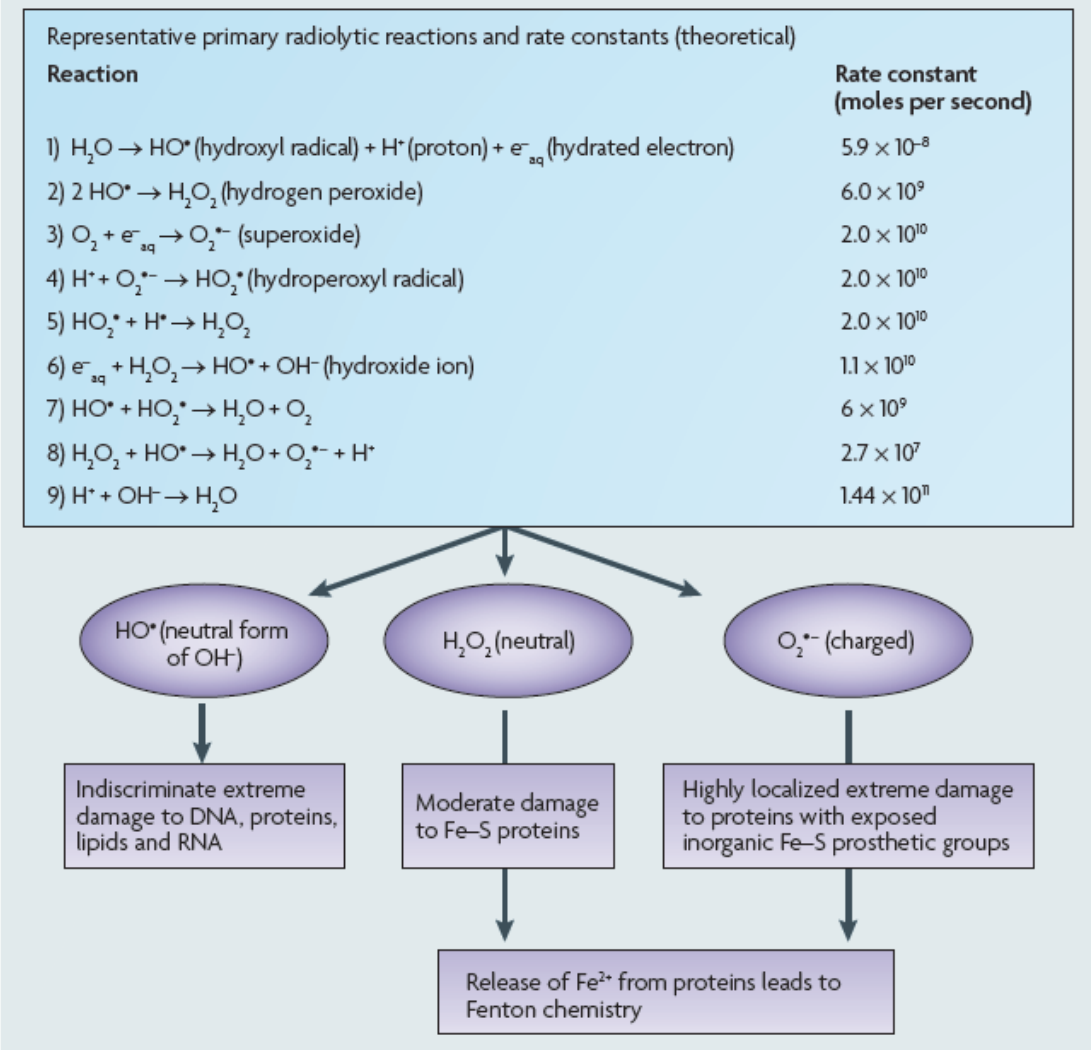

Figure 1-2. Theoretical cellular reactions generating a variety of ROS following ionizing radiation (taken from [22]). Top, expected reactions that result from the radiolysis of water and their rate constants, and IR.

The resulting $HO^{\bullet}$ inflict a barrage of oxidative damage upon cellular components. Hydrogen peroxide also reacts with some other transition metals (Cu^{2+}, Mn^{3+}) bound to the active site of proteins, releasing $HO^{\bullet}$ and damaging the adjacent amino acids,

resulting in inactivation by protein oxidation [20, 21]. While some forms of amino acid oxidation are reversible (*e.g.*, methionine), others are not (cysteine); carbonylation is an irreversible form of protein oxidation [20, 21]. Proteins have also been shown to be inactivated by UV [23]. Thus, IR inflicts severe oxidative damage to the cell which must either be prevented or repaired in order for the cell to survive.

Radioprotection and Damage Repair

In the 1960s, DNA was considered to be the principal target of radiation, and DNA damage was responsible for its lethal effects [24]. Scientists first believed that IR-resistant microorganisms survived high-level radiation because they possessed some way to prevent DNA damage. However, it was later shown that the amount of SSBs, DSBs and base damages were approximately the same for both IR-resistant and IR-sensitive microorganisms [22, 25]. As DNA damage is an inevitable consequence of irradiation, focus then shifted to DNA repair systems, and the investigation of the differences between the repair systems of IR-resistant and IR-sensitive organisms. Whole-genome analysis of *D. radiodurans*, *H. salinarum* and *Pyrococcus furiosus* concluded that these IR-resistant microorganisms encode DNA repair systems, which appear very conventional [22, 26, 27].

While the majority of DNA damage from IR is the formation of SSBs and base modifications, the least frequent but most deleterious are DSBs, which fragment the genome [28]. The mechanisms for DSB repair include homologous recombination (HR), single strand annealing (SSA), extended synthesis-dependent strand annealing (ESDSA),

and non-homologous end-joining (NHEJ) (Fig. 1-3) [29]. HR, SSA and ESDSA require the DNA ends to be processed by exonucleases to generate single-stranded 3' overhangs [30]. HR requires an intact homologous DNA molecule and is used in all three domains of life [31]. ESDSA has only been described in *D. radiodurans* and is a variant of the SSA mechanism where DNA fragment assembly is accompanied by DNA synthesis, producing long 3' overhangs, and it has been suggested that the fidelity of HR that follows is increased by these extended overhangs [15, 30]. NHEJ, which does not require DNA end-processing, is the major pathway of DSB repair in higher eukaryotes [32]. It has been proposed that this mechanism is present in the IR-resistant *D. radiodurans*, facilitated a protein unique to the *Deinococcacea*, PprA [15, 33]. PprA is up-regulated in response to IR, and PprA-deficient strains show slower growth rates and IR-sensitivity when compared to the wild-type, indicating that this protein may be important to the IR resistance in *D. radiodurans* [33]. However, detailed molecular analyses have demonstrated that NHEJ is absent in *D. radiodurans* [34].

Another unique feature of *D. radiodurans* is its single-strand DNA-binding proteins (SSBs), which are different from other bacterial homologs [15]. Compared to *E. coli* SSBs, they are twice the size and form dimers instead of tetramers [15]. While *E. coli* has 200 to 3,000 SSB tetramers per cell, *D. radiodurans* has 19,500 dimers per cell, which increases to 56,000 in response to IR [15]. Along with PprA and SSBs, the "DNA damage response" protein (DdrA) was found to be induced by radiation, presumably to protect DNA fragments from degradation, but mutants deficient of this protein do not lose significant IR resistance [15].

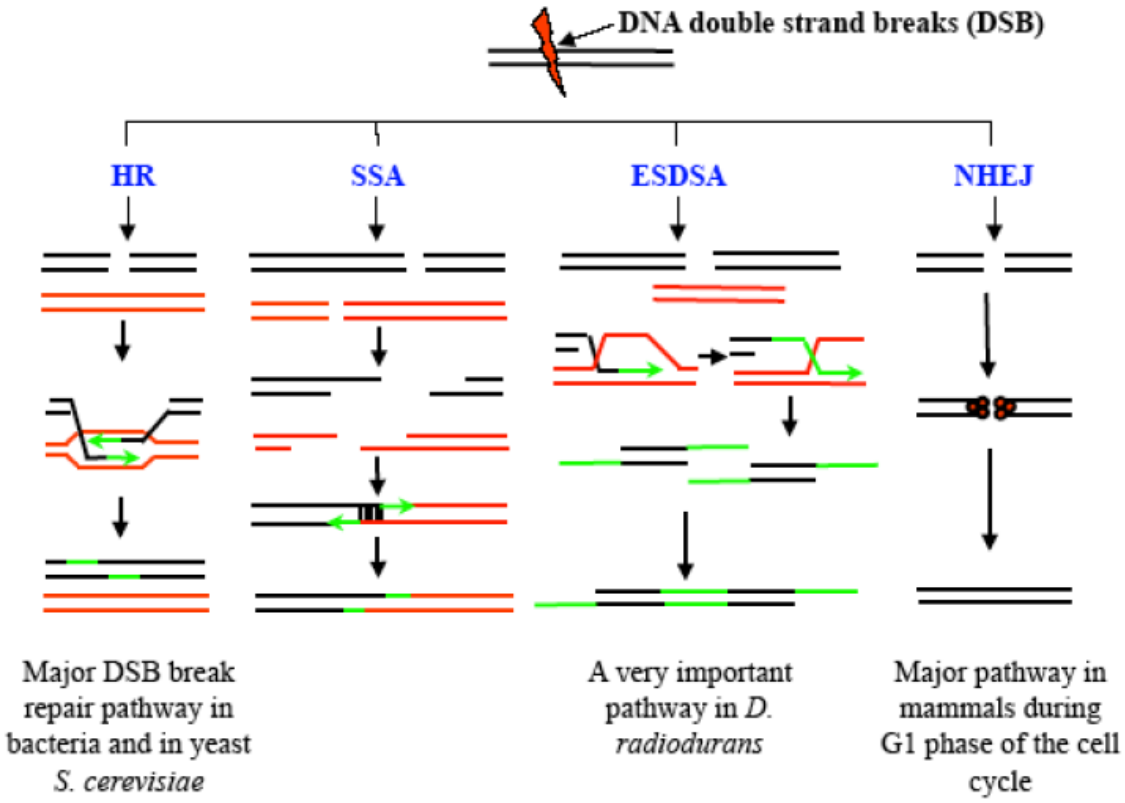

Figure 1-3. Pathways for the repair of DNA double-strand breaks (from [31]). Green lines indicate DNA newly synthesized during repair. Red and black are used to represent two copies of the same chromosomal region.

Compared to bacteria, DSB repair in archaea is less well characterized. In *P. furiosus*, DNA end processing is carried out by Rad50/Mre11 complexes (MR complex) that attach to the DNA ends and recruit nuclease and helicase proteins (NurA and HerA, respectively) to form 3' overhangs [31]. This in turn recruits RadA, a RecA variant [31]. In *H. salinarum*, *nurA* and *herA* homologs are missing, and while Rad50/Mre11 proteins are present, Rad50 is not required for homologous recombination [35]. Additionally,

mutants of *H. salinarum* deficient in both Rad50 and Mre11 (Δ*rad50*-Δ*mre11*) are just as IR-resistant as the wild-type, though the repair of DNA DSBs occur less efficiently [35].

Early radiobiology experiments showed that the activity of purified proteins in aqueous solution could be protected from IR by increasing protein concentration or by the addition of small organic molecules [36, 37]. Du and Gebicki later suggested that proteins are the principal targets of radiation damage in mammalian cells [38]. Consequently, a few researchers began to examine the role of protein oxidation in irradiated cells, and it was shown that protein damage in irradiated prokaryotes was causative in radiation toxicity, not merely correlative [11, 14, 39, 40].

As stated above, $O_2^{\bullet-}$ and H_2O_2 are particularly damaging to proteins, especially those with iron-sulfur groups, therefore the removal of these ROS is key to protecting proteins in the cell. One such way of protecting proteins from IR is through ROS scavenging systems. The key enzymes responsible for the removal of ROS are superoxide dismutase (SOD), catalase and peroxidase. SOD disproportionates $O_2^{\bullet-}$ to H_2O_2 and O_2 (eq. 5 and 6) [41].

(5) $M^{3+} + O_2^{\bullet-} \rightarrow M^{2+} + O_2$

(6) $M^{2+} + 2H^{+} + O_2^{\bullet-} \rightarrow M^{3+} + H_2O_2$

The metal cofactor is represented by M, which can be Mn, Fe, Cu, or Zn [41]. Hydrogen peroxide is then scavenged by peroxidase (eq. 7) which uses an organic reducing agent, represented by R, or by catalase (eq. 8) [21].

(7) $RH_2 + H_2O_2 \rightarrow R + 2H_2O$

(8) $2H_2O_2 \rightarrow O_2 + H_2O$

While SODs are highly efficient, ROS scavenging can also be facilitated by cytoplasmic manganous (Mn^{2+}) complexes [11, 14, 21, 42]. Early evidence showed that the aerotolerant *Lactobacillus plantarum* lacks SOD, but benefits from the accumulation of Mn^{2+} to remove $O_2^{\bullet-}$ [43]. When *L. plantarum* is grown in Mn^{2+}-deficient minimal media it shows greater sensitivity to oxygen [43]. SOD-deficient mutants of *Saccharomyces cerevisiae* and *Escherichia coli* overcame the phenotypic sensitivity to O_2 when these mutants were grown in Mn-enriched media [44, 45]. *In vitro* studies showed that $MnPO_4$ complexes catalytically scavenged $O_2^{\bullet-}$, and when Mn^{2+} was combined with certain amino acids, Mn-amino acid complexes decomposed H_2O_2 [42, 46, 47]. Given its ability to effectively scavenge $O_2^{\bullet-}$, it is not surprising that a mechanistic link has been shown between high Mn/Fe ratios and high resistance to IR, as seen in *D. radiodurans* and *H. salinarum* [11, 22]. A high intracellular concentration of Mn^{2+} confers protection to proteins *in vitro*, and microorganisms with high Mn/Fe ratios show less oxidative protein damage after irradiation than those with low Mn/Fe ratios [11, 14, 18, 39, 48].

Recent studies with the halophilic archaeon *H. salinarum* and bacterium *D. radiodurans* showed that the radiation resistance of these organisms was not dependent on the presence of ROS-scavenging enzymes [11, 49]. Further studies showed that protein-free cell extracts (ultrafiltrates) of *H. salinarum* and *D. radiodurans* had far higher concentrations of Mn^{2+}, peptides, and free amino acids than those of radiation-sensitive organisms such as *E. coli* or *P. putida* [11, 14]. The ultrafiltrates protected enzyme

activity from high levels of IR *in vitro*, whereas ultrafiltrates from radiation-sensitive organisms did not [11, 14]. The radiation resistance of these prokaryotes appeared to reside in the accumulation of manganous (Mn^{2+}) ions, which form antioxidant complexes with peptides, orthophosphate, and other small molecules (Figure 1-4) [11, 14, 15, 50].

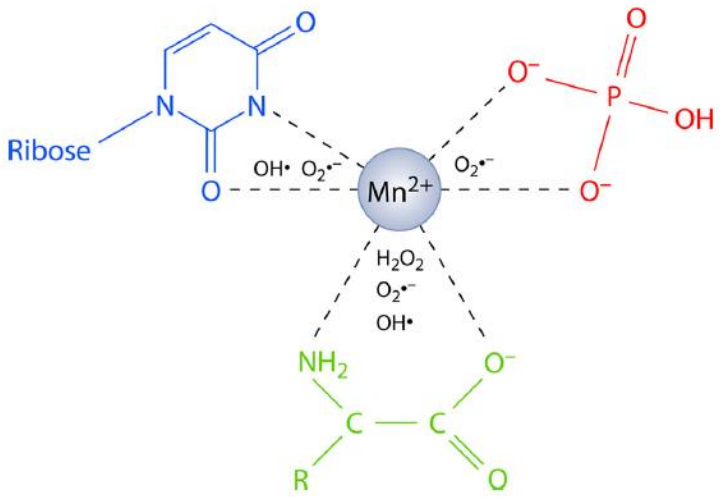

Figure 1-4. Model for manganese-based chemical antioxidants in *D. radiodurans*. Mn^{2+} catalytically scavenges $O_2^{\bullet-}$ in complex with orthophosphate (red). Free amino acids or peptides in complex with Mn^{2+} and orthophosphate catalytically decompose H_2O_2 and scavenge $O_2^{\bullet-}$ (green). Nucleosides (and their analogs) complex with Mn^{2+}-orthophosphate and scavenge $O_2^{\bullet-}$ (blue). Nucleosides, free amino acids, peptides, and other small organic metabolites scavenge hydroxyl radicals $HO^{\bullet}$. From [15].

Additionally, it has been shown that *Bacillus* spores resistant to wet and dry heat benefit from the accumulation of Mn^{2+} coordinated with small molecules including dipicolinic acid (DPA), and possibly α/β-type small, acid-soluble proteins (SASPs) [51]; DPA also formed antioxidant complexes with Ca^{2+} and PO_4, indicating that other divalent metal

ions may contribute to protection from IR [52]. Mn^{2+}-mycosporine-complexes are attributed to facilitating radiation and desiccation resistance in other bacteria [53, 54]. Cellular accumulation of Mn^{2+} together with a variety of organic and inorganic ligands may be a widespread mechanism to surviving oxidative stress, and there is evidence that this may extend also to simple animals such as rotifers [40]. Thus, the idea that protein protection might govern radiation resistance has severely challenged the conventionally held view that DNA damage is paramount in radiation toxicity. By protecting protein function from the damages inflicted by IR, DNA can be repaired by competent proteins, and the cell can survive (Figure 1-5).

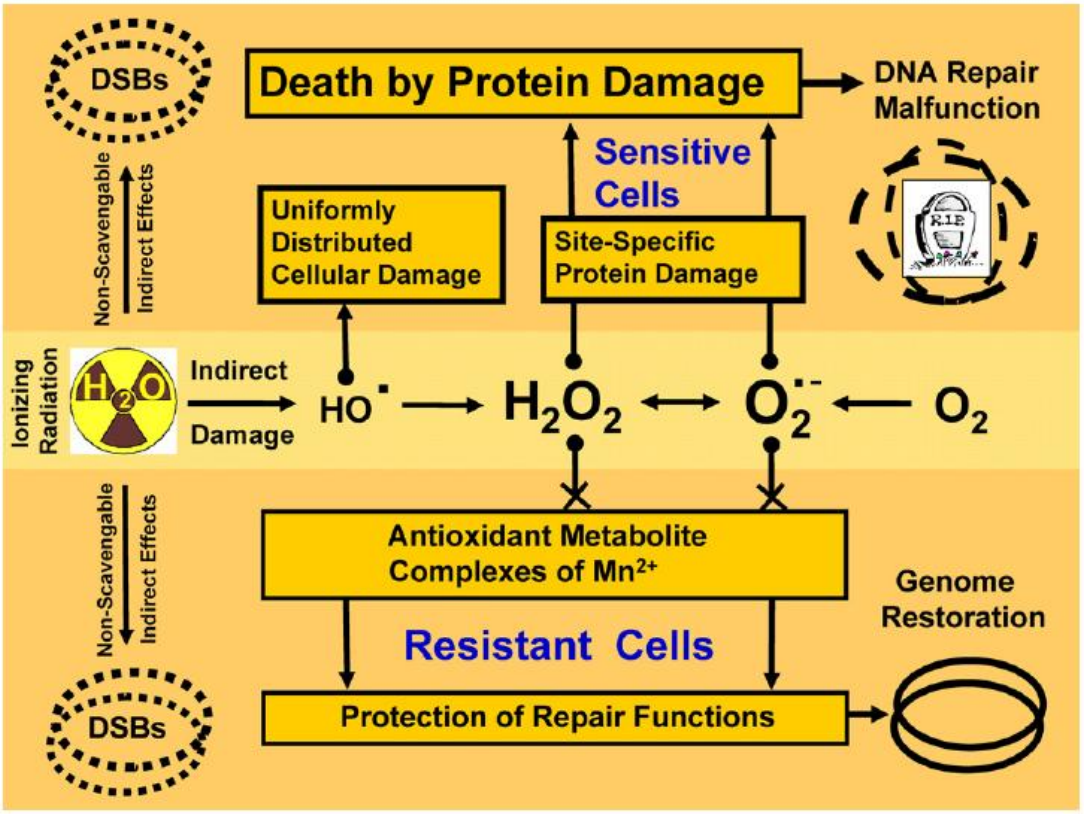

Figure 1-5. Model of death by protein damage in irradiated cells. DSBs in the genomes of cells exposed to IR. $HO^{\bullet}$ are generated by the radiolysis of water react with organic molecules, but also with each other to generate H_2O_2. $O_2^{\bullet-}$ in irradiated cells is generated by the decomposition of H_2O_2 through enzymatic or metal-catalyzed processes and from O_2 in the atmosphere. $O_2^{\bullet-}$ and H_2O_2 are relatively inert, but are extremely damaging to some proteins. Mn^{2+} not bound to proteins forms Mn^{2+}-orthophosphate complexes which can provide protein protection. From [16].

Radiation Resistant Extremophiles

In addition to the halophilic archaeon *H. salinarum* a number of other extremophiles have been found to be resistant to IR (Table 1-1) [14, 55]. Recently, several thermophiles were tested for their resistance to IR, including the sulfate-reducing *Archaeoglobus fulgidus*, as

well as *Methanocaldococcus jannaschii*, a methanogen, and were found to have D_{10} values (the dose of IR at which 10% of the population survives) of approximately 1,000 Gray (1 kGy) [55]. Other thermophilic archaea are even more radiation resistant, such as *P. furiosus* and *Thermococcus gammatolerans*, which have D_{10} values of 3 and 6 kGy, respectively. [56, 57]. Additionally, the thermophilic bacterium *Aquifex pyrophilus* was shown to have a D_{10} of 2.8 kGy, while the phylogenetically distant, thermophilic gram-positive *Rubrobacter radiotolerans* and *Rubrobacter xylanophilus* have D_{10} values of 10 and 6 kGy, respectively [55, 58, 59]. Despite the seeming prevalence of radiation resistant thermophiles, it would be unjustified to assume this is true of all thermophiles, as several have been shown to be radiation sensitive, such as the archaeon *Sulfolobus solfataricus* which has a D_{10} of 0.5 kGy [60]. As discussed earlier, the halophilic archaeon *H. salinarum* is also highly radiation resistant, with a D_{10} value of 5 kGy [12]. Notably, radiation resistance is not exclusive to microorganisms, as the roundworm *Caenorhabditis elegans* and the tetraploid rotifer *A. vaga* can survive far great numbers of radiation-induced DSBs than even *D. radiodurans* [16, 40, 61]. Whether or not mechanisms of radiation resistance are shared between archaea, bacteria and eukaryotes is only now being investigated. This thesis examines features which may be shared between radiation-resistant archaea and bacteria.

Table 1-1. Examples of radiation resistant polyextremophiles

Extremophile	D_{10}	Characteristics
Eukarya		
Adineta vaga	1	Desiccation resistant
Caenorhabditis elegans	1.2	Thermotolerant
Ustilago maydis	6	Thermotolerant, halotolerant
Archaea		
Pyrococcus furiosus	3	Anaerobic thermophile, halotolerant
Halobacterium salinarum	5	Halophile, desiccation and pressure resistant
Thermococcus gammatolerans	6	Anaerobic thermophile
Bacteria		
Aquifex pyrophilus	2.8	Microaerobic thermophile
Rubrobacter xylanophilus	6	Aerobic thermophile, halotolerant, desiccation resistant
Rubrobacter radiotolerans	10	Aerobic thermophile, desiccation resistant
Deinococcus geothermalis	10	Aerobic thermophile, desiccation resistant
Deinococcus radiodurans	12	Desiccation resistant

Radiation Resistant Extremophile Systems:

Rubrobacter xylanophilus and *Rubrobacter radiotolerans*. The obligate aerobic thermophiles *R. xylanophilus* and *R. radiotolerans* are Gram-positive bacteria of the phylum Actinobacteria. Originally named *Arthrobacter radiotolerans*, *R. radiotolerans* was isolated from a radioactive spring in Japan, whereas *R. xylanophilus* was isolated from a thermally polluted industrial runoff in the United Kingdom [59, 62]. Both are pleotrophic, displaying morphologies which vary between rods and cocci, and they are pink as a result of the accumulation of carotenoids in the cells [59, 62]. *R. radiotolerans* has an optimum growth temperature of 48°C whereas *R. xylanophilus* grows optimally at 60°C [59, 62]. These thermophiles are heterotrophs, making them easy to cultivate and use as model systems. *R. radiotolerans* (D_{10}, 12 kGy) is further distinguished from *R. xylanophilus* (D_{10}, 6 kGy) by its higher resistance to IR [62]. Interestingly, DNA related

to these species has been isolated from historically important buildings in Austria and Germany, as well as deserts, a highly desiccating environment [63]. Both *R. xylanophilus* and *R. radiotolerans* have sequenced genomes of 3.2 Mbp and 3.4 Mbp, respectively, but no genetic tools are currently available [64].

R. xylanophilus has been studied extensively for the solutes it accumulates, such as the carbohydrate-derivatives mannosylglycerate (MG) and di-*myo*-inositol phosphate (DIP), as well as the disaccharide trehalose (Fig. 1-6); MG and DIP concentrations increase approximately 2-fold due to salt or heat stress, respectively, whereas trehalose concentrations increase in response to both stressors [65]. Until the detection of this compound in *R. xylanophilus*, DIP was thought to be found only in hyperthermophiles where its concentration is increased in response to heat stress [65, 66]. In contrast, trehalose is ubiquitous, found in diverse organisms throughout the tree of life [67, 68]. *In vitro* studies have shown its protective effects against heat, desiccation, oxidation and freezing [69, 70]. *R. xylanophilus* encodes four pathways for the synthesis of trehalose, two of which have been characterized and confirmed to be metabolically important [71]. One of these pathways is unique to hyperthermophiles, and appears to have been acquired through horizontal gene transfer from a methanogen [71]. The prevalence of multiple pathways dedicated to the synthesis of this simple sugar in *R. xylanophilus* indicates that this compound is important to its survival. Until this study, it was unknown whether or not *R. radiotolerans* accumulates any compatible solutes, and it has not been determined if the compatible solutes accumulated by *R. xylanophilus* and *R. radiotolerans* contribute to the radiation resistance seen in these bacteria.

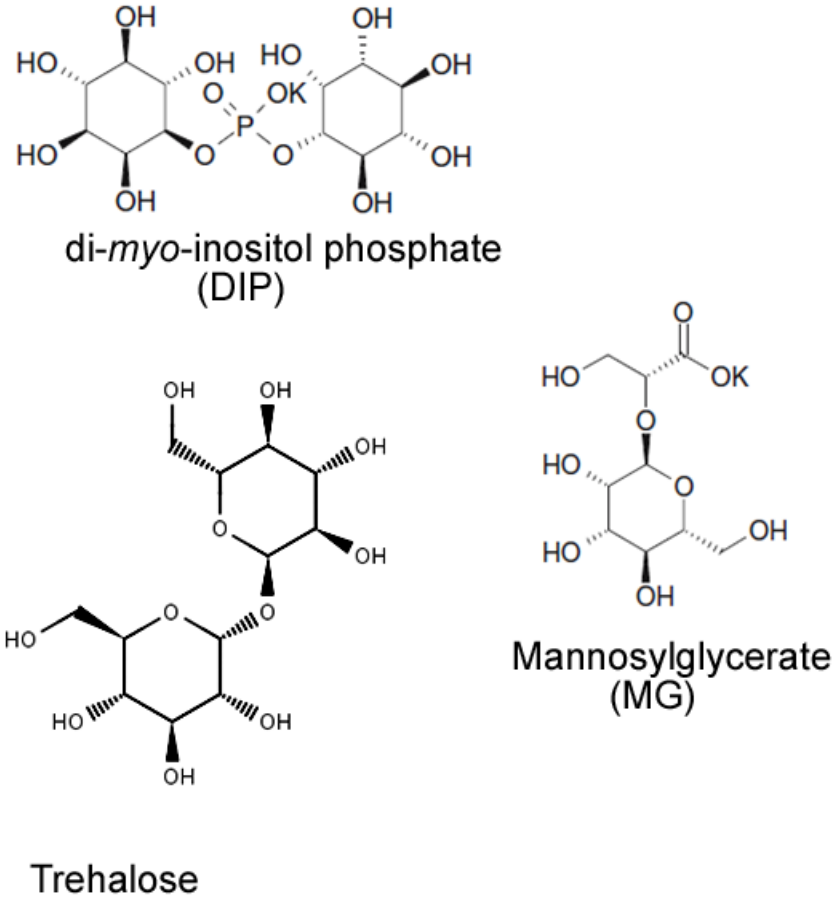

Figure 1-6. Compatible solutes in thermophiles. Mannosylglycerate (MG) and di-*myo*-inositol phosphate (DIP) are anions and depicted as potassium salts, K^+ being the main counter-ion in the organisms from which they originate.

Pyrococcus furiosus and *Thermococcus gammatolerans*

The anaerobic archaeon *Pyrococcus furiosus* was first isolated from a hydrothermal vent near Vulcano Island, Italy and has a D_{10} value of 3 kGy [72, 73]. It is one of the first thermophiles to be studied extensively, including the sequencing of its genome, and is often used as a model hyperthermophile [74]. It can use a wide range of compounds as a carbon source, such as peptides and carbohydrates, and it does not need elemental sulfur for growth when maltose and tungsten are added to the culture media [75]. Proteins have been purified from *P. furiosus* containing Co, Fe, Ni, W, and Zn, and a recent study found that 13 additional metals were incorporated into macromolecular complexes (>5 kDa) [76]. Like the *Rubrobacter* spp., *P. furiosus* accumulates MG and DIP in response to increased salinity and temperature, respectively [66].

The radiation resistance of *P. furiosus* has been investigated extensively [73]. DiRuggiero *et al*. showed that after exposure to 2.5 kGy, no detection of intact chromosomes could be found, indicating that this thermophile can repair its shattered 2Mbp genome within 20 hrs after incubation in fresh media [56]. As stated previously, it has been shown that DNA protection mechanisms are not responsible for the radiation resistance in this archaeon [25]. A whole-genome mRNA microarray analysis of *P. furiosus* in response to radiation yielded the result that very few DNA repair genes were differentially expressed after exposure to IR [73]. The study also showed that the systems involved in oxygen detoxification appeared to be constitutively expressed, but the Dps-like protein (what is DPS) was found to be elevated in response to both IR and H_2O_2, presumably to sequester Fe [73, 77]. These results were also found in a recent study on *P. furiosus* in response to hydrogen peroxide, which concluded that this microorganism maintains constitutive high

level expression of oxidoreductase-related enzymes including superoxide reductase (SOR), rubrerythrin, and alkyl hydroperoxide reductase [77]. *P. furiosus*, like most anaerobic hyperthermophiles, lack the oxygen detoxification enzymes superoxide dismutase (SOD) and catalase which their aerobic counterparts use (Fig. 1-7a) [78]. In their place, *P. furiosus* has a superoxide reductase (SOR), which is a non-heme iron-containing enzyme; instead of catalases, *P. furiosus* has several peroxidases (Fig. 1-7b) [78] including rubrerythrin, alkyl hydroperoxide reductase I and II, and the aforementioned Fe-sequestering Dps-like protein [77-79]. A variation of SOR-mediated $O_2^{\bullet-}$ detoxification was discovered in which SOR- ferrocyanide complexes reduce $O_2^{\bullet-}$ without the formation of H_2O_2, and this system was highly efficient, as the SOR iron site remains reduced, thus eliminating the requirement of oxidoreductases to recycle SOR (Fig. 1-7c) [80].

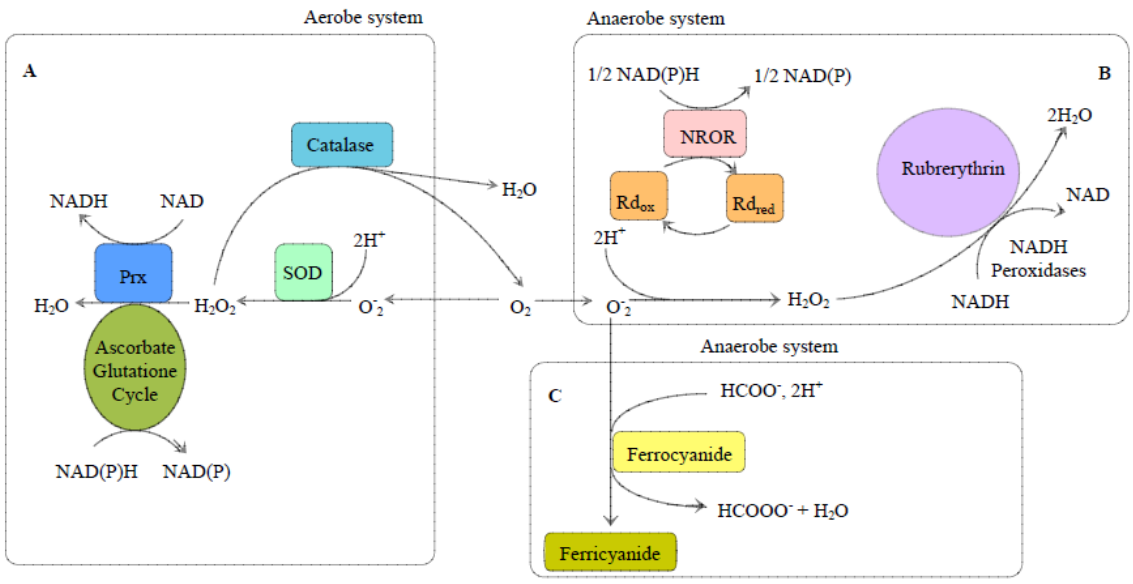

Figure 1-7. Proposed pathways for superoxide detoxification in: (A) aerobic and (B and C) anaerobic organisms (from [31]). Cyt bd: cytochrome bd ubiquinol oxidase, Prx: peroxiredoxin, Rd: rubredoxin, SOD: superoxide dismutase, SOR: superoxide reductase, NROR: NAD(P)H rubredoxin oxidoreductase.

Thermococcus gammatolerans was isolated from enriched samples collected from hydrothermal chimneys after exposure to 30 kGy of radiation, and has a D_{10} value of 6 kGy, making it one of the most radiation-resistant archaea isolated to date [57]. The anaerobic archaeon has an optimal growth temperature of 88°C, and in the presence of elemental sulfur (S°) is able to grow on complex organic compounds [81]. However, unlike *P. furiosus*, it is not able to grow on peptides or free amino acids without the addition of elemental sulfur (S°) [81]. Its 2.0 Mbp genome has been sequenced and has an average coding sequence similarity of 71.5% with *P. furiosus* [81]. While genes have been found in its genome for the synthesis of the solutes MG and DIP, the actual detection of these compounds has not been done for *T. gammatolerans*.

Halobacterium salinarum

H. salinarum is an extremely halophilic archaeon that grows optimally in 4.3 M NaCl at 42°C, and accumulates KCl to maintain osmotic balance [82]. This microorganism is highly resistant to desiccation, pressure and radiation (D_{10}, 5 kGy) [10-12, 83]. Its 2.6 Mbp genome has been sequenced, and many genetic tools are readily available for this halophile, making it a good model system [26, 84, 85]. The stress response of this archaeon has been studied extensively for chemical oxidants, UVC and IR, metals and pressure [11, 27, 83, 86, 87]. From the abundance of these prior studies, there is much we understand about *H. salinarum*'s stress response to oxidizing conditions. With regards to IR, the radiation resistance of *H. salinarum* is not dependent on ROS-scavenging enzymes [11]. As mentioned before, ROS detoxification mutants with Δ*sod1/2*, Δ*perA*, Δ*msrA*, Δ*VNG0018H*, and Δ*VNG0798H* mutations displayed various susceptibilities to chemical oxidants, but not to gamma-radiation [11, 88].

DeVeaux *et al.* selected for super radiation-resistant isolates of *H. salinarum* after multiple successive rounds of high-level IR to explore the potential for increasing the radiation resistance in this archaeon. This type of strain evolution has previously been done with *E. coli* and *Salmonella typhimurium* LT2 [89-91]. A whole-genome transcriptome analysis of two of the super-resistant *H. salinarum* isolates revealed the up-regulation of two single-strand DNA binding proteins (RPAs), one of which was found to be induced in response to UVC light [89, 92]. Up-regulation of genes for both SODs (sod1 and sod2) were also found in these isolates, but as stated previously, these enzymes are not essential for the radiation resistance observed in wild-type *H. salinarum* [11, 89].

Whitehead *et al* combined proteomic and transcriptomic analyses of the IR response systems in wild-type *H. salinarum*, and found that transcript and protein abundances may vary according to gene and temporal shift, complicating the correlation of transcription and translation [27]. The mechanism of radiation and desiccation resistance in *H. salinarum* appears to reside in the accumulation of cytosolic salt and Mn^{2+}-complexes that protect proteins from oxidative damage [11, 87]. Using a similar method employed previously, we propose to select for increased IR-resistant (IR^{+}) isolates of *H. salinarum* and to investigate the change in protein levels expressed in these isolates, which may reveal key metabolic routes or other protein protection systems instrumental in this enhanced IR resistance [89]. This proteomic-based approach will be complemented by a biochemical analysis of the IR^{+} isolates and the metabolites they accumulate.

Research Objectives

The study of extremophiles and the specific environmental extremes they inhabit lead to new insights on the mechanisms of stress response. The diversity of these mechanisms is as diverse as the habitats and organisms themselves. For example, different mechanisms have evolved for halotolerance. Obligate halophiles accumulate high concentrations of salt in the cell, while moderate halophiles or halotolerant organisms remove salt from the cell by Na^{+} transporters and accumulate organic compatible solutes to maintain osmotic balance [82, 93, 94]. The same diversity is found in IR-resistant organisms, whose proteins are protected by the accumulation of Mn^{2+} and a variety of organic molecules [11, 14, 40, 51-53]. Given the diversity of IR-resistant organisms and their natural environments, we do not know if there are universal features of IR resistance, such as the intracellular accumulation of Mn. In the archaeon *H. salinarum*, desiccation and IR

resistance are the result of the high cytosolic salt concentration and Mn^{2+}-complexes that protect proteins from oxidative damage [11, 87]. We hypothesize that the diversity of IR-resistant extremophiles leads to many different paths to IR resistance, and the object of this research is to investigate the diversity of these mechanisms.

My specific aims are as follows:

1. My hypothesis is that there are multiple metabolic routes to increase IR resistance in *H. salinarum*. I will investigate further damage protection mechanisms that underlie the radiation resistance of *H. salinarum* by the selection and analysis of *H. salinarum* super-resistant (IR^+) isolates. Investigation of differential protein expression in IR^+ isolates of *H. salinarum* may reveal Mn-mediated metabolic routes to high IR resistance.
2. My hypothesis is that the accumulation of Mn^{2+}, trehalose, mannosylglycerate (MG), and di-*myo*-inositol phosphate (DIP) are instrumental in the radiation resistance of the thermophiles *Rubrobacter xylanophilus, Rubrobacter radiotolerans, Pyrococcus furiosus,* and *Thermococcus gammatolerans*.

This research established that there are several metabolic routes to high IR resistance. This work revealed the effect of Mn-stimulated central metabolism, which contributes to the IR resistance in 2 of the IR^+ *H. salinarum* isolates. The 3rd IR^+ isolate utilizes an alternative pathway to IR resistance through a high expression of proteins that are typically reserved for stress conditions associated with stationary phase. This work reaffirmed the relevance of single-stranded binding proteins (RPAs) in IR resistance at the protein level. This study also showed that the anaerobic IR-resistant

hyperthermophiles *P. furiosus* and *T. gammatolerans* do not contain high concentrations of Mn, and the basis of their IR resistance is due to their anaerobic lifestyle. Additionally, we showed that the aerobic thermophiles *R. xylanophilus* and *R. radiotolerans* are protected from IR by the accumulation of trehalose and Mn. We conclude that the compatible solutes MG and DIP do not greatly contribute to the IR resistance in thermophiles.

Chapter 2: The Effect of Mn on Metabolic Pathways in Extreme Radiation-Resistant Mutants of *Halobacterium salinarum*

Introduction

Ionizing radiation (IR) is detrimental to biological systems and most of the damage to macromolecules result from radiolysis of water and the production of reactive oxygen species (ROS), such as hydroxyl radicals ($HO^{\bullet}$), superoxide ($O_2^{\bullet-}$) and hydrogen peroxide (H_2O_2) [19]. ROS damage DNA through double strand breaks (DSBs) or base modifications, but evidence suggests that the more threatening damage to the cell is protein oxidation, producing deactivation, fragmentation, and aggregation of proteins [20]. The most susceptible proteins contain exposed iron-sulfur groups, where $O_2^{\bullet-}$ and H_2O_2 can oxidize ferrous ions (Fe^{2+}), resulting in carbonylation of protein residues, as well as releasing Fe^{2+}, which can further damage macromolecules within the cell and generate more $HO^{\bullet}$ by participation in Fenton chemistry [19-21, 95].

For radiation-resistant microorganisms, such as the bacterium *Deinococcus radiodurans* and the halophilic archaeon *Halobacterium salinarum*, the damage inflicted by these highly oxidizing conditions must either be avoided, repaired, or both in order for the cell to survive [11, 14]. DNA repair systems in IR resistant microorganisms continue to be scrutinized (for review, see [15, 31], but researchers have also been investigating the role protein damage plays in IR-related lethality [11, 14, 39, 40]. Given the lack of environments characterized by high radiation, it has been suggested that radiation

resistance is the result of desiccation resistance, as many organisms that are desiccation-resistant are also resistant to IR, including *D. radiodurans* and *H. salinarum* [12, 17, 18].

The role of ROS scavenging systems in IR resistance have been investigated and previous work with *H. salinarum* and *D. radiodurans* revealed that their radiation resistance is not dependent on ROS detoxification enzymes such as superoxide dismutase and catalase [11, 96]. Additionally, SOD-deficient mutants of *Saccharomyces cerevisiae* and *Escherichia coli* were no longer sensitive to O_2 when these mutants were grown in Mn-enriched media, indicating the importance of cellular accumulation of manganese [44, 45]. $MnPO_4$-complexes catalytically scavenge $O_2^{\bullet-}$ *in vitro*, and when Mn^{2+} was combined with certain amino acids, Mn-amino acid complexes decomposed H_2O_2 [43, 46, 47]. Under conditions of high intracellular concentrations of Mn, the metal binding sites of metalloenzymes can replace Fe with Mn, which could prevent Fenton reaction damage to the protein [21]. A mechanistic link has been shown between high Mn/Fe ratios and high resistance to IR, as seen in *D. radiodurans* and *H. salinarum* [11, 22]. Microorganisms with low Mn/Fe ratios have more protein damage after irradiation than those with high Mn/Fe ratios [11, 14, 18, 39, 48].

Protein-free cell extracts (ultrafiltrates) of *D. radiodurans* and *H. salinarum* had higher concentrations of Mn^{2+}, peptides, and amino acids than those of radiation-sensitive organisms, such as *E. coli* or *P. putida* [11, 14]. The ultrafiltrates protected enzyme activity from high levels of gamma irradiation *in vitro*, whereas ultrafiltrates from radiation-sensitive organisms did not [11, 14]. The radiation resistance of these

prokaryotes appeared to reside in the accumulation of manganous (Mn^{2+}) ions, which form antioxidant complexes with peptides, orthophosphate, and other small molecules (Figure 1-3) [11, 14, 15,50].

The halophilic archaeon *Halobacterium salinarum* NRC-1 grows optimally at 4M NaCl, accumulates up to 4M KCl for osmotic balance, and is exposed UV radiation, as well as desiccation and rehydration cycles, in its natural environment [82]. This well-characterized halophile is extremely resistant to desiccation, radiation and pressure [10, 12]. *H. salinarum*'s resistance to these oxidizing stressors is attributed to the accumulation of high intracellular concentrations of salts and Mn^{2+}-complexes that protect proteins from oxidative damage [11, 87]. DeVeaux *et al.* selected for super radiation-resistant isolates of *H. salinarum* after multiple successive rounds of high-level IR to explore the potential for increasing the radiation resistance in this archaeon. This type of strain evolution has previously been done with *E. coli* and *Salmonella typhimurium* LT2 [89-91]. Using a similar method, we selected for IR^+ isolates of *H. salinarum* to investigate the metabolic routes instrumental to this enhanced IR resistance. This proteomic-based approach will be complemented by a biochemical analysis of the IR^+ isolates and the metabolites they accumulate. Our findings indicate that there is a diversity of metabolic routes through which increased radiation resistance can be obtained.

Materials and Methods

Culturing and Growth Conditions. *Halobacterium salinarum* (ATCC 700922) Δ*ura3*, a uracil autotroph which can be used as a counterselectable marker for homologous gene replacement, and cultures of IR^+ isolates were grown in standard GN101 medium (250 g/L NaCl, 20 g/L $MgSO_4 \bullet 7H_2O$, 2 g/L KCl, 3 g/L Na citrate, 10 g/L Oxoid brand peptone), pH 7.2, with the addition of 1 ml/L trace elements solution (31.5 mg/L $FeSO_4 \bullet 7H_2O$, 4.4 mg/L $ZnSO_4 \bullet 7H_2O$, 3.3 mg/L $MnSO_4 \bullet 7H_2O$, 0.1 mg/L $CuSO_4 \bullet 5H_2O$) and supplemented with a final concentration of 50 mg/L uracil (Sigma-Aldrich, St. Louis, MO). Cultures were grown at 42°C with shaking at 220 rpm (Innova 4080 incubator shaker, New Brunswick Scientific, Edison, NJ).

Directed Evolution of *H. salinarum* Δ*ura3* and Selection of IR^+ Isolates. Single picked colonies were grown in GN101 supplemented with uracil to an OD of 0.4 at 600nm and irradiated at the indicated doses with a ^{60}Co gamma source (dose rate = 3.2 kGy/hr; Uniformed Services University of the Health Sciences, Bethesda, MD). Immediately following irradiation, cells were inoculated into fresh media, grown to an OD of 0.4 at 600nm, and stored in 15% glycerol at -80°C. For each subsequent irradiation, the cultures were grown from their glycerol stocks to an OD of 0.4 at 600nm prior to irradiation. Cultures were irradiated at doses up to 23 kGy (Figure 2-1). At the end of 6 to 9 rounds of IR, single picked colonies from each IR^+ cultures were grown to late exponential phase and stored in 15% glycerol at -80°C. Survival tests using 12 kGy as a benchmark were carried out on all cultures and isolates. All isolates were derived from 3 founder strains, F1, F2, and F3, and designated as "Founder-Final Round IR-Isolate #." For example, the IR^+ isolate 392 was the isolate #2 after 9 rounds of IR of Founder 3.

Survival Assay. Following irradiation at the indicated doses, *H. salinarum* cultures were serially diluted in Basal Salt Solution (BSS; 250 g/L NaCl, 20 g/L $MgSO_4 \bullet 7H_2O$, 2 g/L KCl, 3 g/L Na citrate) and plated on GN101 supplemented with 50 mg/L uracil. Plates were incubated at 42°C for 5-7 days. Survival was calculated as the number of colony forming units (CFUs) following treatment divided by the number of CFUs without treatment and graphed with standard error bars. Three replicates were performed.

Preparation of protein-free extracts (ultrafiltrates, UFs). *H. salinarum* cultures were grown to an OD of 0.4 at 600nm, and harvested cells were washed twice with BSS. Pellets were re-suspended in distilled and deionized water (ddH_2O; Sigma-Aldrich, St. Louis, MO) and passed through an Emulsiflex Homogenizer (Avestin, Inc., Ottawa, Canada) at 15,000 psi to lyse the cells. The cell extracts were centrifuged at 12,000 x *g* (60 min, 4°C) and standardized by protein concentration, which was determined by the BioRad Bradford Assay (BioRad, Hercules, CA). The supernatant was further centrifuged at 190,000 x *g* (40 h, 4°C) and then subjected to filtration using 3kDa centrifugal devices (Amicon ultracel 3k filters; Millipore, Billerca, MA). The resulting ultrafiltrates (UF) were concentrated 5 times in a speed vacuum concentrator (Heto Vacuum Centrifuge; ATR, Laurel, MD). Samples were aliquoted and stored at -20°C.

Enzyme Protection Assay. The restriction enzyme *Dde*I was added at a final concentration of 0.5 unit/µl to UFs diluted to 0.2x. The solutions were irradiated using a ^{60}Co gamma source (Uniformed Services University of the Health Sciences, Bethesda, MD, dose rate = 3.2 kGy/hr) at the following doses: 0, 1, 2, 4, 6, 8, 10, and 12 kGy. Samples were kept on ice until digestion of 1 µg of pUC19 DNA using 1U of enzyme from each irradiated solution at 37°C for 1 h. The resulting pUC19 DNA fragments were

separated by electrophoresis on 1 % agarose TBE gels and visualized with ethidium bromide staining, and imaged using BioDoc-It™ Imaging System (UVP, LLC, Upland, CA). The assay was performed 4 times.

Determination of Amino Acid Concentration. Free and total amino acid concentrations in the *H. salinarum* UFs were determined in triplicate using the ninhydrin assay [97]. Briefly, tryptophan standard solutions were prepared at concentrations from 0 to 200 nmol tryptophan. Ninhydrin reagent was added to the UFs and to the standards and boiled for 20 min. Isopropynol was added to 30% final concentration and the absorbance was read at 570 nm. A standard curve was constructed based on tryptophan standards to determine free amino acid concentration in the UFs. Determination of total amino acid concentration was performed with an acid hydrolysis before assaying free amine concentration with the ninhydrin assay. The UFs were diluted 1:10 in 6 N HCl, flushed with nitrogen, and incubated at 100^{o}C for 24 hr. Ninhydrin reagent was added to the resulting digestions and amino acid concentrations were measured as described above.

Amino acid analysis Amino acid analysis was analyzed using Fmoc-derivitization by Dr. Noboru Tomiya (in Appendix A).

ICP-MS and Ion chromatography. Mn, Fe, and PO_4 concentration in *H. salinarum* UFs and cells (Mn, Fe) were determined using ICP-MS (Mn, Fe) and Ion chromatography (PO_4) at the Division of Environmental Health Engineering, JHU School of Public Health as described previously [11].

Protein Extraction and Precipitation. For the founder, F3 and three IR^{+} isolates, 392, 393, and 463, cultures were grown to an OD of 0.4 at 600 nm and cells were harvested by centrifugation 8,000 x *g* (10 min, 4^{o}C). Two separate cultures were grown for F3, and the

three IR^+ isolates, 392, 393, and 463 for biological replicates. The pellet was re-suspended on ice in 1 M cold salt buffer (50 mM potassium phosphate pH 7.0, 1 M NaCl, 1% 2-mercaptoethanol) and subjected to three cycles of sonication for 30 s (Virsonic 100; Virtis, Gardiner, NY) followed by incubation on ice for 30 s. The cell lysate was then fractionated by centrifugation (8000 x *g*, 30 min, 4°C), with the supernatant withdrawn and stored at -20°C. Protein concentration was determined using Bio-Rad Bradford Assay using the manufacturer's protocol. Aliquots containing 200 μg of protein were stored on ice and 8 volumes of -20°C TCA/acetone added. The mixture was vortexed briefly, incubated at -20°C for 4 hr, and then pelleted by centrifugation (16,000 x *g*, 10 min, 0°C) before discarding the supernatant and air-drying the pellet. To measure the yield of protein, another aliquot of 200 μg was subjected to the same protocol but instead of air-drying the pellet, the pellet was re-suspended in a volume of denaturing buffer (50 mM potassium phosphate pH 7.0, 1 M NaCl, 1% 2-mercaptoethanol, 6% sodium dodecyl sulfate) equal to the volume of the original aliquot, and protein concentration was determined with the Bradford Assay. To verify that the TCA/Acetone precipitation process did not result in a loss of a significant amount of proteins, denatured proteins from both TCA treated and non-TCA treated extracts were separated by denaturing acrylamide gel electrophoresis (SDS-PAGE) on a 4-20% gradient gel (15 μg protein per lane) at 150 V, 60 mA for 1.5 hrs. The gel was stained with Bio-Rad Flamingo™ stain (BioRad, Hercules, CA) and imaged using BioDoc-It™ Imaging System (UVP, LLC, Upland, CA) and Typhoon (GE Healthcare Life Science, Piscataway, NJ). The iTRAQ Labeling and LC-MS Analysis were carried out at the Proteomic facility of the Johns Hopkins School of Medicine.

Protein Digestion, iTRAQ Labeling and LC-MS Analysis. The TCA/acetone precipitated protein pellets were re-suspended in 20µL 500mM TEAB (triethyl ammonium bicarbonate) and 1µL 2% SDS. Each sample was reduced by adding 2µL 50 mM TCEP (tris-(2-carboxyethyl) phosphine) for 1 h at 60°C, alkylated by 1µL 200 mM MMTS (methyl methanethiosuphonate) for 15 min at room temperature, then digested at 37°C overnight with trypsin (Promega, Fitchburg, WI) using a 1:10 enzyme to protein ratio. Samples were labeled by adding 100 µL of an iTRAQ reagent (Applied Biosystems, Foster City, CA) dissolved in isopropanol and incubated at room temperature for 2h. All samples were dried to a volume of approximately 30µL and subsequently mixed. The combined peptide sample was dissolved in 8 mL of SCX loading buffer (25% v/v acetonitrile, 10mM KH_2PO_4, pH 2.8) and subsequently fractionated by strong cation exchange (SCX) chromatography on an Agilent 1200 Capillary HPLC system (Agilent Technologies, Santa Clara, CA) using a PolySulfoethyl A column (2.1x100mm, 5µm, 300Å) (PolyLC, Columbia, MD). The sample was loaded and washed isocratically with 25% v/v acetonitrile, 10mM KH_2PO_4, pH 2.8) for 40 min at 250µL/min. Peptides were eluted and collected in 1 min fractions using a 0-350mM KCl gradient in 25% v/v acetonitrile, 10mM KH_2PO_4, pH 2.8, over 40min at 250µL/min, monitoring elution at 214 nm. The SCX fractions were dried, re-suspended in 200µL 0.05% TFA and desalted using an Oasis HLB uElution plate (Waters, Milford, MA). Desalting peptides were loaded for 15 min at 750 nl/ min directly on to a 75 µm x 10 cm column packed with Magic C18 (5 µm, 120Å, Michrom Bioresources, Auburn, CA). Peptides were eluted using a 5-40% B (90% acetonitrile in 0.1% formic acid) gradient over 90 min at 300 nl/min. Eluting peptides were sprayed directly into an LTQ Orbitrap

Velos mass spectrometer (ThermoScientific, Waltham, MA) through an 1 μm emitter tip (New Objective, Woburn, MA) at 1.6 kV. Survey scans (full ms) were acquired from 350-1800 m/z with up to 10 peptide masses (precursor ions) individually isolated with a 1.2 Da window and fragmented (MS/MS) using a collision energy of 45 and 30 s dynamic exclusion. Precursor and the fragment ions were analyzed at 30,000 and 7,500 resolution, respectively

Data Analysis. The MS/MS spectra were extracted and searched against the GenBank database using Mascot (Matrix Science, Boston, MA) through Proteome Discoverer software (ThermoScientific, Waltham, MA) specifying sample's species, trypsin as the enzyme allowing one missed cleavage, fixed cysteine methylthiolation and 8-plex-iTRAQ labeling of N-termini, and variable methionine oxidation and 8-plex-iTRAQ labeling of lysine and tyrosine. Peptide identifications from Mascot searches were processed within the Proteome Discoverer to identify peptides with a confidence threshold 1% False Discovery Rate (FDR), based on a concatenated decoy database search. A protein's ratio is the median ratio of all unique peptides identifying the protein at a 1% false discovery rate (FDR).

Results

Enrichment and selection of IR^+ isolates

We selected for super-IR resistant (IR^+) isolates of *H. salinarum* in order to further investigate the mechanisms contributing to the radiation resistance of this halophile. Five individual cultures of *H. salinarum* (founders) were irradiated as shown in Figure 2-1 for the directed evolution of IR^+ isolates. By using high levels of gamma-radiation, we could eliminate less radiation-resistant members in the culture, and only those possessing increased radiation resistance would survive and proliferate during the recovery phase (Fig. 2-1). After completion of the irradiation-recovery rounds (9 rounds for cultures F1, F2 and F3, and 6 rounds for cultures F4 and F5), a survival test using 12 kGy as a benchmark was conducted. After 9 rounds of irradiation, IR2-9, IR4-6, and IR5-6 reached at least 60% survival to 12 kGy, while only 42% and 23% of the cells survived a dose of 12 kGy in cultures IR1-9 and IR3-9, respectively (Fig. 2-2). Thirty isolates were randomly selected from the cultures (Fig. 2-2) and tested for their survival at 12 kGy (Fig. 2-3).

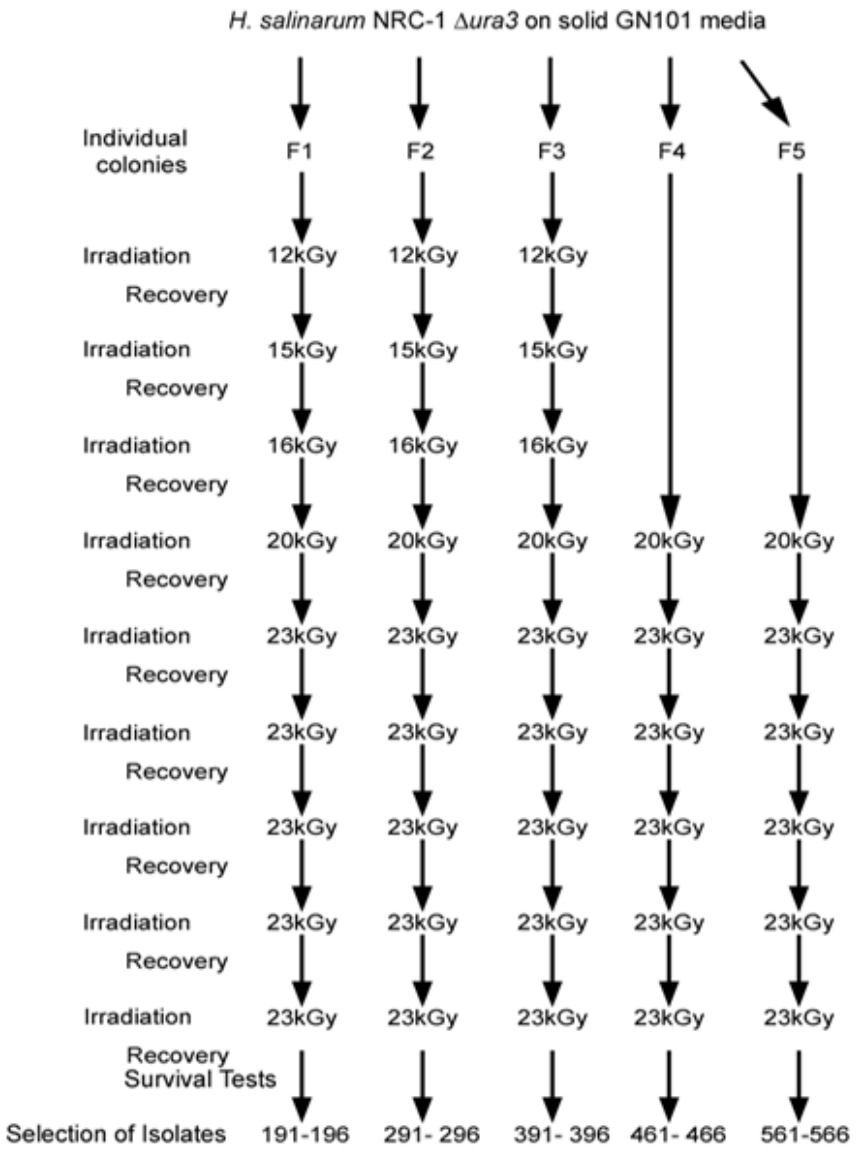

Figure 2-1. Irradiation schedule and IR doses to obtain IR^+ isolates of *H. salinarum*. Founders F1, F2, and F3 were initially exposed to 12 kGy, with the doses gradually increasing to 23 kGy. F4 and F5 were initially exposed to 20 kGy for one round, with all subsequent rounds being at 23 kGy.

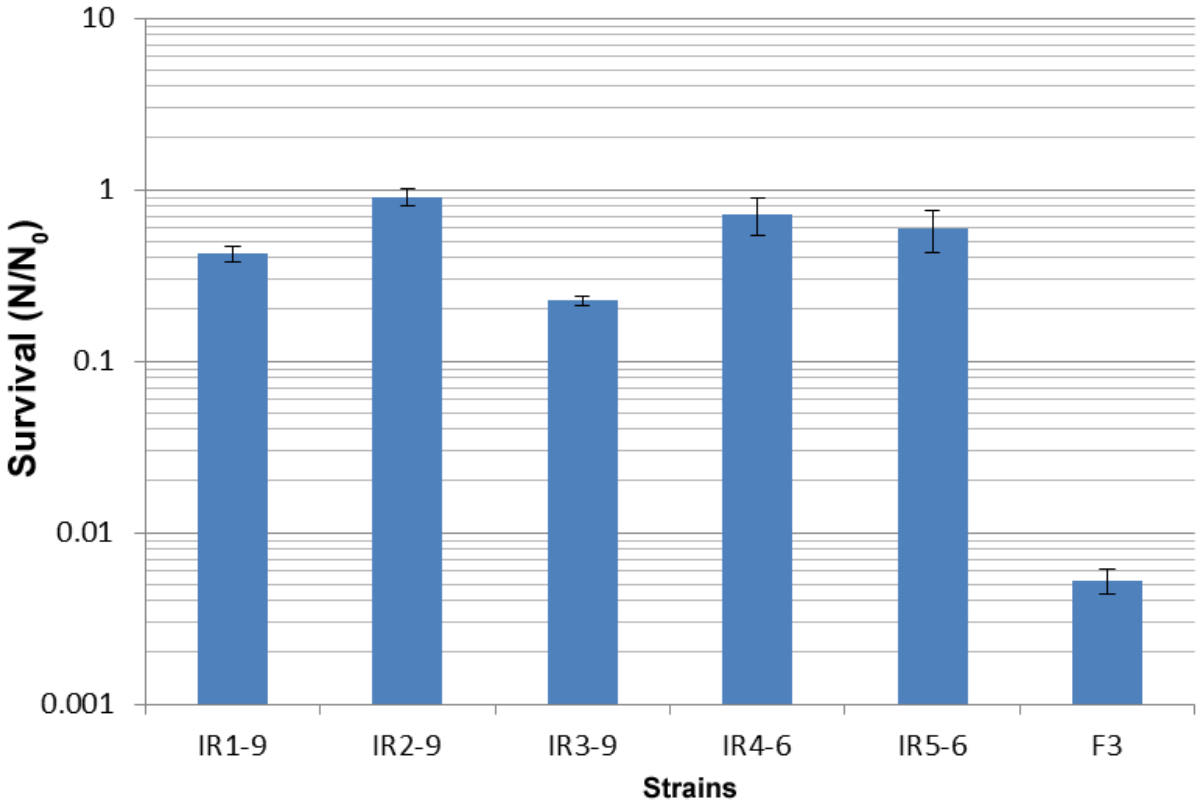

Figure 2-2. Survival of *H. salinarum* cultures completion of the irradiation-recovery rounds and exposed to 12 kGy of IR (from [98]). Survival was calculated as the average ratio (N/N_0) of cfu/ml from irradiated (N) compared to un-irradiated (N_0) cultures, with 3 replicates used for each calculation. The uncertainties are standard errors.

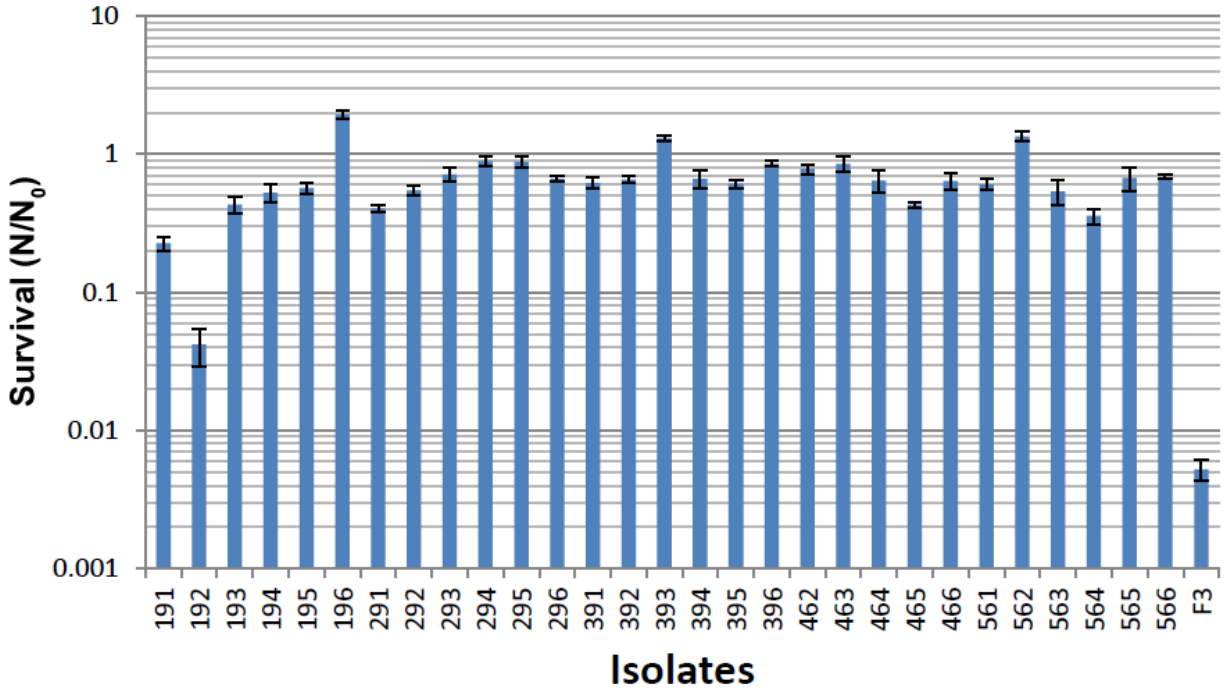

Figure 2-3. Survival of *H. salinarum* isolates at 12 kGy of ionizing radiation (from [98]). Survival was calculated as the average ratio (N/N_0) of cfu/ml from irradiated (N) compared to un-irradiated (N_0) cultures, with 3 replicates used for each calculation. The uncertainties are standard errors. F3 was added for comparison.

Survival for 23 of the 30 selected isolates was > 50% at 12 kGy, and all had significant increases in IR resistance when compared to the founder 3 (F3) strain (Fig. 2-3). Isolates 392, 393, 463, and F3 were selected for further investigation including survival curves, proteomic studies, and biochemical characterization of the enzyme-free cell extract. Isolate 393 was selected because of its high survival to 12 kGy (Fig. 2-3); 392 was selected randomly among isolates with over 50% survival to 12 kGy; and 463 was selected because it came from a culture that was subjected to only 6 rounds of IR,

possibly resulting in different modes of IR^+ resistance than cultures subjected to 9 rounds of IR.

To characterize the survival to IR and calculate the D_{10} (the dose at which 10% of the cells survive) of the selected isolates, survival curves were constructed using doses of 0, 8, 12, 15, and 18 kGy of IR (Fig. 2-4).

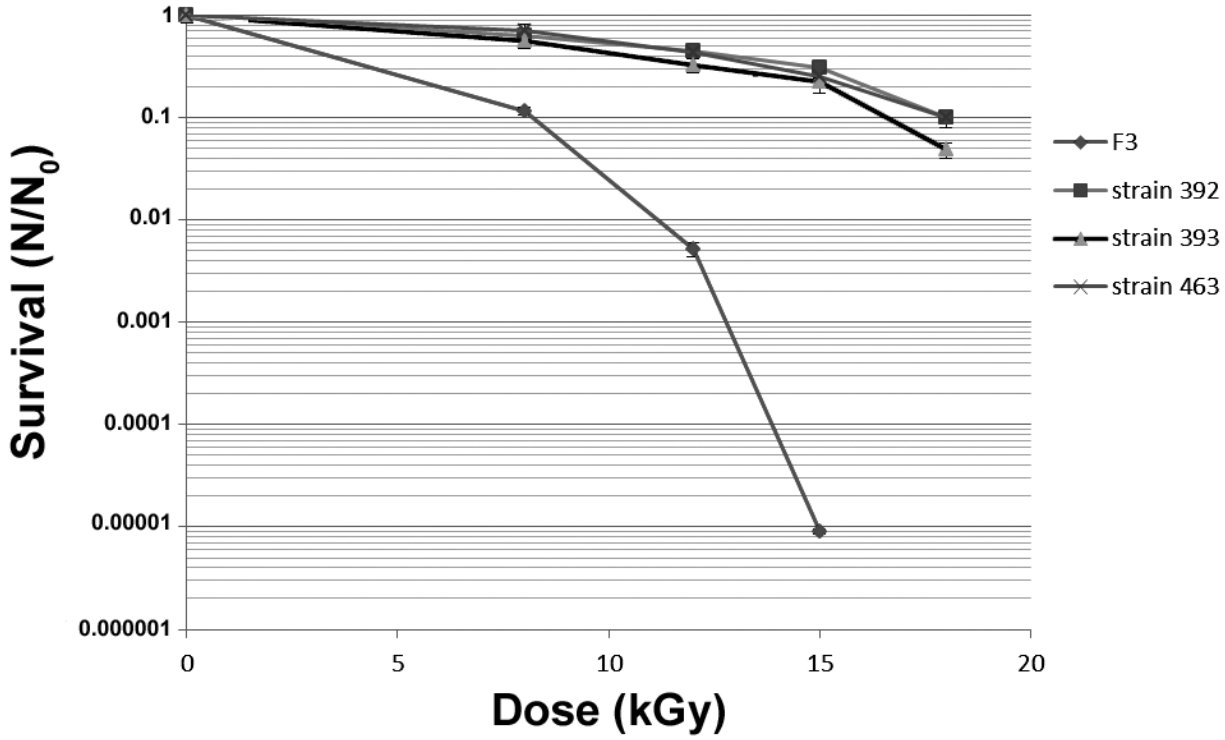

Figure 2-4. Survival curves of *H. salinarum* IR^+ isolates and founder strain F3 exposed to 0, 8, 12, 15, and 18 kGy of IR (from [98]). Survival was calculated as the average ratio (N/N_0) of cfu/ml from irradiated (N) compared to un-irradiated (N_0) cultures, with 3 replicates used for each calculation. The uncertainties are standard errors.

The survival curve of F3 had a moderate shoulder, but as doses increased, it quickly dropped off. The IR^+ isolates displayed a broader shoulder, and at the dose 8 kGy, where F3 survival was reduced to 10%, the isolates were at 80% survival. From the survival curves, a D_{10} value of 17 kGy was calculated for the isolates, a marked improvement from the D_{10} value for wild-type *H. salinarum* of 5 kGy [12].

Ultrafiltrate (UF) protection of enzyme activity from radiation

Non-enzymatic processes significantly contribute to the radiation resistance of *H. salinarum*, and enzyme-free cell extracts (ultrafiltrates, UFs) protected enzyme activity from IR [11]. To investigate the role of antioxidant molecules in the increased IR resistance of *H. salinarum* IR^+ isolates, we prepared UFs from 3 isolates 392, 393 and 463, and the founder strain F3. Using an enzyme protection assay, we determined the level of radioprotection in the UFs. The restriction enzyme *Dde*I was irradiated in the presence of the UFs, and its residual activity determined by its ability to cut pUC19 plasmid DNA (Fig. 2-5). Protection of the enzyme facilitated complete cutting of the plasmid DNA into distinct individual bands on the agarose gel. Inactivation of the enzyme is shown in the gel by one band, indicating the plasmid is still intact. We found residual enzyme activity up to 6 kGy in presence of the UF from F3 but in the presence of UFs from IR^+ isolates, residual activity was detected up to 10 or 12 kGy (Fig. 2-5), demonstrating increased IR protection *in vitro*.

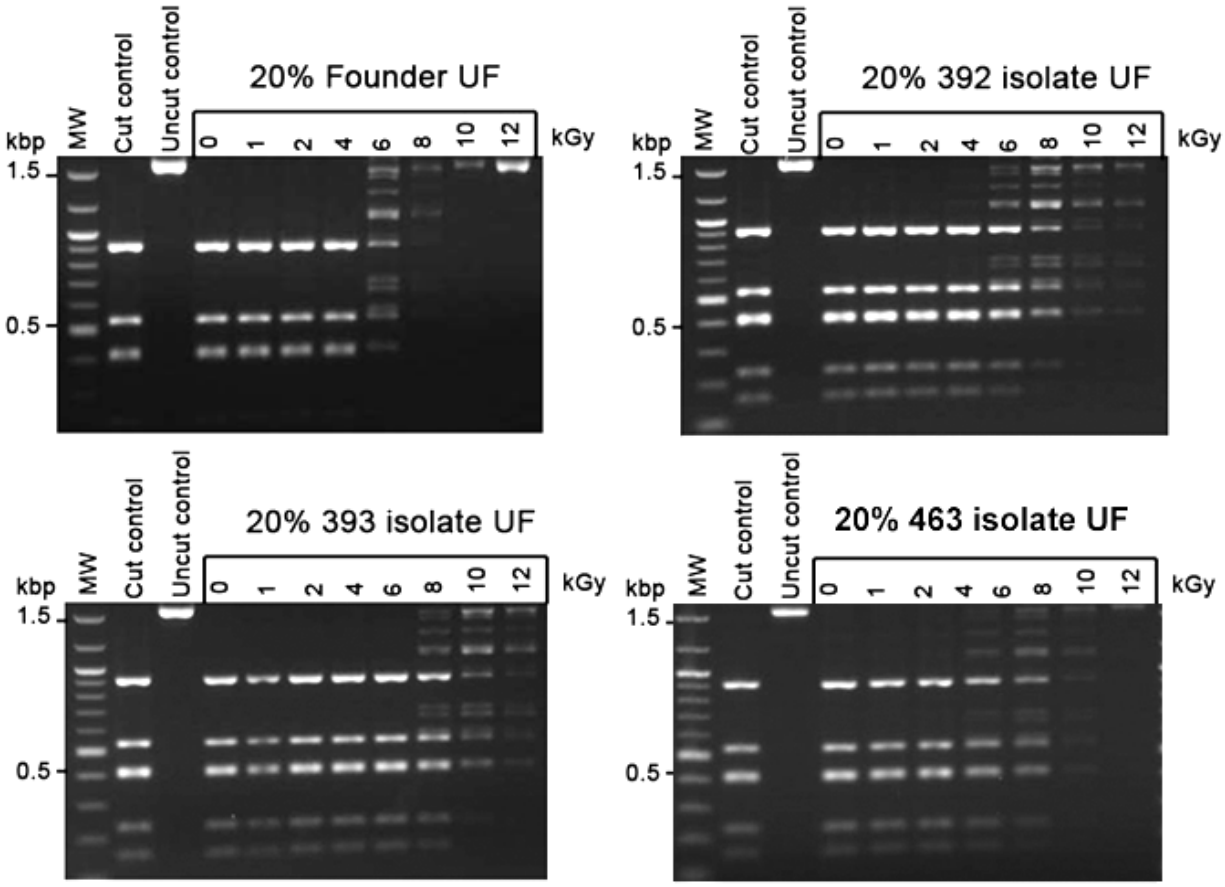

Figure 2-5. Protection of enzyme activity. The restriction enzyme *Dde*I was irradiated up to 12 kGy in enzyme-cell free extracts (UFs) of the *H. salinarum* founder 3 (F3) and the IR^+ isolates 392, 393, and 463 (diluted to 0.2x). Residual restriction enzyme activity was assayed by the digestion of pUC19 plasmid DNA; fragments were analyzed by agarose gel electrophoresis. The first lanes are molecular size ladders.

Ultrafiltrate Composition

The accumulation of intracellular manganous (Mn^{2+}) ions form antioxidant complexes with peptides, orthophosphate, and other small molecules which catalytically scavenge ROS, thus reducing protein damage [11, 14]. Given the increased survival of the IR^+ isolates, and the enhanced protein protection their UFs provide against IR, we measured the concentration of Mn, PO_4, and amino acids in the UFs of the IR^+ isolates and F3. Two of the IR^+ isolates, 392 and 463, had 1.5-fold and 1.3-fold more Mn, respectively, when compared to the F3 UF, $p < 0.05$ (Fig. 2-6). The UF of 392 had 1.5-fold more PO_4, and 2.5-fold more amino acids than the F3 UF, $p < 0.05$ (Fig. 2-6). An analysis of individual amino acids quantified the concentration of glycine in the 392 UF, which was 3 times that of the UF from F3 (Fig. 2-6). The concentrations of Mn, PO_4 and amino acids were comparable to that of the F3 UF (Fig. 2-6). However, given that the 393 UF protected enzyme activity to 12 kGy, it is possible this IR^+ isolate, and potentially the others, accumulates some compounds not tested for here. In order to determine what proteins and metabolic pathways contributed to the increased IR resistance observed in these isolates, we used proteomic analysis to investigate changes in protein abundances of the IR^+ isolates with respect to the founder (F3).

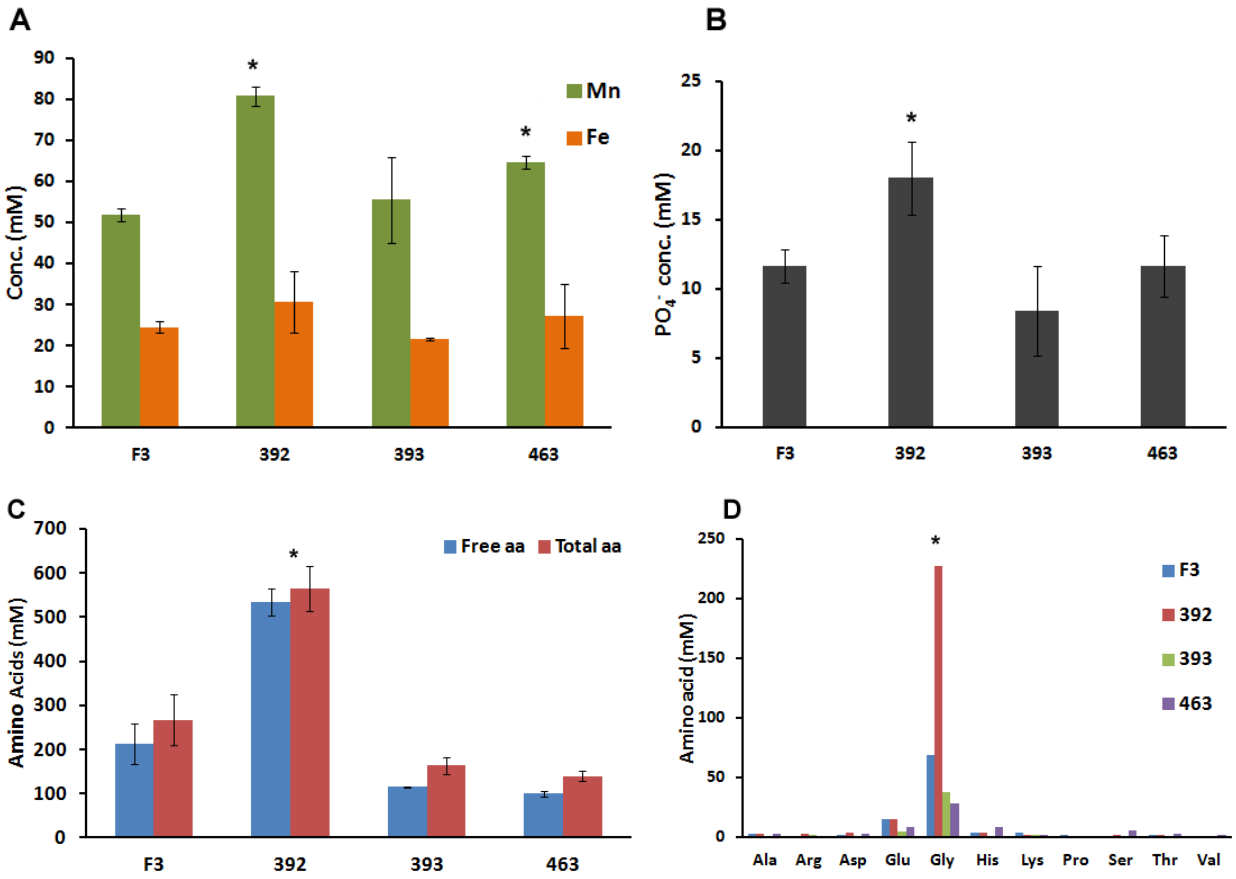

Figure 2-6. Ultrafiltrate composition for Founder 3 (F3) and the IR^{+} isolates 392, 393, and 463.

(A) Manganese (Mn) and iron (Fe) concentrations measured using ICP-MS. (B) Phosphate concentration measured using ion chromatography (C) Free and total amino acid concentrations measured by the ninhydrin assay, total amino acids were determined after acid hydrolysis (D) Individual amino acid concentrations determined by ion chromatography after FMOC derivatization.

* indicates a significant difference from the Founder (F3), $p < 0.05$, determined using Student's t-test.

Proteomic Analysis

We used iTraq analysis to look for differential protein expression in the IR^+ isolates 392, 393, and 463 when compared to the founder (F3). In order to determine the steady-state protein expression levels in each isolate, cells were harvested without irradiation and grown under optimal conditions. Protein digest, iTraq labeling, LC-MS analysis, and data analysis were performed by the Proteomics Facility at Johns Hopkins School of Medicine. iTRAQ analysis of the proteins from the IR^+ isolates and founder produced 386,843 spectra. Using the GenBank database we identified 126,845 peptides that formed 1,266 protein groups and 1,279 merged proteins covering 48% of the *H. salinarum* proteome.

Data validation

We compared the physical properties of the identified proteins in the iTraq dataset with predicted values of the *H. salinarum* proteome to check for any biases (data obtained from the Comprehensive Microbial Resource database, CMR) (Fig. 2-7). The predicted proteome of *H. salinarum* has a mean molecular weight of 31.5 kDa, and a median molecular weight of 27.6 kDa (data from CMR). The iTraq-identified proteins ranged in molecular weight from 10 – 50 kDa, with a mean and median of 34.1 kDa and 29.7 kDa, respectively. With respect to isoelectric point (pI), the calculated pI of iTraq-identified proteins had a mean and median of 4.79 and 4.59, respectively (Fig. 2-7B). These values are close to a median of 4.9 that was previously predicted for the *H. salinarum* proteome [99]. Such low pI values indicate a high negative charge from the abundance of glutamic and aspartic acid residues, and these acidic proteins are an adaptation to remain soluble

and functional in the high salinity environment of the cytoplasm (~4.3 KCl) [99]. Both the molecular weights and the pI values of our identified proteins indicate that the MS analysis of our iTraq dataset is a good representation of the *H. salinarum* proteome without any notable biases (Fig. 2-7).

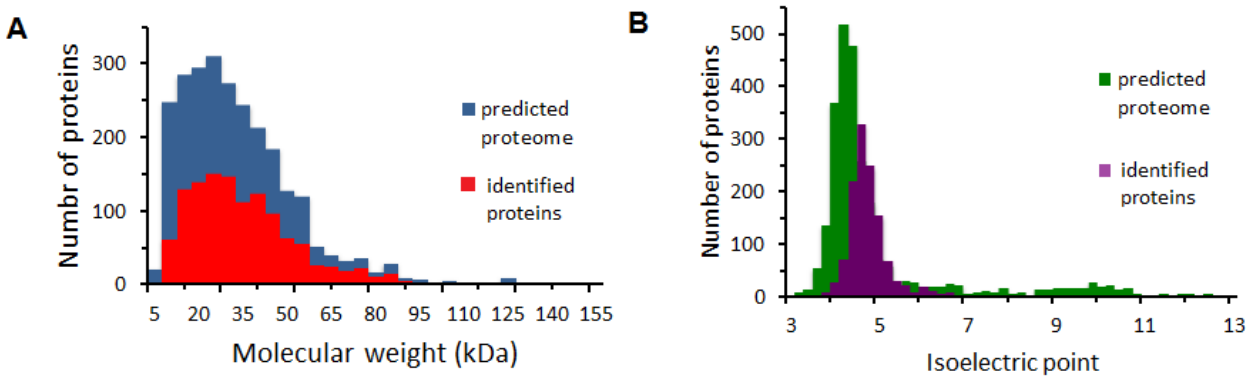

Figure 2-7. Predicted proteome of *H. salinarum* versus iTraq-identified proteins. (A) Histogram of protein molecular weights of predicted proteins in *H. salinarum* and identified proteins in the iTRAQ dataset, (B) Histogram of isoelectric points of predicted proteins in *H. salinarum* and identified proteins in the iTraq dataset (from [98]).

Using the classification from the CMR database, the iTraq-identified proteins and *H. salinarum* predicted proteome were sorted into 18 metabolic categories, which included distinction for hypothetical, unclassified, and proteins of unknown function (Fig. 2-8). This allowed us to evaluate the representation of our identified proteins with respect to cellular function when compared to the predicted proteome. For both datasets (identified and predicted), hypothetical and unclassified proteins were the largest categories, and for proteins of known function, energy metabolism out-numbered all other processes (Fig. 2-8). The iTraq-identified proteins correlated with the predicted proteome for all the

categories, save for underrepresentation of the cell envelope proteins and transport proteins, which is likely the result of our protein extraction method (Fig. 2-8).

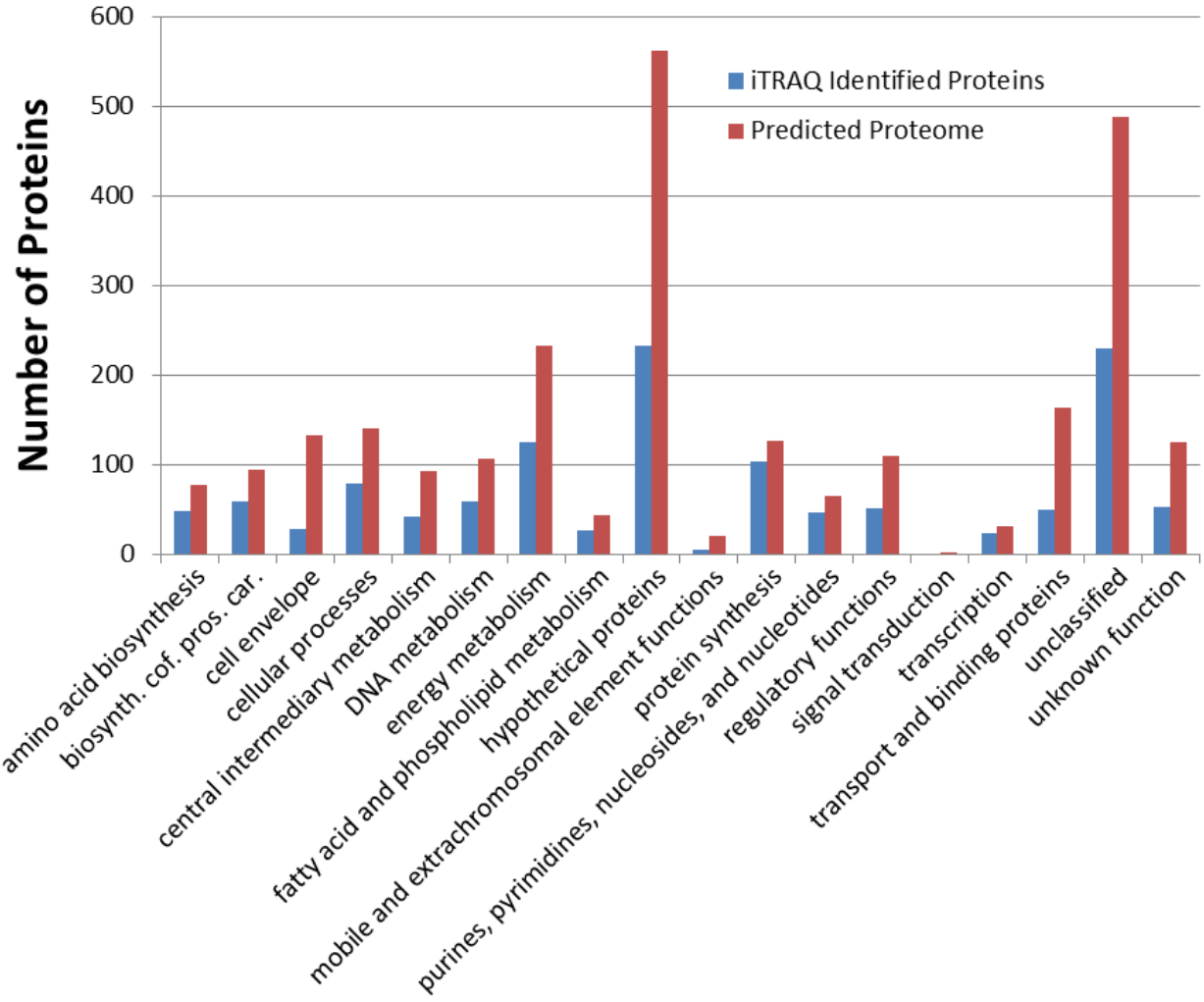

Figure 2-8. Classification of iTraq-identified proteins and predicted proteome of *H. salinarum* according to the CMR database. "biosynth. cof. pros. car." = biosynthesis of cofactors, prosthetic groups, and carriers (from [98]).

Ratios of protein expression levels were calculated using Proteome Discoverer (Thermo Scientific, Waltham, MA) between pairs of biological replicates and between each IR^{+}

isolate (392, 393 and 463) and the founder (F3) (Fig. 2-9). Figure 2-9A is the graph of the two founder replicates, F3-1 and F3-2, and the ratio of each protein is close to 1, as they are biological replicates under identical growth conditions. Differences were found, with one protein at a ratio of 1.5, and the lowest ratio being 0.22; these reflect variation between biological replicates. When comparing the IR^+ isolates to the founder, we see significant variation in protein expression ratios, ranging from 0.07 to 6.9, representing differential protein expression levels in the IR evolved isolates when compared to the founder strain (Fig. 2-9).

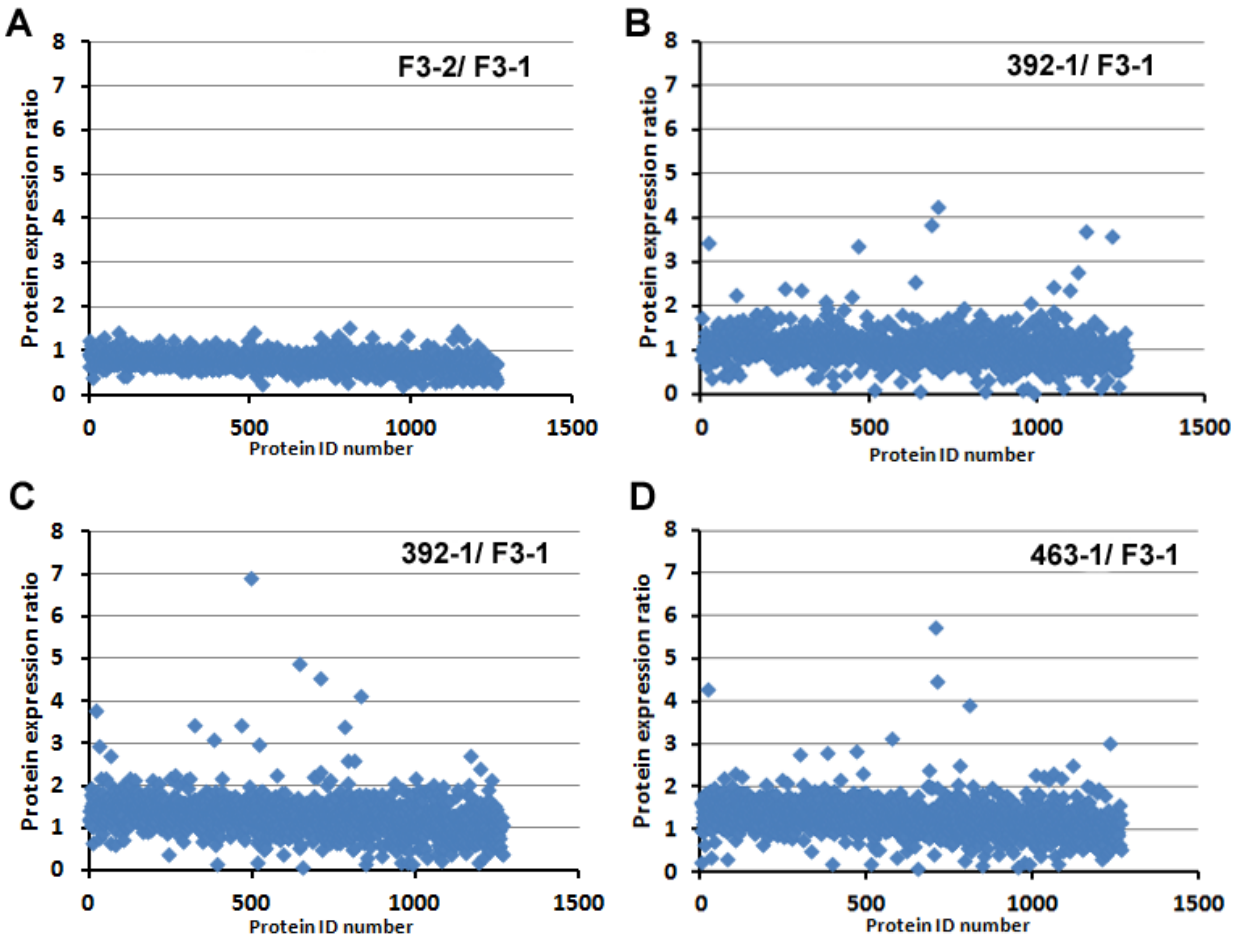

Figure 2-9. Ratios of protein expression levels between (A) F3-2 and F3-1, (B) 392-1 and F3-1, (C) 393-1 and F3-1, and (D) 463-1 and F3-1 (from [98]). The ratios for the biological replicates are close to 1 as expected, while the ratios between the IR^+ isolates and the founder are significantly varied.

Differential Protein Expression in IR^+ Isolates

Protein expression ratios (PER) were calculated for each protein using unique MS-identified peptides for the protein, and an overall score is assigned. This score (A4 score) is the sum of the absolute probabilities for the unique peptides identifying the protein in the PER; for example, an A4 score of 200 indicates that the sum of the unique peptide probabilities contributing to the PER is 10^{-20}. A threshold of > 100 A4 score was used to remove proteins with poor peptide coverage (determined using Proteome Discoverer). To identify proteins that were differentially expressed in the IR^+ isolates with respect to the founder we selected cut off ratios of <0.4 and >1.5 for a false discovery rate (FDR) of <6%. FDR were calculated by counting outliers in all biological replicate comparisons at specific cut off ratios. A FDR of 6% indicates that there is less than 6% chance that the expression level of a protein was not significantly increased or decreased at ratios above 1.5 or below 0.4, respectively. To determine differential protein expression between the IR+ isolate and the founder (F3), there are four possible PER (isolate-1 with F3-1; isolate-2 with F3-1; isolate-1 with F3-2; and isolate-2 with F3-2) which were averaged. This average represents the overall PER of the IR^+ isolate when compared to F3 for a given protein. Using the 6% FDR, PER <0.4 are considered decreased (Fig. 2-10, Table 1 in Appendix B), and PER >1.5 are considered increased (Fig. 2-11, Table 2 in Appendix B).

Decreased Protein Expression Ratios in IR^+ Isolates

All of the decreased PER fell into 1 of 4 functional categories: transcription, regulation, cellular processes, and unknown (Table 1 in Appendix B). Five of the 14 decreased PER

were common among the three IR^+ isolates, including 3 gas vesicle proteins GvpC, GvpN and GvpO (VNG7026, VNG7027 and VNG7028), chromosome partitioning protein SojB (VNG7029), and a putative signal-transducing histidine kinase/ response regulator protein (VNG7030). The phenotype of gas vesicle-deficient *H. salinarum* has red (versus pink) plated colonies than the wild-type, and the cells do not float in liquid culture as observed for the wild-type. The decreased PER for gas vesicle proteins in the IR^+ isolates indicates these proteins are not as abundant as in the founder strain, and the confirmation of the observed phenotype of the IR^+ isolates provides us with experimental validation of the iTraq analysis. As all three IR+ isolates were gas vesicle-deficient, we verified that the loss of gas vesicle did not contributed to the IR^+ resistance observed in our IR^+ isolates. We isolated a spontaneous F3*vac*$^-$ isolate that had not been exposed to any IR. We determined the F3*vac*$^-$ isolate's resistance to IR was less than that of F3, and concluded that the loss of gas vesicle function itself did not contribute to IR^+ resistance (Fig. 1 in Appendix C).

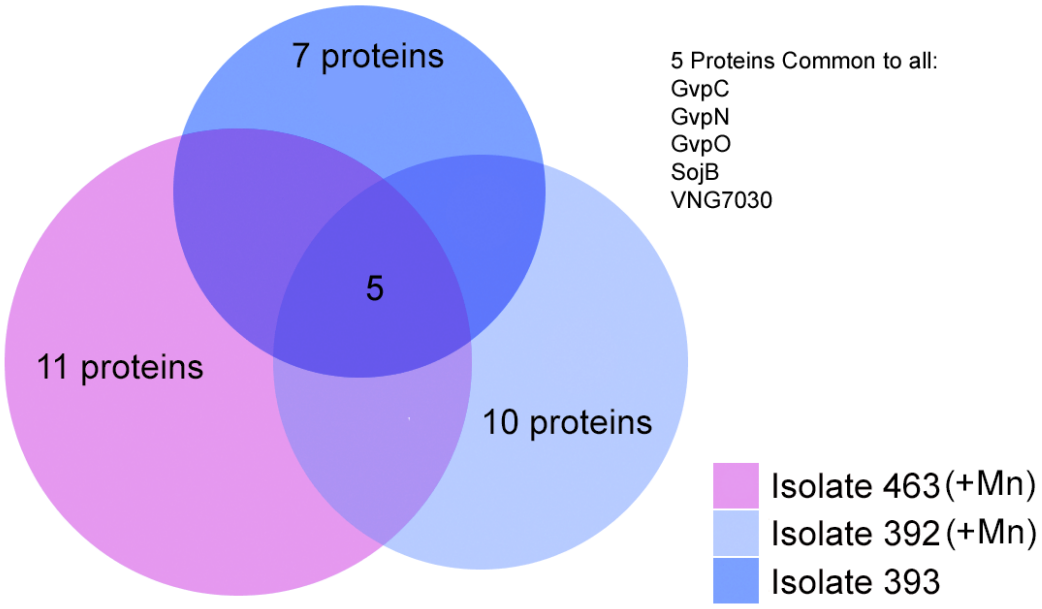

Figure 2-10. Decreased protein expression ratios (< 0.4) in IR^+ isolates. Details of common and unique proteins can be found in Table 1 in Appendix B. Isolates 392 and 463 have increased Mn accumulation.

Increased Protein Expression Ratios in IR$^+$ Isolates

IR$^+$ isolate 393 had 78 increased PER; isolate 392 had 262 increased PER; and isolate 463 had 435 increased PER (Fig. 2-11). Twenty-nine of the 537 increased PER were common for all 3 of the IR$^+$ isolates (Fig. 2-11). These included: a ArgK-type transport ATPase (VNG0674C); 2 single-strand DNA binding proteins (Rfa3, Rfa8); threonine synthase (VNG2430G); both superoxide dismutases (Sod1, Sod2); a cell division cycle protein (Cdc48b); a general stress protein 69 (Gsp); glyceraldehyde-3-phosphate dehydrogenase (GapB); phosphoenolpyruvate synthase (PpsA); carboxypeptidase (Cxp); 2-oxoglutarate ferredoxin oxidoreductase subunit alpha (PorA); and a V-type ATP synthase subunit E (VNG2142) (Table 2 in Appendix B).

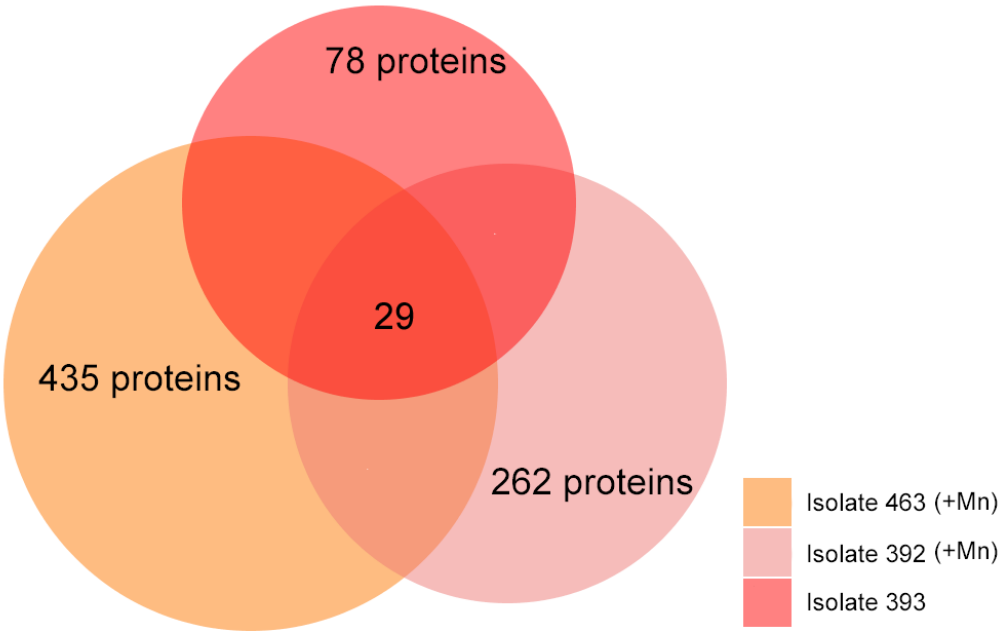

Figure 2-11. Increased protein expression ratios (> 1.5) in IR$^+$ isolates. Details of common and unique protein expression ratios can be found in Tables 2 in the Appendix B. Isolates 392 and 463 have increased Mn accumulation.

While we were able to investigate the 14 decreased PER individually among the IR^+ isolates (Fig. 2-10), a more practical approach was required for the 537 increased PER (Fig. 2-11). The increased PER were manually evaluated for further annotation and better categorization. Additionally, the Transcription and Regulatory categories from the CMR database were combined as follow: Protein Synthesis and Translation categories were combined; "biosynthesis of cofactors, prosthetic groups, and carriers" was annotated as Cofactors and 2° Metabolites; and Hypothetical, Unclassified and Unknown protein categories were combined to Unknown. This approach allowed us to investigate trends in protein function for the increased PER among the IR^+ isolates (Fig. 2-12).

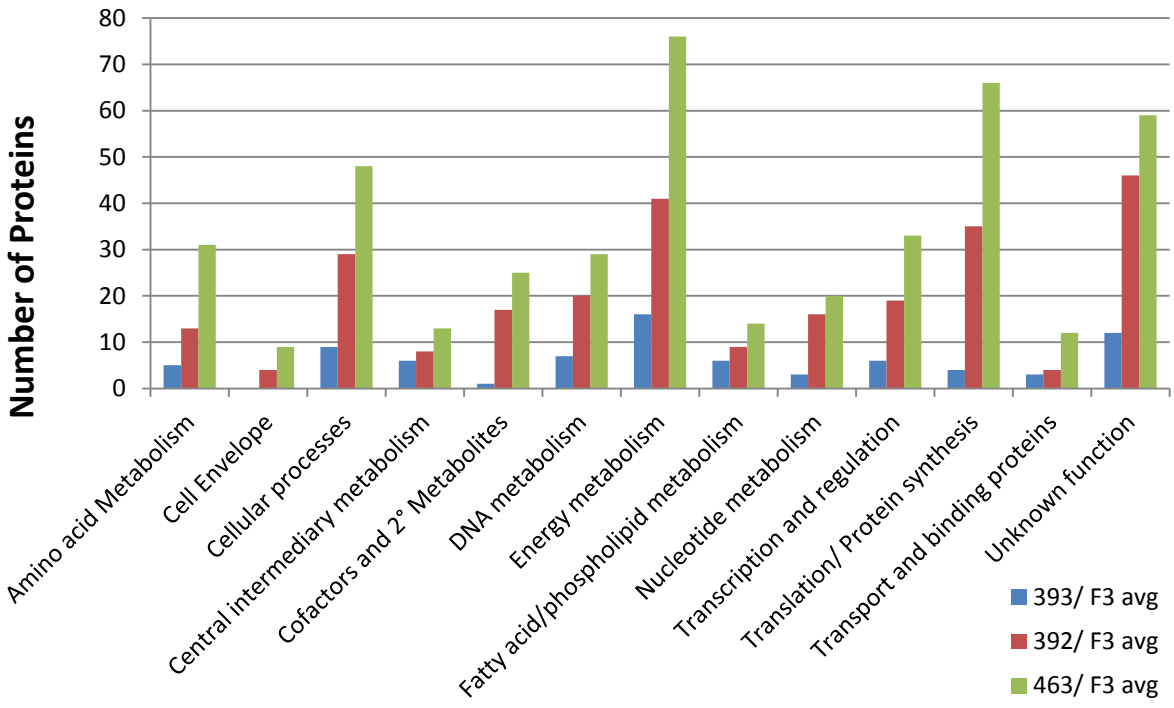

Figure 2-12. Classification of protein function for increased protein expression ratios among the three IR^+ isolates. Isolates 392 and 463 have increased Mn accumulation.

Investigating increased PER at the >1.5 cutoff allowed us to find metabolic trends among the IR^+ isolates. Isolate 463 had the highest amount of increased PER among the 3 isolates (435). Excluding the 29 increased PER common to all isolates, 463 had 18 and 148 increased PER common with isolates 393 and 392, respectively (Fig. 2-11). The 18 increased PER common only between 463 and 393 included: a flavin-dependent oxidoreductase (Mer); phosphoglycerate dehydrogenase (SerA3); alcohol dehydrogenase (Adh2); and a putative glutathione S-transferase (VNG2281C) (Table 2 in Appendix B). Isolates 463 and 392 have many PER in common (177, including the 29 increased PER common to all IR^+ isolates), and the overall metabolic trends are very similar, which also correlates with the increase in Mn observed in the UFs of these 2 isolates. Isolates 463 and 392 had increases of Mn in their UFs, but isolate 393 did not (Fig. 2-6). The 177 increased PER common between isolates 392 and 463 accounted for 68% of the total increased PER for isolate 392. We found a trend among the protein function categories of the increased PER both isolates 392 and 463; both had increased PER associated with energy metabolism, cellular processes, cofactor biosynthesis, and translation/ protein synthesis (Figs. 2-12). The majority of the increased PER associated with translation/ protein synthesis are ribosomal proteins (Table 2 in Appendix B) presumably to synthesize the high levels of enzymes required to meet the demands of increased PER found in the 392 and 463 isolates. (Figs. 2-12). Thirty-two of the 177 increased PER common between 392 and 463 were classified as energy metabolism proteins and included: phosphoglyceromutase (GpM); a cytochrome-like protein (Fbr); phosphopyruvate hydratase (Eno); NADH oxidase (NoxA); phosphoglycerate kinase (Pgk); fructose-bisphosphate aldolase (Fbp); and a pyruvate dehydrogenase component

(Dsa) (Table 1 in Appendix B). Two PER common between isolates 392 and 463 were transport proteins, a hypothetical K^+ transport system that binds Mn (VNG0983C) and arsenical pump-driving ATPase (ArsA1). Cellular processes was also a dominant category for common PER between isolates 392 and 463, with a hypothetical peptidase (VNG0437C), a heat shock protein (Hsp2), 2 chemotaxis proteins (CheW1, CheC1), and 2 cell division proteins (FtsZ3, FtsZ4). There were 7 PER related to cofactor biosynthesis in common between the 392 and 463 isolates, which included two NAD synthesis proteins L-aspartate oxidase (NadB) and NAD synthetase (NadE). There were 239 increased PER that were unique to isolate 463 alone. These included 8 peptidases, 6 universal stress response proteins, 7 proteins associated with oxidative phosphorylation, and a starvation induced DNA-binding protein (DpsA) (Table 2-1).

Table 2-1. Examples of increased protein expression ratios unique to IR^+ isolate 463

Peptidases:	Universal Stress Response:	Oxidative Phosphorylation:
PepQ1	VNG0743	Cytochrome C oxidase subunit I
PepQ2	VNG1536	Cytochrome C oxidase subunit II
PepB2	VNG1658	HcpC
PepB3	VNG2520	NdhG5
YjbG	VNG2521	NolD
YwaD	VNG2523	Sdh
VNG0096C		VNG0891
VNG1866G		

There were 15 increased PER common only between isolates 392 and 393 (Fig. 2-11, Table 2 in Appendix B) including: a bacterio-opsin linked protein (VNG1463); a NADH dehydrogenase/oxidoreductase-like protein (VNG1932); a acyl-CoA dehydrogenase (VNG1191); and a photolyase/cryptochrome protein (Phr1). Isolate 392 alone had 4 increased PER in the NAD synthesis pathway, quinolinate synthetase (NadA), nicotinate-

nucleotide pyrophosphorylase (NadC), NadB and NadE. Additionally, the average PER for NadA, NadB and NadC were 5.0, 6.9 and 3.2, respectively, and were among the highest increased PER for isolate 392.

The increased PER for isolate 393 contrasted with isolates 392 and 463, as no increased PER for isolate 393 related to cell envelope functions were found, and cofactor biosynthesis was not a dominant protein function category (Fig. 2-12). Categories for energy metabolism, cellular processes, unknown function, and DNA metabolism were the groups with the most increased PER in isolate 393 (Fig. 2-12). We looked at the increased PER with respect to KEGG (Kyoto Encyclopedia of Genes and Genomes) pathway classification and saw that categories for isolates 392 and 463 were very similar, while isolate 393 had distinctly more varied categories (Fig. 2-13). Isolate 393 had increased PER involved in arginine and proline metabolism, fatty acid metabolism, geraniol degredation, and gluconeogenesis, whereas isolates 392 and 463 did not (Fig. 2-13). Increased PER unique to isolate 393 included: serine protein kinase (Prk); transcription regulator (Trh5); TRK potassium uptake system protein (VNG1924G); and phytoene dehydrogenase (VNG1755G).

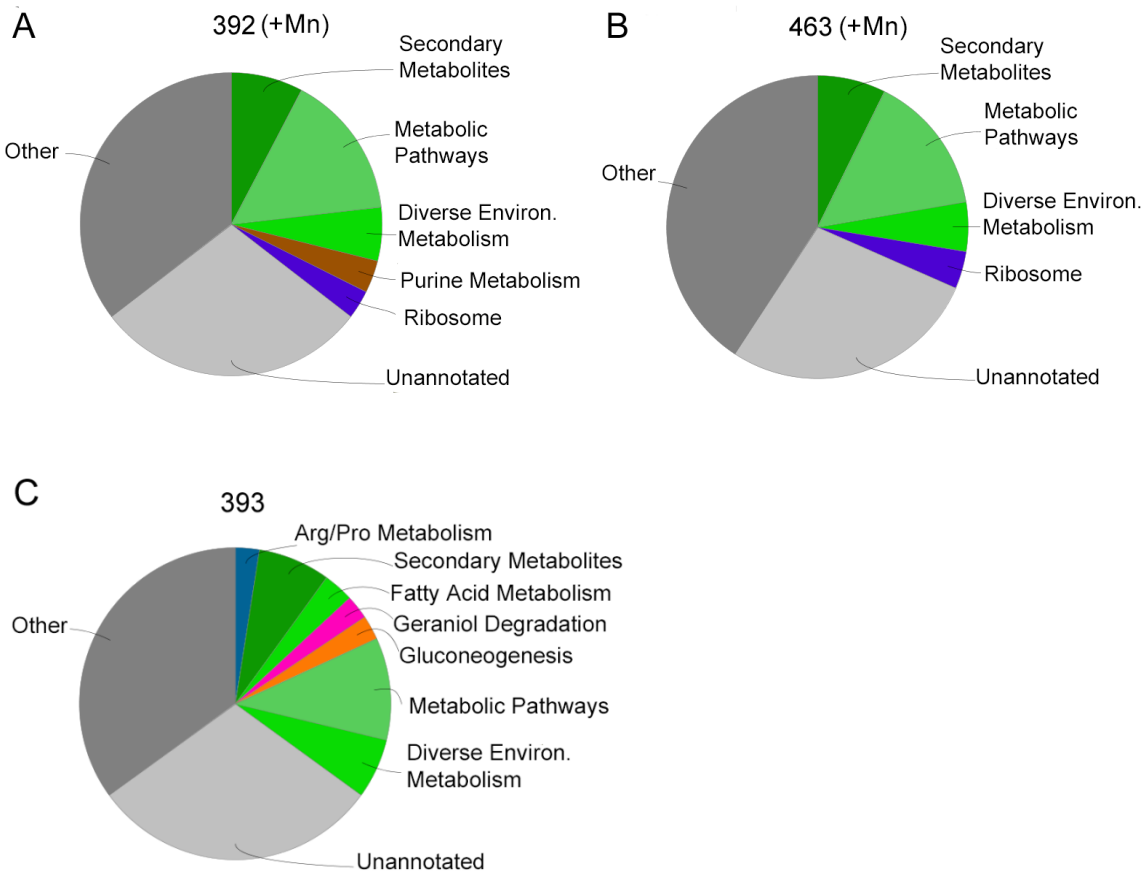

Figure 2-13. KEGG pathways associated with increased protein expression ratios for (A) Isolate 463, (B) Isolate 392, and (C) Isolate 393. Isolates 392 and 463 have increased Mn accumulation.

Discussion

To investigate the metabolic routes contributing to IR resistance, we selected for super-resistant (IR^+) isolates of *H. salinarum* after subjecting founder strains to successive rounds of high-level IR exposure followed by recovery (directed evolution). The selection of IR^+ isolates through directed evolution has been successful previously with *E. coli*, *S. typhimurium* LT2, and *H. salinarum* [89-91]. DeVeaux *et al* isolated 2 strains of IR^+ *H. salinarum* after 4 successive rounds of high-level IR (D_{10} = ~12 kGy), which

were 2 times more resistant than that of the wild-type (D_{10} = 5kGy) [89]. Here we have selected for IR^+ isolates of *H. salinarum* that are 3 times more IR-resistant than the wild-type after 6 or 9 rounds high-level IR exposure.

In Vitro Protection and Small Molecule Accumulation in IR^+ Isolate UFs

We prepared ultrafiltrates (UFs) from our IR^+ isolates and found a 1.6- to 2-fold increase in radioprotection from all 3 UFs when compared to the founder strain (F3 UF) (Fig. 2-5). We attribute the increased protection observed in the 392 UF to increased concentrations of Mn, PO_4 and glycine when compared to the founder UF (Fig. 2-6). The dramatic increase of glycine in the 392 UF eclipsed all other small molecules measured in the UFs, which may be the result of a metabolic pathway modification. Interestingly, the 393 UF did not have increased concentrations of any small molecules analyzed, but we did see increased radioprotection from its UF. This indicated that there might be other small organic metabolites accumulated in the UF with radioprotection properties, but due to the high salt content of these UFs (4 M), traditional biochemical analyses proved to be difficult. UF of *H. salinarum* and *D. radiodurans* were enriched with Mn, PO_4 and amino acids and peptides when compared to IR-sensitive microorganisms, and these UFs protected enzyme activity to higher doses of IR than the UFs of IR-sensitive strains *in vitro* [11, 14]. The increase of Mn is likely the cause of the enhanced the radioprotection conferred by the 463 UF. We conclude that increases in Mn in the 463 UF, and Mn, PO_4 and free amino acids in the 392 UF confer more protein protection from IR *in vitro*.

Proteomic Analysis of Protein Expression in IR^+ Isolates Compared to the Founder

Using proteomic analysis, we attempted to elucidate the metabolic pathways contributing to the IR^+ phenotype of these isolates. Our proteomic analysis compared the protein abundances of the IR^+ isolates to the *H. salinarum* founder strain (F3) and found a large number of proteins differentially expressed, potentially contributing to the increase IR^+ tolerance of the isolates. We chose this proteomic approach to avoid complications presented from variation in transcript abundances according to gene and temporal shift, as previously reported for *H. salinarum* IR response systems [27].

The iTRAQ analysis identified 1,279 proteins, a 48% coverage of the predicted *H. salinarum* proteome, which fell within the range of previous iTraq studies (39% - 63%) [27, 100]. The physical characteristics (molecular weight, isoelectric point) and metabolic classification of the proteins identified in our iTRAQ dataset were similar to the predicted proteome, indicating little bias in our analysis for most protein function categories except for membrane and transport proteins, which is likely an artifact of the protein extraction method used, or the loss of lysine and arginine residues from the tryptic digest. Given the multitude of differentially expressed proteins in our dataset, we chose cutoffs of > 1.5 and < 0.4 to be significant, which corresponded to a 6% false discovery rate (FDR). For protein expression ratios (PER) to be considered increased, the average of the 4 ratios (two replicates of the IR^+ isolate, two replicates of the founder) must > 1.8. For PER to be considered decreased, its average was < 0.4.

Overall, the IR^+ isolates had far less decreased PER than increased PER. This is a limitation of the iTraq analysis, as proteins absent, or with expression levels below the limit of detection, in the IR^+ isolates were not represented in the MS analysis. The majority of the decreased PER were gas vesicle proteins. Gas vesicles are protein complexes that accumulate gases through the hydrophobic exclusion of water, providing buoyancy to the cell [101]. In *H. salinarum* these proteins are expressed from two gene clusters containing 14 genes [102]. GvpC is a structural protein, and GvpO is regulatory transcription protein for one of the gene clusters [101]. All three isolates had decreased PER for the GvpC and GvpO proteins, indicating a disruption in gas vesicle formation. We observed the gas vesicle-deficient phenotype in the IR^+ isolates, and this provided some experimental validation of the iTraq analysis. One of the 2 IR^+ isolates selected by DeVeaux *et al* was also gas vesicle-deficient [89]. Ten of the 14 *gvp* genes are essential for gas vesicle formation; a mutation in any 1 of these 10 renders the cell gas vesicle-deficient, presenting an easy target under high-level IR [101]. The wild-type *H. salinarum* has a moderate frequency of spontaneous loss of this function (1%) [103]. Despite this frequency, we concluded that the loss of gas vesicle function itself did not increase IR resistance (Fig. 1 in Appendix C).

Increased Expression of RPA Proteins in IR^+ Isolates

Of the 537 increased PER among the 3 isolates, only 29 proteins were found to be common among the 3 IR^+ isolates. Two of these proteins were Rfa3 and Rfa8, which are single-stranded DNA binding proteins, also called Replication factor A (RFA), and are homologs to Replication protein A (RPA) in eukaryotes. These proteins are essential for

many aspects of DNA metabolism including replication, repair and recombination [104]. The *rfa3* and *rfa8* genes are part of an operon in *H. salinarum* that encodes for *rfa3, rfa8* and *ral*, but only Rfa3 and Rfa8 proteins had increased PER. Genetic studies of the *rfa3* and *rfa8* homologs in a closely-related halophilic archaeon determined these proteins are not involved with the repair of pryrimidine dimers or single-strand breaks caused by UV or mitomycin C exposure [105]. Given the increased expression of the Rfa3 and Rfa8 proteins in our IR^+ isolates, we propose that these proteins may be used to stabilize single-stranded DNA during homologous recombination (HR). DNA double-strand breaks (DSBs) increase with respect to dose of IR, and the crucial maintenance of genome integrity is facilitated by HR [15, 35]. The high steady-state expression of these proteins (Rfa3 and Rfa8) in the IR^+ isolates provide stability to single-strand DNA for efficient HR, and increases of these proteins have been observed in other studies of *H. salinarum*'s IR and UVC resistance. In wild-type *H. salinarum* the *rfa3* and *rfa8* genes were induced in response to UVC light [92]; and both genes were found to be up-regulated in the early response to IR [27]. In the whole-genome transcriptome analysis of two IR^+ *H. salinarum* isolates, the *rfa3* and *rfa8* genes were up-regulated 3.2-fold and 1.9-fold, respectively [89]. We are currently investigating if the increased expression of these proteins is ubiquitous among the other IR^+ isolates in our collection.

Increased Expression of Stationary Phase-Associated Proteins in IR^+ Isolates

We looked for global trends among the 537 increased PER across all 3 IR^+ isolates. While the proteins for our iTraq dataset were harvested from cells in the mid-exponential phase of growth, we found that 98 (18%) of the increased PER were proteins typically

associated with stationary phase, such as peptidases and universal stress response proteins. Other stationary phase-associated increased PER for all 3 isolates included: GapB, the ArgK-type transport ATPase (VNG0674); the oxidoreductase YusZ1; Sod2; threonine synthase; and Rfa8. The two isolates 392 and 463 had 17% and 18% of their increased PER associated with stationary phase proteins, respectively, and isolate 393 had the highest percentage of stationary phase-associated PER, which was 33%, despite the proteins extracted for iTraq quantification came from cells grown in exponential phase. While isolate 393 had the high percentage of stationary phase-associated PER, the other two isolates had more PER associated with stationary phase due to the overall increased PER in these isolates.

Stationary phase-associated PER unique to isolate 393 included: a serine protein kinase (VNG0749); a phytoene dehydrogenase (VNG1755); transcription regulator Trh5; a TRK potassium uptake system protein (VNG1924); and two hypothetical proteins VNG1063 and VNG1746. A large scale study of *H. salinarum* determined that approximately 33% of its genes increased expression as the culture transitioned to stationary phase, indicating genes possibly related to the stresses associated with nutrient depletion and increased oxidation of cellular constituents, as the cell shifts focus from reproduction and growth to stress maintenance and repair [106, 107]. The high steady-state expression of proteins normally reserved for stress conditions contributed to the IR^+ resistance in the 3 isolates, particularly isolate 393 by having stress response proteins readily available in the cell to neutralize oxidative stress.

Effects of Mn Accumulation on Cellular Metabolism Pathways

Both isolates 392 and 463 had accumulated significantly more Mn in their UFs than the founder (F3 UF) (Fig. 2-6), and the effect of Mn on the cellular processes and energy metabolism may contribute greatly to the IR resistance observed in these isolates, above and beyond its ROS scavenging capabilities. Both the 392 and 463 isolates had increased PER associated with energy metabolism, cellular processes, cofactor biosynthesis, and translation/ protein synthesis.

The majority of the proteins for translation/ protein synthesis are ribosomal proteins, which facilitates the synthesis of the many of enzymes required to meet the demands of the increased rate of energy metabolism. While the accumulation of antioxidant Mn-complexes can confer radioprotection to the cell, it has also been reported that the amount and diversity of Mn-dependent enzymes may be far greater than originally thought [108]. In both 392 and 463 isolates we found an increase in PER related to enzymes involved in central metabolism (*e.g.*, peptidases, phosphatases and phosphoglycerate mutase) (Table 2 in Appendix B), which can be stimulated or activated by the accumulation of Mn [108, 109]. As *H. salinarum* does not use sugars for its carbon source, the increase of peptidases facilitates the breakdown of peptides to amino acids for energy conversion [110]. The stimulation of the central metabolism would allow for increased production of reducing equivalents, which would be depleted under the oxidative stress inflicted by IR. In particular, 392 had dramatic increases in 3 proteins in the NAD synthesis pathway, NadA, NadB and NadC; average protein ratios of 5.0, 6.9 and 3.2, respectively, which

were among the highest ratios reported for this isolate. Studies of *H. salinarum* have previously outlined its voracious metabolism, which ferments arginine simultaneously with respiration of amino acids (including essential amino acids leucine, lysine, isoleucine, methionine and valine) in addition to the energy the organisms derives from light [110]. Additionally, many of the proteins involved in oxidative phosphorylation were increased in isolate 463 (Table 2-1).

Concerning Mn transport, the ABC transporter proteins primarily associated with Mn transport in *H. salinarum* (ZurA, ZurM and YcdH) were not present in our iTraq data. However, there are several other transport proteins significantly increased among the 392 and 463 isolates, including a hypothetical K^+ transporter that binds Mn (VNG0983) (Table 7 in Appendix B). The ABC transporter is regulated by SirR, which has a global effect on several other genes (~90), but the expression of this protein was not found to be significantly increased among the 3 IR^+ isolates. [86, 111]. Mn accumulation can affect gene regulation, including genes not related to its own transport, and in some cases Mn regulation is part of a larger global response system within the cell [112, 113]. In yeast, regulation of Mn accumulation and transport is part of nutrient and stress sensing complexes: two transcription factors (Gis1p and Msn2/Msn4p) downstream of a serine/threonine kinase (Rim15p) typically regulate a large set of genes in a cooperative manner [114]. However, with respect to Mn, loss of Gis1p increased the Mn antioxidant capabilities in yeast cells, while the loss of Msn2/Msn4p decreased Mn antioxidant activity [112]. Additionally, Rim15p (and its downstream transcription factors) is negatively regulated by a phosphate-sensing complex (Pho80p/Pho85p) and a nitrogen-

sensing protein (Sch9p), indicating that Mn regulation may play a large role in cell homeostasis and central metabolism. [112]. We conclude that not only the increased concentration of Mn can directly aid in ROS scavenging, but also Mn-stimulated metabolism contributes to the IR resistance in isolates 392 and 463.

Chapter 3: Radioprotection by Compatible Solutes and Mn^{2+} in Thermophilic Bacteria and Archaea

Introduction

Thermophilic bacteria and archaea inhabit diverse environments and can survive multiple stresses including desiccation, radiation, pressure and pH extremes together with high temperature [1, 55, 56]. In studying the mechanisms underlying their survival under extreme conditions, we gain insight into the diversity of their defense strategies and the prospect of harnessing those capabilities for practical purposes [6]. It has long been recognized that desiccation tolerance and extreme ionizing radiation (IR) resistance are closely linked [17, 18]. Cellular desiccation generates reactive oxygen species (ROS) by endogenous processes, which damage proteins and DNA in a manner that is analogous to oxidative damage caused by the radiolysis of water during exposure to γ-rays [18, 115]. Both conditions are highly oxidizing, producing hydroxyl radicals ($HO^{\bullet}$), superoxide ($O_2^{\bullet-}$) and hydrogen peroxide (H_2O_2), which cause DNA double strand breaks (DSBs) and base modifications, carbonylation of protein residues, protein cross-linking, and ultimately protein inactivation [19-21, 95]. Initially, it was believed that the DNA damage was the lethal radiation target [24]. However it was later shown that DNA in IR resistant bacteria was no less susceptible to radiation damage than in IR sensitive organisms [22]. Radiation research examined the role of protein oxidation in irradiated cells and found that IR resistant microorganisms had less protein damage after irradiation than IR sensitive microorganisms [39, 40, 48]. Thus, IR resistant organisms must be able to protect their proteins, while IR sensitive organisms cannot. If proteins are protected and remain functional, they can then repair DNA damage inflicted by IR [16].

Previous studies with the bacterium *Deinococcus radiodurans* and the halophilic archaeon *Halobacterium salinarum* NRC-1 suggested that the mutual nature of radiation and desiccation resistance resides in cytosolic Mn-dependent antioxidant processes that protect against oxidative damage [11, 14]. For example, in *H. salinarum* resistance to IR is not dependent on the major enzymes responsible for ROS detoxification (*e.g.*, superoxide dismutase and catalase), but rather, is built on the accumulation of manganous (Mn^{2+}) ions that form antioxidant complexes with peptides, orthophosphate, and other small molecules [11]. Similarly, highly efficient ROS-scavenging Mn^{2+} complexes have been identified in *D. radiodurans* [14]. These complexes were shown to protect protein activity *in vitro* [11, 14]. Additionally, Mn^{2+}-dipicolinic complexes are implicated in contributing to the myriad of stress resistance phenotypes of *Bacillus* spores, including IR, wet and dry heat [51], and cyanobacteria, which are extremely resistant to IR and desiccation, accumulate Mn^{2+} and mycosporine-like amino acids [53]. Generally, cellular accumulation of Mn^{2+} together with a variety of organic and inorganic ligands may be a widespread mechanism to surviving oxidative stress, and this may extend also to simple animals such as rotifers [40].

Thermophiles are distinguished by their ability to grow at or above, and survive temperatures exceeding 50°C [2], which demand that their macromolecules resist not only the thermal denaturing effects of heat, but also the attendant burden of elevated oxidative stress arising from physico-chemical and metabolic processes. Many thermophiles are also halotolerant [65, 116] and collectively, these organisms are characterized by the accumulation of amino acids, sugars, polyols, and derivatives thereof

(compatible solutes) [117]. Compatible solute accumulation is conventionally attributed to protecting cells from osmotic stress and heat shock, and have been shown to stabilize proteins *in vitro* [116, 118]. Mannosylglycerate (MG) is widely distributed among thermophiles and generally thermophiles will increase the cellular concentration of MG in response to salt stress [116]. Di-*myo*-inositol phosphate (DIP) is a compatible solute that is exclusively thermophilic and has not been found in mesophiles, and is accumulated in response to thermal stress [66, 116]. Both MG and DIP have been studied for their ability to protect proteins *in vitro* against thermal stress and freeze-drying [119-122].

Several thermophiles have been shown to be radiation resistant, including the thermophilic bacteria *Rubrobacter xylanophilus* and *Rubrobacter radiotolerans* [63, 123]. *R. radiotolerans* is more IR resistant (the IR dose at which 10% of the cells survive [D_{10}] is 12 kGy) than *R. xylanophilus* (D_{10} = 6 kGy) [62], and DNA related to these species has been isolated from the surfaces of historically important buildings in Austria and Germany, as well as deserts [63]. *R. radiotolerans* has not been investigated for compatible solutes, but *R. xylanophilus* has been shown to accumulate MG, DIP and trehalose [65]. MG and DIP concentrations increase approximately 2-fold due to salt or heat stress, respectively, whereas trehalose concentrations increase in response to both stressors [65]. Trehalose is not exclusive to thermophiles and is found in diverse organisms including bacteria, fungi and plants [67, 68]. *In vitro* studies have shown its protective effects against heat, desiccation, oxidation and freezing [69, 70].

Recently, several hyperthermophiles were tested for IR resistance, including *Archaeoglobus fulgidus* and *Methanocaldococcus jannaschii* (D_{10} = 1 kGy for both organisms) [55]. Other hyperthermophiles are even more radiation resistant, such as *P. furiosus* (D_{10} = 3 kGy) and *Thermococcus gammatolerans* (D_{10} = 6 kGy) [56, 57]. Beblo *et al* did not find a correlation between desiccation resistance and IR resistance in hyperthermophiles, but this is because many of the hyperthermophiles tested were obligate anaerobes, and any exposure to oxygen, let alone desiccation, is lethal [55]. It has been determined that the IR resistance of *P. furiosus* is not dependent on mechanisms protecting DNA from IR damage [25]. While *P. furiosus* shows 75% survival at 2.5 kGy, intact chromosomes could not be detected, and this hyperthermophile repaired its fragmented genome within 20 hrs after incubation in fresh media [56]. Whole genome transcript analysis of *P. furious* in response to IR and H_2O_2 showed that the enzymes involved in oxygen detoxification (superoxide reductase and peroxidases) are highly constitutively expressed, but there was an up-regulation in genes coding for proteins that sequester free iron within the cell, presumably to reduce further ROS production [73, 77]. The hyperthermophile *Thermococcus gammatolerans* (D_{10} = 6 kGy) was isolated from enriched samples collected from hydrothermal chimneys after exposure to 30 kGy of radiation, and is one of the most radiation-resistant archaea to date [57]. The anaerobic archaeon has an optimal growth temperature of 88°C, and in the presence of elemental sulfur (S°) is able to grow on complex organic compounds, peptides and amino acids [81]. Interestingly, its IR resistance is not dependent on growth phase, as seen with *D. radiodurans* or *H. salinarum*, but *T. gammatolerans* becomes less IR resistant when

irradiated minimal media consisting 20 amino acids and S° [22, 27, 124]. Its 2.0Mbp genome has been sequenced and has an average coding sequence similarity of 71.5% with *P. furiosus* [81]. While the genes have been found for the synthesis of the solutes MG and DIP, the actual detection of these compounds has not been confirmed for *T. gammatolerans* [125].

Compatible solutes have been shown to protect proteins from various stressors *in vitro*, and the concurrent accumulation of these compounds with increases of salt or heat stress indicate that these compounds aid in osmotic homeostasis and protein stability *in vivo*. In this study, we demonstrate that under aerobic conditions, compatible solutes accumulated by thermophilic prokaryotes confer IR resistance to enzymes *in vitro*, and that radioprotection is facilitated by the presence of Mn^{2+}. With regard to hyperthermophiles, the anaerobic environment contributes to their IR resistance, which was the most significant factor for protection of enzymes *in vitro*.

Materials and Methods

Culturing and Growth Conditions. *Rubrobacter radiotolerans* (DSMZ5868) and *Thermococcus gammatolerans* (DSMZ 15229) were obtained from the DSMZ. *Rubrobacter xylanophilus* (DSMZ 9941) was a gift from Dr. Gaidamakova. *Rubrobacter* spp. were grown in TM media (1g/L tryptone, 1g/L yeast extract, 0.7g/L $NaNO_3$, 0.1g/L Na_2HPO_4, 0.1g/L nitrilotriacetic acid, 0.1g/L $MgSO_4 \cdot 7H_2O$, 0.1g/L KNO_3, 60mg/L $CaSO_4 \cdot 2H_2O$, 8mg/L NaCl, 2.2mg/L $MnSO_4 \cdot H_2O$, 0.5mg/L $ZnSO_4 \cdot 7H_2O$, 0.5mg/L H_3BO_3, 25µg/L $CuSO_4 \cdot 5H2O$, 25µg/L $Na_2MoO_4 \cdot 2H_2O$, 46µg/L $CoCl_2 \cdot 6H_2O$, 10ml/L

0.17mM $FeCl_3$•$6H_2O$, final pH 8.2). Cultures were grown at 48°C for *R. radiotolerans,* and at 60°C for *R. xylanophilus,* with shaking at 220 rpm in a Gyromax 737 shaker (Amerex Instruments, Lafayette, CA). *Pyrococcus furiosus* strain (DSMZ 3638) was grown in the absence of sulfur with 100µM Na_2WO_4 and 0.5% (wt/vol) maltose in a medium we designated "Pf medium" containing 24g/L NaCl, 4g/L Na_2SO_4, 0.7g/L KCl, 0.2g/L $NaHCO_3$, 0.1g/L KBr, 0.03g/L H_3BO_3, 10.8g/L $MgCl_2$•$6H_2O$, 1.5/Lg $CaCl_2$•$2H_2O$, 0.025g/L $SrCl_2$•$6H_2O$, 0.08% Na_2S•$9H_2O$, 5g/L tryptone, 1g/L yeast extract, 1 ml/L resazurin (0.2 g l^{-1} solution), final pH = 6.8 in 100 ml serum bottles or 1L bottles at 95°C under anaerobic conditions [126]. *Thermococcus gammatolerans* was grown in ASW-YTP medium (38g/L NaCl, 14.5g/L $MgCl_2$•$6H_2O$, 5g/L tryptone, 5g/L yeast extract, 5g/L sodium pyruvate, 5.6g/L $MgSO_4$•$7H_2O$, 2.5g/L $CaCl_2$•$2H_2O$, 2.6g/L Na_2SO_4, 1g/L KCl, 80mg/L Na_2CO_3, 80mg/L NaBr, 64mg/L KBr, 58mg/L $SrCl_2$•$6H_2O$, 42g/L H_3BO_3, 8.1mg/L Na_2HPO_4, 2.4mg/L NaF, 0.4mg/L $NaSiO_4$, 50µg/L KI, 0.08% Na_2S•$9H_2O$, 1ml/L resazurin (0.2 g l^{-1} solution), final pH = 6.8) in 100ml serum bottles or 1L bottles under anaerobic conditions at 88°C.

Preparation of enzyme-free cell extracts. Cultures of *R. xylanophilus, R. radiotolerans*, *P. furiosus,* and *T. gammatolerans* were grown in appropriate media and conditions to 0.4 $OD660_{nm}$, cells were harvested by centrifugation 8,000 x *g* (10 min, 4°C). *Rubrobacter* spp. cells were washed twice with TM-BSS (TM media lacking tryptone and yeast extract, final pH 8.2); *P. furiosus* cells with Pf-BSS (Pf medium lacking carbon sources, tungsten, and Na2S•$9H_2O$, final pH 6.8), and *T. gammatolerans* cells with ASW-BSS (ASW-YTP medium lacking carbon sources and Na2S•$9H_2O$, final pH 6.8). Pellets were re-suspended in distilled and deionized water (ddH_2O, Sigma-Aldrich) and passed

through an Emulsiflex Homogenizer (Avestin, Inc., Ottawa, Canada) at 15,000 psi to lyse the cells. Cell extracts were then centrifuged at 12,000 x *g* (60 min, 4°C) and standardized by protein concentration, which was determined by the BioRad Bradford Assay (BioRad, Hercules, CA). The supernatant was further centrifuged at 190,000 x *g* (40 h, 4°C) and subjected to filtration using 3kDa centrifugal devices (Amicon ultracel 3k filters; Millipore, Billerca, MA). The resulting protein-free cell extracts, called ultrafiltrates (UF), were concentrated 5 times in a speed vacuum concentrator (Heto Vacuum Centrifuge; ATR, Laurel, MD) and stored at -20°C. The UF for H. salinarum was prepared as described in [11].

Enzyme Protection Assay. The restriction enzyme *Dde*I was added at a final concentration of 0.5 unit/µl to UFs diluted to 0.2x, to 25 mM phosphate buffer (P_iB), pH 7.0, to a 20 mM solution of trehalose, mannosylglycerate (MG), or di-*myo*-inositol phosphate (DIP), with or without the addition of 250 µM or 25 µM $MnCl_2$, and to distilled and deionized water (ddH_2O, Sigma-Aldrich). Residual storage buffer present in all irradiations contains: 5µM EDTA, 10 µg/ml BSA, 2.5% glycerol, 2.5 mM KCl, 0.5 mM Tris-HCl, 0.05 mM DTT. Assays performed under anaerobic conditions were purged with ultra-high purity Ar (99.999%) (ValleyNational Gases, Frederick, MD). The solutions were irradiated on ice using a ^{60}Co gamma source (Uniformed Services University of the Health Sciences, Bethesda, MD, dose rate = 3.2 kGy/hr) at the following doses: 0, 1, 2, 3, 4, and 5 kGy, or 0, 1, 2, 4, 6, 8, 10, and 12 kGy. Samples were kept on ice until digestion of 1 µg of pUC19 DNA using 1U of enzyme from each irradiated solution at 37°C for 1 h. The resulting pUC19 DNA fragments were separated

by electrophoresis on 1 % agarose TBE gels and visualized with ethidium bromide staining.

Determination of Amino Acid Concentration. Free and total amino acid concentrations in the UFs of *R. xylanophilus, R. radiotolerans, P. furiosus,* and *T. gammatolerans* were determined using the ninhydrin assay [97]. Briefly, tryptophan standard solutions were prepared at concentrations from 0 to 200 nmol tryptophan. Ninhydrin reagent was added to the UFs and to the standards and boiled for 20 min. Isopropynol was added to 30% final concentration and the absorbance was read at 570 nm. A standard curve was constructed based on tryptophan standards to determine free amino acid concentration in the UFs. Determination of total amino acid concentration was performed with an acid hydrolysis before assaying free amine concentration with the ninhydrin assay. The UFs were diluted 1:10 in 6 N HCl, flushed with nitrogen, and incubated at 100^{o}C for 24 hr. Ninhydrin reagent was added to the resulting digestions and amino acid concentrations were measured as described above.

ICP-MS and Ion Chromatography. Mn, Fe, and PO_4 concentration in *R. xylanophilus, R. radiotolerans, P. furiosus,* and *T. gammatolerans* UFs and cells (Mn, Fe) were determined using ICP-MS (Mn, Fe) and Ion chromatography (PO_4) at the Division of Environmental Health Engineering, JHU School of Public Health. For ICP-MS analysis, 50 µl of UF was transferred to a pre-cleaned 15 ml polystyrene tube and diluted to a final volume of 1.5 ml with 1 % HNO_3 + 0.5 % 1N HCl. Cells were prepared by adding 1.5 ml of concentrated HNO_3 to a pellet of 10^9 cells, vortexing, and diluting 50 µl of the digest into 4.95 ml of H_2O, yielding a 1% final concentration of HNO_3. Internal standards (Mn or Fe) were added to each sample to monitor for sample matrix effects of the

plasma. Analysis was performed with an Agilent 7500ce Induced Coupled Plasma-Mass Spectrometer (Agilent Technologies, Santa Rosa, CA). A standard calibration curve was generated from multi-element standards (Elements INC, Shasta Lake, CA) at the following concentrations: 0, 1, 5, 10, 50, 100, 500, 1000 µg/L. Reported sample concentrations of Mn and Fe were blank and dilution corrected. SRM 1643e (NIST, Gaithersburg, MD) was used to test the accuracy of sample preparation, and was prepared in the same manner as the samples. For ion chromatography analysis, 25µl of UF was transferred into a pre-cleaned Dionex IC vial (Dionex Corp, Sunnyvale, CA), MilliQ water was added up to 1.5 mL final volume, and the sample was vortexed to ensure thorough mixing. Analysis was performed using a Dionex DX600 Ion Chromatograph (Dionex Corp, Sunnyvale, CA). A standard calibration curve was generated from a multi-anion solution (Elements INC, Shasta Lake, CA) containing the anion of interest (PO_4). Concentrations of the calibration curve were as follows: 0, 1, 2, 4, 6, 12, 16, 20 µg/ml. Samples were run on an IonPac AS14A Anion exchange column (4 x 250 mm; Dionex Corp, Sunnyvale, CA) and AS14A Guard column (3 x 150 mm, Dionex Corp, Sunnyvale, CA) column using 1.08 mM Na_2CO_3 and 1.02 mM $NaHCO_3$ as eluent. Samples were suppressed using an ASRS 4 mm suppressor (Dionex Corp, Sunnyvale, CA) with a current of 100 mA. Samples were eluted for 30 min to ensure complete anion exchange. Anion retention times (+/-5%) were determined based upon the certificate of analysis for the column. Sample concentrations of PO_4 were reported as the average of the two replicates after blank and dilution correction.

Preparation of Ethanol Extracts. Cells were harvested and washed with BSS. Pellets of 10^9 cells were re-suspended in 80% ethanol before broken via French press. Cell

lysates underwent centrifugation at 10,000 x *g* (50 min, 4°C) to remove cell debris. Cells and ethanol were on ice throughout the process. The solvent was removed by speed vacuum concentrator (Heto Vacuum Centrifuge, ATR, Laurel, MD), and the residue was re-suspended in ultra-pure water (ddH_2O, Sigma-Aldrich), before filtration through a 10kDa filter (Amicon ultracel 10k filters; Millipore, Billerca, MA). Matching cell pellets of 10^9 cells were re-suspended in distilled and deionized water (ddH_2O, Sigma-Aldrich) before lysis by French press and centrifugation. The protein contents of the cells were determined by the BioRad Bradford Assay (Hercules, CA).

High-Performance Anion-Exchange Chromatography. High-performance anion-exchange chromatography (HPAEC) was carried out on Dionex DX 500 with a CarboPac PA-10 column and a PA-10 guard column (Dionex, Sunnyvale, CA) and pulsed amperometric detection (PAD). An aliquot of the ethanol extract was diluted 10- to 100-fold and injected into a CarboPac PA-1 column equilibrated 16mM sodium hydroxide. Elution was performed with a linear gradient from 16mM sodium hydroxide to 0.5M sodium acetate/0.1M sodium hydroxide. Standards of 0.25, 0.5, 1, 2, and 4nmol of trehalose, MG, and DIP were run for quantification. Mannosylglycerate (MG) and di-*myo*-inositol phosphate (DIP) were obtained from Bitop AG, Witten, Germany.

Results

Composition Analysis of Ultrafiltrates. Protein-free cell extracts (ultrafiltrates; UFs) of IR-resistant bacteria and archaea were found to be enriched in Mn^{2+} and small organic molecules that included amino acids and peptides [11, 14]. When combined *in vitro* at physiologically-relevant concentrations, these constituents formed potent antioxidant

complexes in orthophosphate buffer (P_iB) [11, 14]. To determine the potential role of Mn and compatible solutes in the radiation resistance of thermophiles, we prepared UFs for *R. xylanophilus, R. radiotolerans, P. furiosus,* and *T. gammatolerans* and measured the concentrations of metal ions, phosphates, and compatible solutes in their UFs and in whole cells (Tables 3-1 and 3-2). UFs for the IR-resistant *Rubrobacter* species were enriched in Mn relative to that of IR-sensitive bacteria, yielding high Mn/Fe ratios similar to those found in *H. salinarum* (Table 3-1). The concentrations of Mn found in the UFs of the anaerobic archaea *T. gammatolerans* and *P. furiosus* were more than an order of magnitude lower than the values for the *Rubrobacter* species UFs, resulting in Mn/Fe ratios similar to that of the radiation sensitive bacteria *E. coli* and *P. putida* (Table 3-1). The Mn/Fe ratios in whole cells followed the trend observed with the analysis of Mn/Fe ratios in the UFs (Table 3-1).

R. radiotolerans and *R. xylanophilus* UFs both contained high amounts of trehalose with 29mM and 17mM, respectively. We found more mannosylglycerate (MG) in *R. xylanophilus* UF (99 mM) than in the UF of *R. radiotolerans* (64 mM), whereas only the *R. xylanophilus* UF contained di-*myo*-inositol phosphate (DIP) (33 mM) (Table 3-2). In contrast to data reported for *D. radiodurans,* the amino acid and peptide concentrations were not significantly elevated in the *Rubrobacter* species UFs or that of *P. furiosus*, whereas *T. gammatolerans* UF had significantly high free amino acid concentrations (Tables 3-1 and 3-2). *P. furiosus* accumulated 52 mM of MG and 6 mM of DIP, which was significantly more than the concentrations found in the *T. gammatolerans* UF (Table 3-2). Thus, the UFs of aerobic and anaerobic thermophiles reported here all accumulated

some type of small organic molecules (Tables 3-1 and 3-2) but only the aerobic thermophile UFs, *R. radiotolerans* and *R. xylanophilus*, accumulated significant amounts of Mn^{2+}. We used high-performance anion-exchange chromatography (HPAEC) to quantify the compatible solutes in the UFs. To estimate intracellular concentrations of the compatible solutes in the thermophiles, we analyzed ethanol extracts using HPAEC (Table 3-2, Table 1 in Appendix D). Previous analyses of these compatible solutes were done by NMR, but our HPAEC method yielded similar results [65, 66]. For instance, Martins and Santos calculated the concentration of MG in *P. furiosus* to be 0.25µmol/ mg protein [66]; using cells grown in similar growth conditions with respect to salinity and temperature, we calculated the concentration of MG to be 0.22 µmol/ mg protein. We also calculated the approximate cellular concentration of MG and DIP for *P. furiosus* and *T. gammatolerans*, using the cellular volume of 4.5 µl/ mg protein from previous literature [66]; for *P. furiosus*, MG and DIP concentrations were 49 mM and 10 mM, respectively; for *T. gammatolerans*, MG and DIP concentrations were 21 mM and 11 mM, respectively (Table 1 in Appendix D). The whole cell concentration of MG and DIP were similar to those found in the UFs (Table 3-2). For the *Rubrobacter* species, cellular concentrations were calculated using our experimentally determined estimate of 6.76 µl/ 10^9 cells; *R. xylanophilus* had concentrations of 27 mM trehalose, 54 mM MG, and 13 mM DIP; *R. radiotolerans* had concentrations of 20 mM trehalose and 28 mM MG (Table 1 in Appendix D). The *Rubrobacter* UFs have increased MG concentrations compared to whole cell concentrations (Table 1 in Appendix D), which may be due to the preparation and concentration the UFs. In the preparation of UFs, cell lysates are standardized to 17mg/ml protein concentration prior to ultracentrifugation, which allows

for comparison across different species [11]. The 17mg/ml protein concentration does not correlate with cellular concentration of the compatible solutes in the *Rubrobacter* species. To investigate the role of those small molecules in radiation resistance, we then tested the ability of the UFs, and of reconstituted preparations, to protect the activity of purified enzymes irradiated under aerobic or anaerobic conditions.

Table 3-1. Ultrafiltrates and whole cells concentrations of Mn and Fe.

			Conc. In:					
			Ultrafiltrates			Whole cells		
Organism	D_{10}[a] (kGy)	Genome (Mbp)	Mn (μM)	Fe (μM)	Mn/ Fe	Mn (ng/10^9 cells)	Fe (ng/10^9 cells)	Mn/Fe
P. putida[b]	0.1	6.2	0.9	6.1	0.1	18	1045	0.02
E. coli[b]	0.5	4.6	0.6	3.5	0.2	14	645	0.02
H. salinarum NRC-1[b]	5	2.6	87	8.9	9.8	155	818	0.19
R. xylanophilus	6	3.2	79	8.2	9.6	549	290	1.9
R. radiotolerans	10	3.4	211	18	11.8	300	340	0.88
P. furiosus	3	1.9	5.3	113	0.1	14	345	0.04
T. gammatolerans	6	2.1	6.3	15	0.4	3	235	0.01

[a] Dose at which viable cells are reduced to 10% of the population
[b] From [11]

Table 3-2. Ultrafiltrates and ethanol extracts concentrations for PO4, amino acids, and compatible solutes.

	Conc. In:								
	Ultrafiltrates (mM)						Ethanol extracts (µmol/mg protein)		
	Amino Acids								
Organism	Free	Total	PO_4	Trehalose	MG	DIP	Trehalose	MG	DIP
H. salinarum NRC-1 [a]	325	642	22	nd	nd	nd			
R. xylanophilus	87	115	10	17	99	33	1.5	3.0	0.7
R. radiotolerans	134	159	24	29	64	- [b]	1.7	2.4	nd
P. furiosus	15	35	5.4	nd	52	6	nd	0.2	0.04
T. gammatolerans	221	235	19	nd	10	2.3	nd	0.1	0.05

[a] From [11]
[b] Not detected
nd, not determined

Protection against IR by UFs and Compatible Solutes under Aerobic Conditions.

We tested the radioprotective properties of UFs prepared from *R. xylanophilus* and *R. radiotolerans* on the activity of *Dde*I, a restriction endonuclease (Fig. 3-1). *Dde*I is typically deactivated by less than 500 Gy of IR when incubated in 0.8M KCl during irradiation [11]. After irradiation, the residual activity of the enzyme was measured by its ability to cut plasmid DNA; the restriction fragments were analyzed by agarose gel electrophoresis. Under our experimental conditions, the *R. xylanophilus* and *R. radiotolerans* UFs displayed protection of *Dde*I activity at doses extending to 6 and 8 kGy, respectively, which was comparable to levels of protection conferred by *H. salinarum* UF (Fig. 3-1).

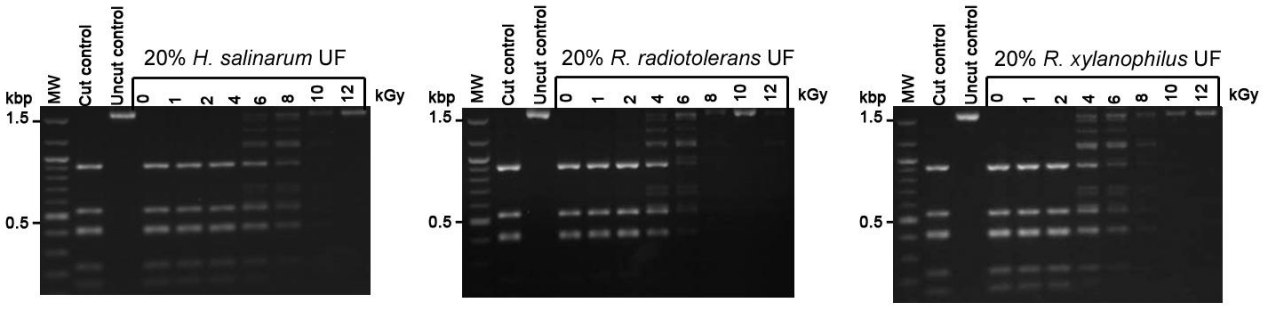

Figure 3-1. Protection of enzyme activity. The restriction enzyme *Dde*I was irradiated up to 12 kGy in enzyme-free cell extracts (UFs) of *H. salinarum*, *R. radiotolerans* and *R. xylanophilus* (diluted to 0.2x). Residual restriction enzyme activity was assayed by the digestion of pUC19 plasmid DNA; fragments were analyzed by agarose gel electrophoresis. The first lanes are molecular size ladders.

We next tested the ability of the compatible solutes we found in the UFs and the cells of both *Rubrobacter* species for their ability to protect enzyme activity against IR, at physiologically-relevant concentrations. While 20 mM trehalose protected enzyme activity to 2 kGy, this was comparable to the IR-resistance of *Dde*I in phosphate buffer (P_iB). When trehalose and P_iB were combined we saw a significant increase in the protection, up to 6 kGy (Fig. 3-2). The addition of 0.25 mM Mn (determined to be physiologically relevant from whole cell analysis) to trehalose conferred radioprotection to the *Dde*I enzyme to 6 kGy. However, when trehalose, phosphate and Mn were combined, the radioprotection increased dramatically to 12 kGy (Fig. 3-2). We established that P_iB alone or combined with 0.25mM Mn conferred protection of the DdeI enzyme up to 2 kGy (Fig. 3-3). After adding 25mM concentrations of MG, we could not detect any increase in radioprotection contributed by MG. In the case of DIP, the addition of 25 mM of this compound removed any detectible protection of enzyme activity (Fig. 3-3). It is important to note that these experiments were conducted with 2-kGy intervals of IR except for the 1 kGy dose (Fig. 3-2).

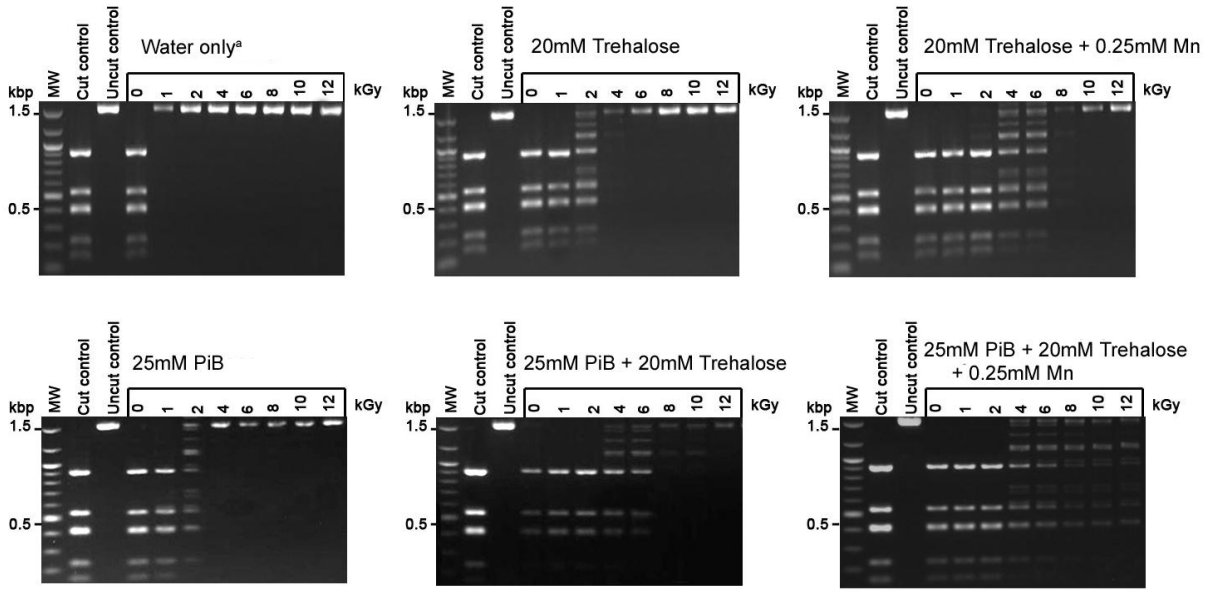

Figure 3-2. Protection of enzyme activity with trehalose, PO_4 and Mn^{2+} under aerobic conditions. The restriction enzyme *Dde*I was irradiated up to 12 kGy in water or 25 mM phosphate buffer (P_iB) with the addition of 20 mM trehalose or 20 mM trehalose + 0.25 mM Mn^{2+}. Residual restriction enzyme activity was assayed by the digestion of pUC19 plasmid DNA; fragments were analyzed by agarose gel electrophoresis. The first lanes are molecular size ladders. [a]Ultra pure water (ddH_2O, Sigma-Aldrich) was added prior to irradiation.

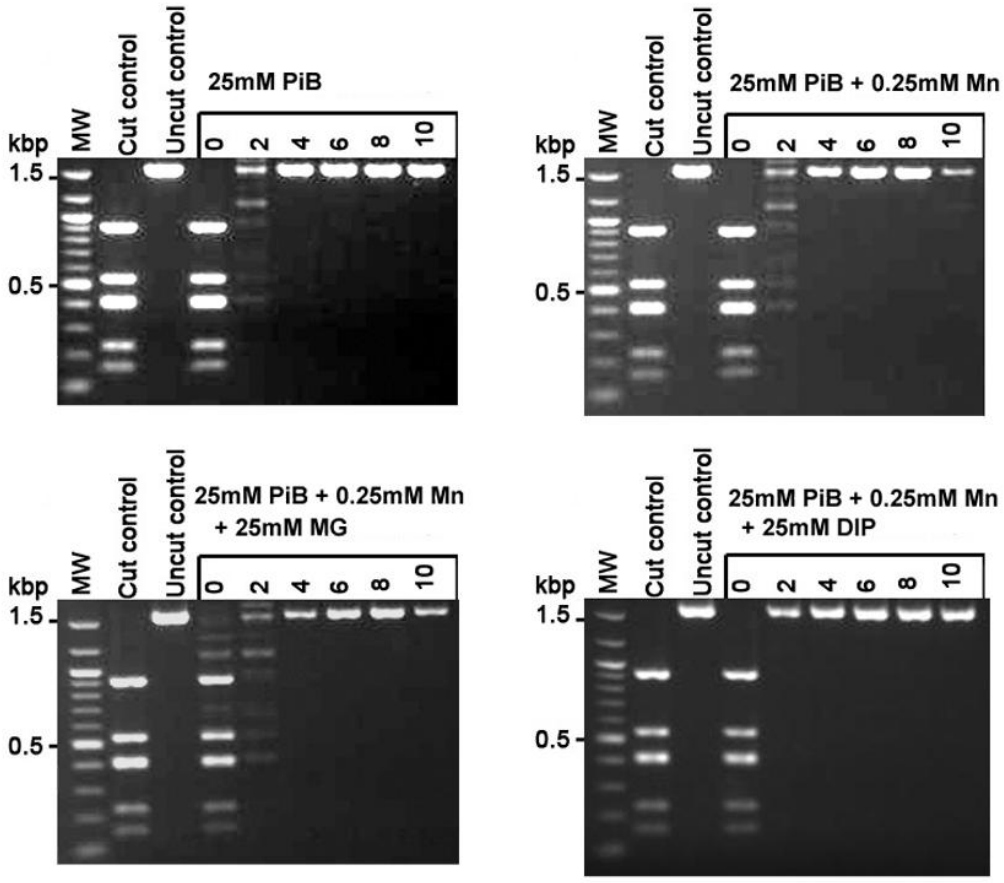

Figure 3-3. Protection of MG and DIP combined with PO_4 and Mn^{2+} under aerobic conditions. The restriction enzyme *Dde*I was irradiated up to 10 kGy in 25mM phosphate buffer (P_iB) with the addition of 0.25mM Mn. Residual restriction enzyme activity was assayed by the digestion of pUC19 plasmid DNA; fragments were analyzed by agarose gel electrophoresis. The first lanes are molecular size ladders.

Protection against IR by UFs and compatible solutes under anaerobic conditions.

In contrast to the *Rubrobacter* UFs, UFs of the anaerobes *P. furiosus* and *T. gammatolerans* did not protect *Dde*I at doses greater than 1 kGy under aerobic conditions (Fig. 3-4). To determine whether or not this lack of radioprotection was due to the presence of dioxygen (O_2), we tested their properties under anaerobic conditions (Fig. 3-4). In the absence of O_2, UFs of *P. furiosus* and *T. gammatolerans* protected *Dde*I up to 4 kGy, representing an increase of 3 kGy over aerobic conditions (Fig. 3-4). The addition of 0.025 mM Mn^{2+} to UFs of *P. furiosus* and *T. gammatolerans* provided a marginal increase of radioprotection, under both aerobic and anaerobic conditions. While this Mn concentration (0.025 mM) is physiological relevant for *P. furiosus* and *T. gammatolerans*, it is 10 to 100-fold less than the Mn concentration found in the cells of the aerobic radiation resistant *Rubrobacter* species (Table 3-1).

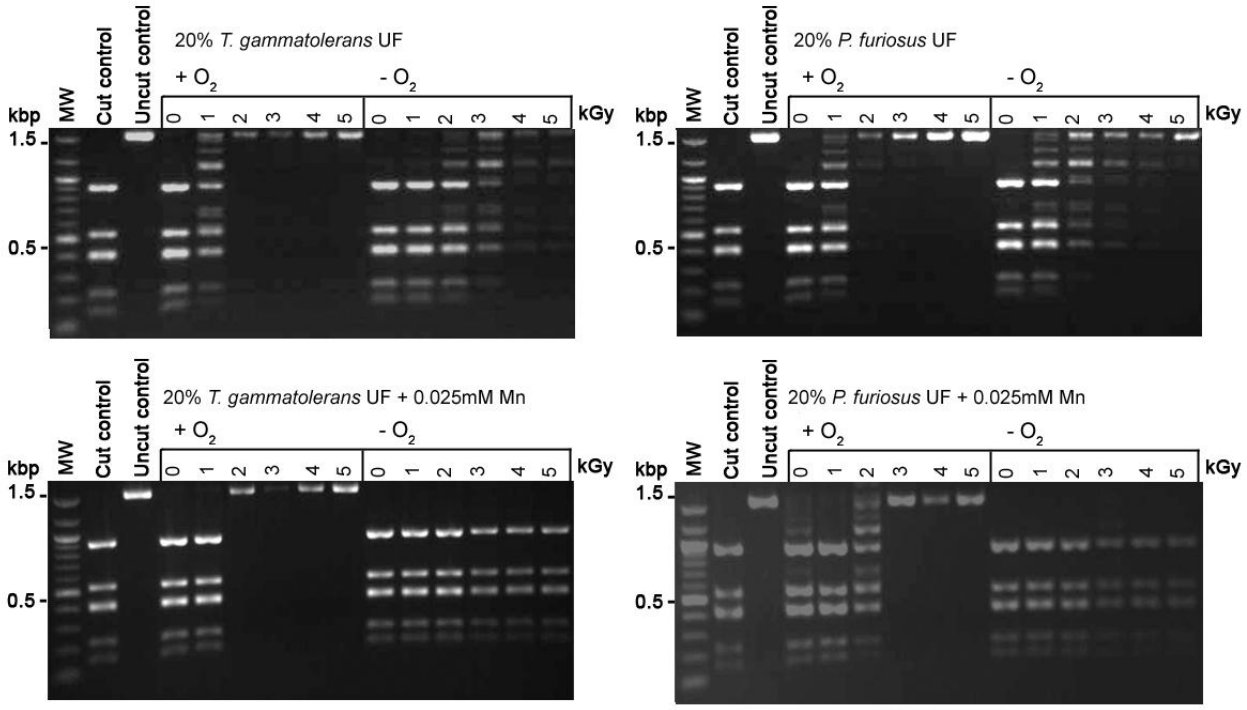

Figure 3-4. Protection of enzyme activity in aerobic and anaerobic conditions. The restriction enzyme *Dde*I was irradiated up to 5 kGy in the presence or absence of oxygen in enzyme-free UFs of *T. gammatolerans* and *P. furiosus* (diluted to 0.2x). Residual restriction enzyme activity was assayed by the digestion of pUC19 plasmid DNA; fragments were analyzed by agarose gel electrophoresis. The first lanes are molecular size ladders.

While the four thermophiles investigated here accumulated MG and DIP to various extents, we did not see significant protection of enzyme activity by these compatible solutes under aerobic conditions (Fig. 3-5); note that experiments in Fig. 3-5 were conducted with 1-kGy intervals of IR. In contrast, under the anaerobic conditions found in the intracellular milieu of *P. furiosus* and *T. gammatolerans*, MG protection of the *Dde*I enzyme was extended to 5 kGy. Protection of enzyme activity was also extended under anaerobic conditions whether the enzyme was irradiated in water, 0.025 mM Mn, MG with Mn, but not in the presence of 20 mM DIP alone. These experiments show that incubation of the enzyme under anaerobic conditions during irradiation was the single most effective condition for extending enzyme activity to higher doses of IR.

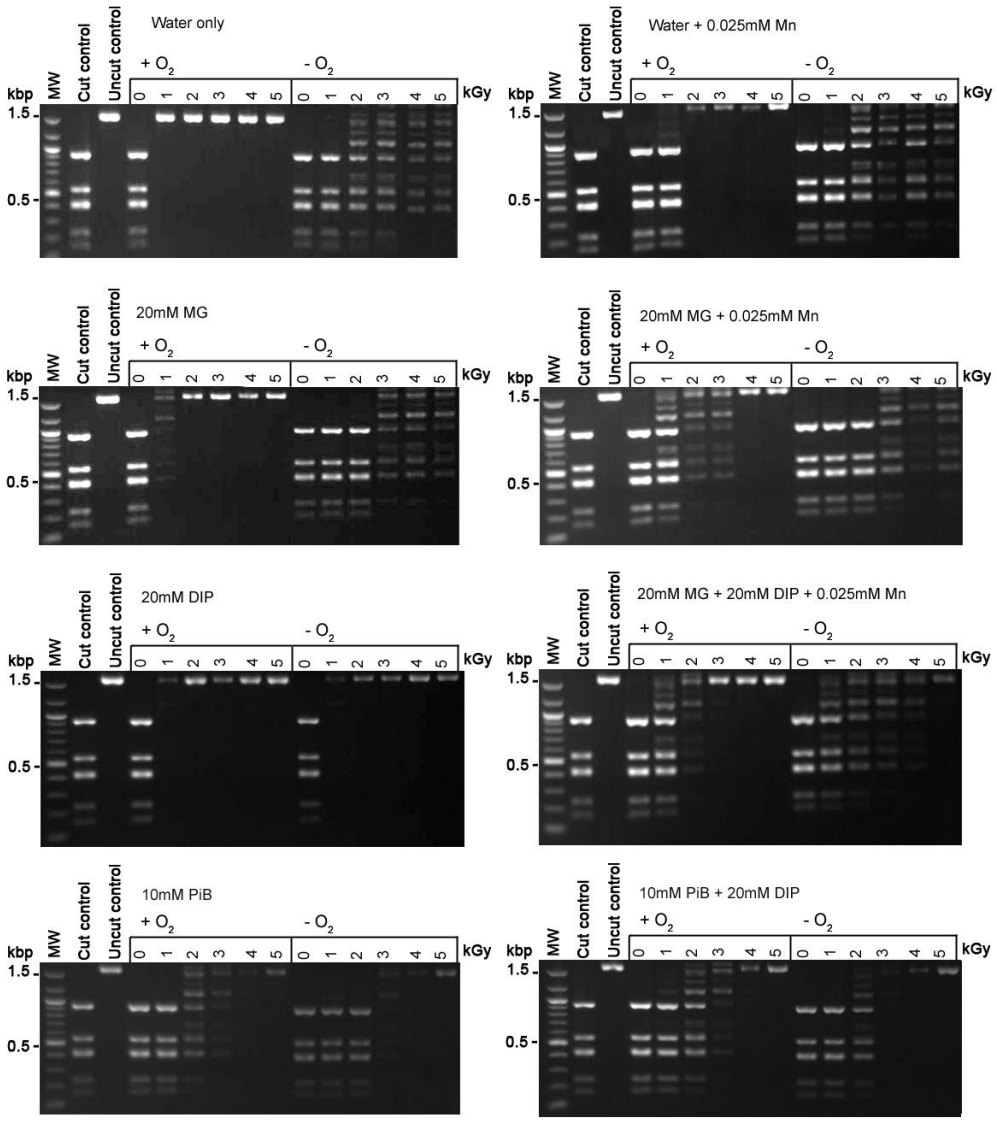

Figure 3-5. Protection of enzyme activity with compatible solutes. The restriction enzyme *Dde*I was irradiated up to 5 kGy in the presence or absence of oxygen, in water or with the addition of 20 mM MG, 20 mM MG and 0.025 mM Mn, 20 mM DIP, or 20 mM MG, 20 mM DIP and 0.025 mM Mn. The 20 mM solution of DIP had a pH of 9.5, thus 10 mM P_iB was added for a final pH of 7.5. Residual restriction enzyme activity was assayed by the digestion of pUC19 plasmid DNA; fragments were analyzed by agarose gel electrophoresis. The first lanes are molecular size ladders.

Discussion

Thermophiles are defined by their requirement for high temperatures, however within such groups there is an enormous diversity in the environments they inhabit and the metabolic capabilities they possess [6]. Here we investigated the radiation resistance of two groups of thermophiles that are phylogenetically and metabolically distinct. The bacteria *R. xylanophilus* and *R. radiotolerans* represent IR resistant thermophiles from aerobic environments, while the archaea *T. gammatolerans* and *P. furiosus* are IR resistant hyperthermophiles from anaerobic environments.

Radiation-resistant bacteria and archaea have high cellular Mn/Fe ratios, and this was confirmed for both *R. xylanophilus* and *R. radiotolerans* [11, 22]. Previous studies showed that Mn^{2+} boosts protein protection in cells by interacting synergistically with the pool of small-molecules, including P_i, and forming catalytic $O_2^{\bullet-}$- and H_2O_2-scavenging complexes [11, 16]. Both of the aerobic *Rubrobacter* species UFs were enriched in Mn and protected the enzyme activity of *Dde*I from similarly high doses of IR *in vitro* compared to the UF from the halophilic aerobe *H. salinarum*. This suggests that the cellular constituents present in the *Rubrobacter* spp. provide protein protection *in vivo*, as proposed for *H. salinarum*. While the *Rubrobacter* UFs did not contain high concentrations of amino acids, they were enriched in compatible solutes trehalose, MG and DIP.

The compatible solutes of thermophiles have been studied extensively for their protein-stabilizing properties and possible preservative applications in freeze-drying and

temperature tolerance [121]. A number of thermophiles are radiation-resistant, and herein we evaluated the possible antioxidant properties of these molecules with respect to radiation. Prior to this work, the compatible solutes present in *R. radiotolerans* had not been investigated. We found that this bacterium accumulated trehalose and mannosylglycerate (MG) to similar amounts as *R. xylanophilus*, but not di-*myo*-inositol phosphate (DIP) when grown at 48°C. DIP is associated mostly with hyperthermophiles (optimal growth temperature >80°C), and *R. radiotolerans* is considered moderately thermophilic with an optimal growth temperature of 48°C [62]. *R. xylanophilus* has an optimal growth temperature of 60°C, which is the lowest reported among organisms known to accumulate DIP [125]. As previously reported, *R. xylanophilus* accumulates trehalose, MG and DIP under its optimal growth conditions and increases the concentration of these compatible solutes in response to heat or osmotic stress [65]. We have determined that the *R. radiotolerans* also maintains basal millimolar cellular concentrations of trehalose and MG, representing organic solutes constitutively present in the cell, with potential for antioxidant properties.

Trehalose protected protein activity from radiation *in vitro* when combined with phosphate and Mn^{2+}. Trehalose is present in a wide variety of organisms including bacteria, yeast, fungi, plants and invertebrates, and we add IR to the list of stressors it has been shown to protect proteins from including heat, osmotic stress, desiccation and oxidation [67]. Additionally, strains of *Chroococcidiopsis*, a desiccation and IR-resistant cyanobacterium, have been shown to accumulate trehalose, though no connection was drawn between the accumulation of trehalose and IR resistance [127, 128]. Under aerobic

conditions, MG and DIP did not confer as much radioprotection to the *Dde*I enzyme as trehalose. Both MG and DIP are charged compatible solutes, while trehalose is neutral. Various sites of negative charge on the protein may repel the charge of MG or DIP, leaving an area susceptible to ROS attack.

Additionally, with respect to freeze-drying, the protection conveyed by MG can vary somewhat from protein to protein [120]. While both MG and DIP have previously been shown to be efficient scavengers of $HO^{\bullet}$, they do not appear to scavenge $O_2^{\bullet-}$ and H_2O_2 generated under the aerobic conditions in our *in vitro* assay [121]. We conclude that the majority of the radioprotection conferred by the *Rubrobacter* UFs is from the phosphate, trehalose and Mn present within the cells, which fits our current model of radiation resistance by the accumulation of small organic molecules and Mn^{2+}. While the *Rubrobacter* UFs do not have high concentrations of amino acids when compared to *H. salinarum*, the trehalose makes up for this deficit. This work is the first to determine trehalose protects proteins from IR.

In contrast to the aerobic thermophiles, the anaerobic hyperthermophiles *P. furiosus* and *T. gammatolerans* had Mn/Fe concentrations that were similar to radiation-sensitive microorganisms such as *E. coli* and *P. putida*. The low Mn/Fe ratios were attributed to the numerous proteins present in anaerobes that utilize Fe, such as dehydrogenases and ferredoxin, which *P. furiosus* uses as an electron carrier in place of NAD [129-131]. We suggest that high concentrations of Mn are critical for IR-resistance in aerobic organisms, as Mn^{2+}-dependent ROS scavenging is limited to $O_2^{\bullet-}$- and H_2O_2, formed predominantly

under aerobic irradiation conditions [132, 133]. In the presence of O_2, the formation of $O_2^{\bullet-}$ is a 1-step process in which a free electron (e^-) reacts with O_2 ($2.0E^{10}$ M^{-1} s^{-1}). This is much faster than in the absence of O_2, where the formation of $O_2^{\bullet-}$ is dependent upon concentrations of $HO^{\bullet}$ and H_2O_2 ($2.7E^7$ M^{-1} s^{-1}) [132]. In our *in vitro* protection assay, the *P. furiosus* and *T. gammatolerans* UFs and the compatible solutes display more protection in an anaerobic environment, which leads us to believe that part of the radiation resistance observed in *P. furiosus* and *T. gammatolerans* quite likely is attributed to the anaerobic environment itself.

P. furiosus, like most anaerobic hyperthermophiles, lacks the oxygen detoxification enzymes superoxide dismutase (SOD) and catalase which their aerobic counterparts use [78]. In their place, *P. furiosus* has a SOR (superoxide reductase), which is a non-heme iron-containing enzyme; instead of catalases, *P. furiosus* has several peroxidases [78] including rubrerythrin, alkyl hydroperoxide reductase I and II, and the aforementioned Fe-sequestering Dps-like protein [77-79]. A whole-genome mRNA microarray analysis of *P. furiosus* in response to radiation showed that SOR, rubrerythrin and both alkyl hydroperoxide reductases were constitutively expressed [73]; these results were also found in response to H_2O_2, though alkyl hydroperoxide reductase II expression was elevated [77]. The Dps-like protein was found to be elevated in response to both IR and H_2O_2, presumably to sequester Fe that could be released from damage to Fe-containing proteins under the oxidizing conditions [73, 77]. Genes in the SOR pathway were shown to be the most highly expressed in *P. furiosus* under normal anaerobic growth conditions, and to date any increased expression of SOR cannot be found in response to IR or H_2O_2,

indicating that this protein may be functioning at max capacity at all times [73, 77, 130]. Additionally, a variation of SOR-mediated $O_2^{\bullet-}$ detoxification was discovered in which SOR complexed with ferrocyanide reduces $O_2^{\bullet-}$ without the formation of H_2O_2, and this system was highly efficient, as the SOR iron site remains reduced, thus eliminating the requirement of oxidoreductases to recycle SOR [80].

While ROS detoxification enzymes have been shown to be dispensable for the aerobic archaeon *H. salinarum*, the intracellular Mn-complexes protect the cell from IR [11]. The highly constitutively expressed SOR and peroxidases play a part in removing ROS threats to the cell and maintaining the anaerobic cellular environment. As *P. furiosus* and *T. gammatolerans* lack high Mn/Fe ratios, we conclude that the anaerobic environment contributes to the IR resistance observed.

Chapter 4: Conclusions

The study of extremophiles and how they meet the physical and chemical challenges found in environmental extremes they inhabit lead to new insights on the mechanisms of stress response. Many extremophiles are found to be resistant to ionizing radiation (IR), and the dearth of environments characterized by high IR suggested that radiation resistance is a fortuitous consequence of a high tolerance to other environmental stressors (*e.g.*, desiccation). Given the diversity of IR-resistant extremophiles and their natural environments, we do not know if there are universal features of IR resistance, such as high intracellular concentration of Mn [11, 14].

The IR-resistance found in *Halobacterium salinarum* NRC-1 is attributed to high intracellular concentrations of salts and Mn^{2+}-complexes that protect proteins from oxidative damage [11, 87]. To further investigate possible metabolic routes contributing to the IR-resistance of *H. salinarum,* we used directed evolution to select for super IR resistance (IR^{+}) isolates and confirmed to have IR^{+} isolates that are 3 times more resistant than the wild-type, the most IR-resistant strains of *H. salinarum* reported to date [89]. We chose 3 isolates for biochemical characterization and proteomic analysis. The protein-free cell extracts (UFs) prepared from the IR^{+} isolates protected protein activity from IR *in vitro* to a dose higher than that of the founder UF, suggesting that the intracellular *milieu* of these isolates protected proteins *in vivo* more efficiently. Two of the IR^{+} isolates (392 and 463) had increased Mn concentrations in the UFs and thusly, the cell; one of these also had increased glycine and PO_4 concentrations (isolate 392). While the accumulation

of antioxidant Mn-complexes can confer radioprotection to the cell, enzymes involved in central metabolism (*e.g.*, peptidases and phosphatases) can be stimulated or activated by the accumulation of Mn [108, 109]. Proteomic analysis of these 2 IR^+ isolates found increased expression of proteins related to proteins involved in energy metabolism, cellular processes, cofactor biosynthesis, and translation/ protein synthesis when compared to the founder strain. The stimulated central metabolism allows for increased production of reducing equivalents, which would be depleted under the oxidative stress, as well as the production of energy required for repairing cellular damage inflicted by IR.

The role of this Mn-enhanced metabolism could be investigated through deletion mutants of putative Mn transporter genes *zurA*, *zurM*, and *ycdH*, or the Mn autorepressor *sirR* gene [86]. There may be other Mn transporters, as many transport proteins were increased in expression in the 392 and 463 isolates. The Mn accumulation of these mutants could provide more insight to the role Mn regulation may play in cell homeostasis and central metabolism, as well as its impact on IR resistance.

The 3rd IR^+ isolate (393) did not have increased concentrations of Mn, PO_4, or amino acids, but its UF had elevated radioprotection when compared to the founder UF. We conclude that there may be other small molecules UFs contributing to the enhanced radioprotection that we did not quantify. Additionally, the increased protein expression profile of this isolate was different from the Mn-enhanced isolates. For instance, increased expression of proteins related to cofactor biosynthesis were not as prevalent in this isolate as seen in the other 2 IR^+ isolates. In fact, isolate 393 had the fewest proteins

expressed more than the founder. However, of the increased protein expression, 33% of these proteins were associated with stationary phase processes, despite the proteins for the proteomic analysis were harvested in mid-exponential phase of growth. Proteins associated with stationary phase are often related stresses associated with nutrient depletion and increased oxidation of cellular constituents, as the cell shifts focus from reproduction and growth to stress maintenance and repair [106, 107]. Isolates 392 and 463 had 17-18% stationary phase-associated proteins that were increased in expression, but more stationary phase-associate proteins than isolate 393. We conclude that the increased expression of proteins normally reserved for stress conditions contributed to the IR^+ resistance in the 3 isolates.

One feature that was common between the 3 IR^+ isolates was the increased expression of Replication factor A (RFA) proteins, also known as single-strand DNA binding proteins in bacteria, or Replication protein A (RPA) in eukaryotes [104]. *H. salinarum* preserves the integrity of its genome and repairs double-strand breaks (DSBs) using homologous recombination [87]. We propose that the increased expression of these proteins provide stability to single-strand DNA for efficient HR, and the genes of these proteins are increased in expression in other studies of *H. salinarum*, implicating their contribution IR and UVC resistance [27, 88, 92]. This is the first study to confirm the increase of RPA proteins in IR resistance at the protein level. Further investigation of the other IR^+ isolates will confirm if this is a universal trend for high IR resistance.

The second focus of this work was to evaluate the IR resistance mechanisms in IR-resistant thermophiles to investigate the diversity or common methods they used to avoid IR damage.

While thermophiles are adapted to their high-temperature environments, they must also defend against other stressors, such as fluctuations in salinity and temperature. These microorganisms use compatible solutes such as trehalose, mannosylglycerate (MG), and di-*myo*-inositol phosphate (DIP), to maintain cell homeostasis and preserve protein stability [116, 121]. The aerobic *R. xylanophilus* and *R. radiotolerans* fit the current model of IR resistance through protein protection which is facilitated by Mn^{2+}-complexes found in the cytoplasm [11, 14]. The accumulation of Mn^{2+} in combination with other small molecules is key to scavenge the $O_2^{\bullet-}$ and H_2O_2 formed within the cell during irradiation under aerobic conditions, and we have shown that these organisms accumulate extremely high concentrations of Mn. These bacteria also benefit from the accumulation of trehalose, which protected enzyme activity *in vitro*, and this was synergistically increased by the addition of Mn.

In contrast, cell extracts of the anaerobic archaea *T. gammatolerans* and *P. furiosus* did not contain significant amounts of Mn, and were radioprotective of enzymes only under anaerobic conditions. The compatible solutes MG and DIP have previously been shown to scavenge $HO^{\bullet}$, but we are unable to detect any significant contribution to IR resistance from these compatible solutes [121]. We conclude that the anaerobic environment

contributes to the IR resistance observed in the hyperthermophiles *P. furiosus* and *T. gammatolerans*.

This work has shown that for aerobic IR-resistant microorganisms, Mn is universally essential, but there is diversity in the metabolic routes to Mn-mediated IR resistance. The IR^+ isolates of *H. salinarum* had varying but increased concentrations of small molecules, and different metabolic pathways were up-regulated in different isolates. Isolates 392 and 463 had Mn-stimulated central metabolism, but isolate 393 had increased proteins that varied greatly from the other two isolates. Our analysis of the compatible solutes of the thermophilic bacteria and archaea has shown that not all small molecules contribute to IR resistance equally, and that there is diversity of the small molecule accumulation with Mn (*e.g.*, amino acids in *H. salinarum*, trehalose in *R. xylanophilus* and *R. radiotolerans*). Our analysis of the anaerobic hyperthermophiles revealed that Mn is not universally accumulated in all IR-resistant organisms. The anaerobic environment and lifestyle protect against IR damage, providing evidence of an alternative route to IR resistance.

Appendix A –Detailed Materials & Methods

ICP-MS For ICP-MS analysis, 50 µl of UF was transferred to a pre-cleaned 15 ml polystyrene tube and diluted to a final volume of 1.5 ml with 1 % HNO_3 + 0.5 % 1N HCl. Cells were prepared by adding 1.5 ml of concentrated HNO_3 to a pellet of 10^9 cells, vortexing, and diluting 50 µl of the digest into 4.95 ml of H_2O, yielding a 1% final concentration of HNO_3. Internal standards (Mn or Fe) were added to each sample to monitor for sample matrix effects of the plasma. Analysis was performed with an Agilent 7500ce Induced Coupled Plasma-Mass Spectrometer (Agilent Technologies; Santa Rosa, CA). A standard calibration curve was generated from multi-element standards (Elements INC; Shasta Lake, CA) at the following concentrations: 0, 1, 5, 10, 50, 100, 500, 1000 µg/L. Reported sample concentrations of Mn and Fe were blank and dilution corrected. SRM 1643e (NIST; Gaithersburg, MD) was used to test the accuracy of sample preparation, and was prepared in the same manner as the samples. For ion chromatography analysis, 25µl of UF was transferred into a pre-cleaned Dionex IC vial (Dionex Corp; Sunnyvale, CA), MilliQ water was added up to 1.5 mL final volume, and the sample was vortexed to ensure thorough mixing. Analysis was performed using a Dionex DX600 Ion Chromatograph (Dionex Corp; Sunnyvale, CA). A standard calibration curve was generated from a multi-anion solution (Elements INC; Shasta Lake, CA) containing the anion of interest (PO_4). Concentrations of the calibration curve were as follows: 0, 1, 2, 4, 6, 12, 16, 20 µg/ml. Samples were run on an IonPac AS14A Anion exchange column (4 x 250 mm, Dionex Corp; Sunnyvale, CA) and AS14A Guard column (3 x 150 mm, Dionex Corp; Sunnyvale, CA) column using 1.08 mM Na_2CO_3 and 1.02 mM $NaHCO_3$ as eluent. Samples were suppressed using an ASRS 4 mm suppressor

(Dionex Corp; Sunnyvale, CA) with a current of 100 mA. Samples were eluted for 30 min to ensure complete anion exchange. Anion retention times (+/-5%) were determined based upon the certificate of analysis for the column. Sample concentrations of PO_4 were reported as the average of the two replicates after blank and dilution correction.

Amino Acid Analysis. The UFs underwent Fmoc-derivitization in parallel with a 17 standard amino acid mixture (Sigma-Aldrich, St. Louis, MO). In brief, 2 µl of sample or standard were added to 2 µl L-Norleucine and 6 µl water, diluted 10-fold in 0.1 M sodium bicarbonate-HCl buffer (pH 7.7). 100 µl of 10 mM acetonitrile Fmoc-Cl (Sigma-Aldrich, St. Louis, MO) was added, vortexed, and incubated at room temperature for 1 min. Excess Fmoc-OH was extracted with n-hexane (1 mL) 10 times. Aqueous layer was recovered and diluted 100-fold with 50 mM sodium acetate (pH 4.2). 10 µl was injected onto a YMC-Triart C18 column (1.9 µm, YMC Co., Ltd.) using a Nexera SIL-30AC with RF-20Axs fluorescence detector (Shimadzu Scientific Instruments, Columbia, MD) at 264nm. Eluent A: 4:1 mixture of 50 mM sodium acetate and acetonitrile; Eluent B: 1:10 mixture of 50 mM sodium acetate and acetonitrile. A concave gradient of 90% eluent A, 10% eluent B to 100% eluent B over 60 minutes was used. Flow rate 0.8 ml/ min.

Protein Extraction and Precipitation. For the founder, F3 and three IR^+ isolates, 392, 393, and 463, cultures were grown to mid exponential phase and cells were harvested. Two biological replicates were performed. The pellet was resuspended on ice in 1 M cold salt buffer (50 mM potassium phosphate pH 7.0, 1 M NaCl, 1% 2-mercaptoethanol) and subjected to three cycles of sonication for 30 s (Virsonic 100, Virtis, Gardiner, NY) followed by incubation on ice for 30 s. The cell lysate was then fractionated by centrifugation (8000 *g*, 30 min, 4°C), with the supernatant withdrawn and stored at -

20°C. Protein concentration was determined using Bio-Rad Bradford Assay (Hercules, CA) using the manufacturer's protocol. Aliquots containing 200 µg of protein were stored on ice and 8 volumes of -20°C TCA/acetone added. The mixture was vortexed briefly, incubated at -20°C for 4 hr, and then pelleted by centrifugation (16,000 x *g*, 10 min, 0°C) before discarding the supernatant and air-drying the pellet. To measure the yield of protein, another aliquot of 200 µg was subjected to the same protocol but instead of air-drying the pellet, the pellet was resuspended in in a volume of denaturing buffer (50 mM potassium phosphate pH 7.0, 1 M NaCl, 1% 2-mercaptoethanol, 6% sodium dodecyl sulfate) equal to the volume of the original aliquot, and protein concentration was determined with the Bradford Assay. To verify continuity between TCA and non-TCA treatments, denatured proteins from both TCA treated and non-TCA treated extracts were separated by denaturing acrylamide gel electrophoresis (SDS-PAGE) on a 4-20% gradient gel (15 µg protein per lane) at 150 V, 60 mA for 1.5 hrs. The gel was stained with Bio-Rad Flamingo™ stain and imaged with UVP BioDoc-IT™ Imaging System and Typhoon.

Protein Digestion, iTRAQ Labeling and Strong Cation Exchange Fractionation.

The TCA/acetone precipitated protein pellets were re-suspended in 20µL 500mM TEAB (triethyl ammonium bicarbonate) and 1µL 2% SDS. Each sample was reduced by adding 2µL 50 mM TCEP (tris-(2-carboxyethyl) phosphine) for 1 h at 60°C, alkylated by 1µL 200 mM MMTS (methyl methanethiosuphonate) for 15 min at room temperature, then digested at 37°C overnight with trypsin (Promega, sequencing grade, www.promega.com) using a 1:10 enzyme to protein ratio. Samples were labeled by adding 100 µL of an iTRAQ reagent (dissolved in isopropanol) and incubating at room

temperature for 2h. All samples were dried to a volume of approximately 30µL and subsequently mixed. The combined peptide sample was dissolved in 8 mL of SCX loading buffer (25% v/v acetonitrile, 10mM KH_2PO_4, pH 2.8 and subsequently fractionated by strong cation exchange (SCX) chromatography on an Agilent 1200 Capillary HPLC system using a PolySulfoethyl A column (2.1x100mm, 5µm, 300Å, PolyLC, polylc.com). The sample was loaded and washed isocratically with 25% v/v acetonitrile, 10mM KH_2PO_4, pH 2.8 for 40 min at 250µL/min. Peptides were eluted and collected in 1 min fractions using a 0-350mM KCl gradient in 25% v/v acetonitrile, 10mM KH_2PO_4, pH 2.8, over 40min at 250µL/min, monitoring elution at 214 nm. The SCX fractions were dried,resuspended in 200µL 0.05% TFA and desalted using an Oasis HLB uElution plate (Waters, www.waters.com).

LC-MS Analysis. Desalting peptides were loaded for 15 min at 750 nl/min directly on to a 75 µm x 10 cm column packed with Magic C18 (5 µm, 120Å, Michrom Bioresources, www.michrom.com). Peptides were eluted using using a 5-40% B (90% acetonitrile in 0.1% formic acid) gradient over 90 min at 300 nl/min. Eluting peptides were sprayed directly into an LTQ Orbitrap Velos mass spectrometer (ThermoScientific, www.thermo.com/orbitrap) through an 1 µm emitter tip (New Objective, www.newobjective.com) at 1.6 kV. Survey scans (full ms) were acquired from 350-1800 m/z with up to 10 peptide masses (precursor ions) individually isolated with a 1.2 Da window and fragmented (MS/MS) using a collision energy of 45 and 30 s dynamic exclusion. Precursor and the fragment ions were analyzed at 30,000 and 7,500 resolution, respectively

Data Analysis. The MS/MS spectra were extracted and searched against the GenBank database using Mascot (Matrix Science, www.matrixscience.com) through Proteome Discoverer software (v1.2, Thermo Scientific) specifying sample's species, trypsin as the enzyme allowing one missed cleavage, fixed cysteine methylthiolation and 8-plex-iTRAQ labeling of N-termini, and variable methionine oxidation and 8-plex-iTRAQ labeling of lysine and tyrosine. Peptide identifications from Mascot (Matrix Science) searches were processed within the Proteome Discoverer to identify peptides with a confidence threshold 1% False Discovery Rate (FDR), based on a concatenated decoy database search. A protein's ratio is the median ratio of all unique peptides identifying the protein at a 1% FDR.

Appendix B

Table1. IR^+/F3 avg, all proteins < 0.4 cutoff and > 100 A4 score

Functional Category	Locus	Description	392 avg	393 avg	463 avg
cellular processes	VNG0960G	FlaB1	0.4		
cellular processes	VNG7025	gas vesicle synthesis protein GvpA	0.1		0.1
cellular processes	VNG7026	gas vesicle protein GvpC	0.1	0.2	0.2
cellular processes	VNG7027	gas vesicle protein GvpN	0.2	0.4	0.2
cellular processes	VNG7028	gas vesicle protein GvpO	0.1	0.3	0.2
transcription and regula	VNG0726C	hypothetical protein VNG0726C		0.4	
transcription and regula	VNG7114	transcription factor	0.4		0.4
unknown	VNG6012H	hypothetical protein VNG6012H	0.2	0.3	
unknown	VNG6126H	hypothetical protein VNG6126H			0.3
unknown	VNG7029	chromosome partitioning protein SojB	0.2	0.4	0.2
unknown	VNG7030	hypothetical protein VNG7030	0.4	0.3	0.4
unknown	VNG7086	hypothetical protein VNG7086			0.3
unknown	VNG7102	hypothetical protein VNG7102			0.2
unknown	VNG7103	hypothetical protein VNG7103			0.3

Table 2. IR^+/F3 ratios for proteins > 1.5 cutoff and > 100 A4 score
Bolded proteins are associated with Stationary Phase

Functional categories	locus	Description	392 avg	463 avg	393 avg
Unclassified	VNG0043H	hypothetical VNG0043H	1.7	1.8	1.2
Cell envelope	VNG0046G	UDP-glucose dehydrogenase [Halobac	1.5	1.7	0.8
Nucleotide metabolism	VNG0047Gm	dTDP-glucose pyrophosphorylase [Hal	1.4	1.5	0.5
Cell envelope	VNG0051G	LPS biosynthesis [Halobacterium sp. N	1.6	1.7	0.5
Energy metabolism	VNG0063G	galE2; UDP-glucose 4-epimerase	1.3	1.5	1.2
Energy metabolism	VNG0065G	GDP-D-mannose dehydratase [Haloba	1.5	1.7	1.3
Cofactors and 2° Metabolite	VNG0081G	moaE; bifunctional molybdopterin-gua	1.3	1.5	1.1
Energy metabolism	**VNG0095G**	**gapB; glyceraldehyde-3-phospha**	**2.0**	**2.3**	**1.6**
Amino acid Metabolism	VNG0096C	Aminopeptidase (Similar to leucyl amir	1.4	1.6	1.1
Cellular processes	**VNG0097G**	**Hsp2 [Halobacterium sp. NRC-1]**	**1.5**	**1.7**	**1.4**
Translation/ Protein synthes	VNG0099G	50S ribosomal protein L10e [Halobact	1.5	1.7	1.2
Energy metabolism	**VNG0104G**	**SerA3; Phosphoglycerate dehydr**	**1.4**	**1.6**	**2.0**
DNA metabolism	VNG0106G	rmeM; RmeM; K03427 type I restrictic	1.6	1.7	1.2
DNA metabolism	VNG0107G	RmeS [Halobacterium sp. NRC-1]	1.4	1.5	1.1
Central intermediary me	**VNG0115G**	**yusZ1; oxidoreductase**	**1.7**	**1.6**	**1.5**
Unknown function	VNG0144H	hypothetical VNG0144H	1.2	1.5	1.1
Hypothetical proteins	VNG0153C	hypothetical VNG0153C	1.5	2.2	1.2
Amino acid Metabolism	VNG0161G	GdhB; glutamate dehydrogenase (NAI	1.5	2.2	1.4
DNA metabolism	VNG0163G	mutS1; DNA mismatch repair protein I	1.5	1.5	1.0
Cellular processes	VNG0166G	psmB; proteasome subunit alpha	1.4	1.6	1.2
Translation/ Protein synthes	VNG0177G	50S ribosomal protein L15e [Halobact	1.6	1.8	1.1
Regulatory functions	VNG0179C	hypothetical Serine/threonine protein I	1.5	1.6	1.1
Cellular processes	VNG0192G	cell division protein FtsZ	1.4	2.0	1.2
DNA metabolism	VNG0209H	hypothetical protein VNG0209H [Halol	1.3	1.3	1.6
Cellular processes	VNG0234C	hypothetical protein VNG0234C [Halol	1.7	1.4	1.8
Transcription and regulatior	VNG0237H	DNA-directed RNA polymerase subuni	1.5	1.4	1.1
Translation/ Protein synthes	VNG0239C	50S ribosomal protein L37Ae [Halobac	1.9	2.1	1.4
Nucleotide metabolism	VNG0245G	deoxycytidine triphosphate deaminase	1.4	1.4	1.5
Energy metabolism	VNG0249G	Fbr; cytochrome-like protein	2.3	3.2	1.1
Unknown function	VNG0252C	geranylgeranylglyceryl phosphate synt	1.6	1.7	1.2
Transcription and regulatior	VNG0258H	hypothetical protein VNG0258H [Halol	1.1	1.5	1.1
Energy metabolism	VNG0259G	ipp; inorganic pyrophosphatase	1.2	1.6	1.3
Central intermediary metab	VNG0264H	hypothetical VNG0264H	1.2	1.6	1.1
Cellular processes	VNG0265G	FtsZ4 [Halobacterium sp. NRC-1]	1.5	1.7	1.2
Cellular processes	VNG0283C	hypothetical protein VNG0283C [Halol	1.3	1.5	1.3
Cofactors and 2° Metabolite	VNG0294G	N-methyltransferase-like protein	1.4	1.8	1.4
Cellular processes	VNG0303G	lon; ATP-dependent protease Lon;	1.3	1.6	1.2
Amino acid Metabolism	**VNG0309C**	**fructose-bisphosphate aldolase [I**	**1.6**	**1.4**	**1.2**
Amino acid Metabolism	VNG0310C	3-dehydroquinate synthase [Halobacte	1.5	1.8	1.2
Cell envelope	**VNG0321G**	**Ids; Bifunctional short chain isop**	**1.0**	**1.7**	**1.1**
Energy metabolism	VNG0330G	ppsA; phosphoenolpyruvate synthase	2.2	2.0	1.7
DNA metabolism	**VNG0342G**	**smc1; chromosome segregation p**	**1.6**	**1.8**	**1.2**
Translation/ Protein synthes	VNG0345G	aspartyl/glutamyl-tRNA amidotransfer	1.4	1.6	1.3
Cellular processes	**VNG0355G**	**Htr14 [Halobacterium sp. NRC-1]**	**1.0**	**1.6**	**1.0**
Transport and binding p	**VNG0365G**	**ArsA1; arsenical pump-driving AT**	**1.6**	**1.7**	**1.2**
Hypothetical proteins	VNG0367H	hypothetical protein VNG0367H [Halol	1.3	1.5	1.4
Unclassified	**VNG0368C**	**hypothetical VNG0368C**	**1.4**	**1.5**	**1.5**
Unclassified	VNG0373H	hypothetical VNG0373H	1.5	1.6	1.3
Cellular processes	VNG0376G	cell division protein FtsZ	1.8	2.8	1.2

Amino acid Metabolism	VNG0382G	aroE; hypothetical skikimate dehydrog	1.4	1.8	1.5
Amino acid Metabolism	VNG0384G	TrpE2 [Halobacterium sp. NRC-1]	1.5	1.4	1.2
Transcription and regulatior	VNG0401G	epf2; mRNA 3'-end processing factor-l	1.5	1.6	1.2
Translation/ Protein synthes	VNG0403G	prolyl-tRNA synthetase [Halobacterium	1.5	1.6	1.2
Hypothetical proteins	VNG0405C	hypothetical NAD-dependent epimeras	1.4	1.5	1.2
Amino acid Metabolism	VNG0409C	hypothetical protein VNG0409C [Halol	1.3	1.2	1.6
Cofactors and 2° Metabolite	VNG0412G	hypothetical protein VNG0412G [Halol	1.6	1.5	1.1
Unclassified	**VNG0419C**	**hypothetical VNG0419C**	**1.1**	**1.5**	**1.3**
Energy metabolism	VNG0422G	Cyc [Halobacterium sp. NRC-1]	1.6	1.2	1.8
Transcription and regulatior	VNG0424C	nascent polypeptide-associated compl	1.6	1.4	1.3
Central intermediary metab	VNG0425G	pimT2; L-isoaspartyl protein carboxyl	1.7	1.7	1.2
Transcription and regulatior	VNG0426G	rpoM; DNA-directed RNA-polymerase	1.7	2.3	1.3
Fatty acid/phospholipid met	VNG0428G	fad2; enoyl-CoA hydratase	1.2	1.5	1.3
Amino acid Metabolism	VNG0431G	apa; diadenosine tetraphosphate pyro	1.5	1.6	1.3
Cellular processes	**VNG0437C**	**hypothetical peptidase**	**1.5**	**1.7**	**1.4**
Unknown function	**VNG0440C**	**probable metallo-beta-lactamase**	**1.4**	**1.6**	**1.2**
Cofactors and 2° Metabo	**VNG0442G**	**cyc; cytochrome P450**	**1.3**	**1.8**	**1.3**
Energy metabolism	**VNG0446G**	**gcd; glucose dehydrogenase**	**1.3**	**1.7**	**1.0**
Hypothetical proteins	VNG0447H	hypothetical protein VNG0447H [Halol	1.5	1.4	1.0
Transport and binding prote	VNG0452G	pstB2; phosphate ABC transporter ATI	1.3	1.5	1.2
Cellular processes	VNG0459G	nodP; nodulation protein; K00390 phc	1.5	1.6	1.1
Translation/ Protein synthes	VNG0461G	aspS; aspartyl-tRNA synthetase	1.5	1.6	1.2
Energy metabolism	**VNG0467G**	**yafB; aldehyde reductase**	**1.5**	**1.7**	**1.4**
Fatty acid/phospholipid met	VNG0468C	Oxidoreductase (Geranylgeranyl hydrc	1.4	1.7	1.3
Energy metabolism	VNG0473G	2-oxoglutarate ferredoxin oxidoreduct	1.6	1.7	1.4
Energy metabolism	VNG0474G	porA; hypothetical 2-oxoglutarate ferr	1.7	1.8	1.6
Central intermediary metab	VNG0479G	YajO1; oxidoreductase	1.2	1.8	1.5
Fatty acid/phospholipid met	VNG0481G	McmA1 [Halobacterium sp. NRC-1]	1.2	1.5	1.1
Transcription and regula	**VNG0482H**	**hypothetical N-acetyltransferase**	**1.3**	**1.5**	**1.2**
Translation/ Protein synthes	VNG0487H	N-acetyltransferase activity	1.6	1.6	1.5
Amino acid Metabolism	**VNG0502G**	**aspB1; aspartate aminotransfera**	**1.3**	**1.7**	**1.1**
Translation/ Protein synthes	VNG0504G	translation-associated GTPase [Haloba	1.5	1.7	1.1
Cellular processes	VNG0510G	proteasome-activating nucleotidase [H	1.5	1.2	1.3
Cellular processes	VNG0514C	chromosome segregation protein [Hal	1.5	1.4	1.3
DNA metabolism	VNG0521G	polB1; DNA polymerase B1; DNA poly	1.5	1.7	1.3
Energy metabolism	**VNG0523G**	**inb; oxidoreductase-like protein**	**1.5**	**1.7**	**1.2**
Cofactors and 2° Metabolite	VNG0525C	hypothetical protein VNG0525C [Halol	1.6	1.3	1.4
Cellular processes	VNG0527C	hypothetical protein VNG0527C [Halol	1.5	1.5	1.4
Unclassified	VNG0533H	hypothetical VNG0533H	1.2	1.9	1.3
Unclassified	VNG0534C	Metal dependent phosphohydrolase	1.2	1.5	1.2
Cell envelope	VNG0540G	imp; hypothetical VNG0540G	1.7	1.9	1.1
Amino acid Metabolism	VNG0541G	hypothetical protein VNG0541G [Halol	1.3	1.5	1.1
Hypothetical proteins	VNG0546C	hypothetical VNG0546C	1.6	1.6	1.2
Unclassified	**VNG0557H**	**hypothetical protein VNG0557H [**	**1.5**	**1.2**	**1.2**
Nucleotide metabolism	VNG0559G	apt; adenine phosphoribosyltransferas	1.7	1.6	1.2
Cofactors and 2° Metabolite	VNG0572G	hypothetical protein VNG0572G [Halol	1.5	1.2	1.0
Amino acid Metabolism	VNG0575G	ywaD; aminopeptidase	1.4	1.6	1.3
Energy metabolism	VNG0582C	Cytochrome bc1 complex cytochrome	1.3	1.7	1.1
Energy metabolism	VNG0584H	hypothetical VNG0584H	1.3	1.9	1.1
DNA metabolism	VNG0608C	hypothetical CoA binding, NAD(P)H bi	2.0	1.4	1.5
Transport and binding prote	VNG0617H	hypothetical VNG0617H; Pfam: ABC-t	1.4	2.3	1.5
Cellular processes	VNG0620G	Edp; proteinase	1.2	2.1	1.2

Amino acid Metabolism	VNG0628G	gdhA1; glutamate dehydrogenase	1.6	1.9	1.6
Amino acid Metabolism	VNG0629G	aspB2; aspartate aminotransferase	1.4	1.7	1.2
Nucleotide metabolism	**VNG0632G**	**PurK [Halobacterium sp. NRC-1]**	**1.6**	**1.0**	**1.1**
Energy metabolism	VNG0637G	ndhG5; NADH dehydrogenase/oxidore	1.3	1.7	1.1
Energy metabolism	VNG0640G	nolD; NADH dehydrogenase/oxidored	1.3	2.0	1.2
Transcription and regula	**VNG0651G**	**imd1; inosine-5'-monophosphate**	**1.3**	**1.5**	**1.2**
Fatty acid/phospholipid met	VNG0653G	McmA1 [Halobacterium sp. NRC-1]	1.3	1.5	1.2
Transcription and regula	**VNG0654C**	**hypothetical protein VNG0654C [**	**1.5**	**1.4**	**1.4**
Regulatory functions	**VNG0674C**	**ArgK-type transport ATPase**	**1.5**	**1.6**	**1.5**
Unclassified	**VNG0675C**	**hypothetical Alpha/beta hydrola**	**1.3**	**1.6**	**1.4**
Fatty acid/phospholipid met	VNG0678G	3-ketoacyl-CoA thiolase [Halobacteriur	0.6	1.6	1.2
Fatty acid/phospholipid met	VNG0679G	Acd4 ; acyl-CoA dehydrogenase	1.8	1.7	1.8
Energy metabolism	VNG0680G	fdfT; farnesyl-diphosphate farnesyltra	1.4	1.5	1.0
Fatty acid/phospholipid met	VNG0681G	3-hydroxyacyl-CoA dehydrogenase [H	1.6	1.4	1.6
Energy metabolism	VNG0683C	fructose-bisphosphate aldolase, class	2.0	1.9	1.4
DNA metabolism	VNG0705C	hypothetical protein VNG0705C [Halol	1.2	1.5	1.2
Cellular processes	**VNG0711C**	**Alkyl hydroperoxide reductase/ T**	**1.2**	**1.6**	**1.1**
Unclassified	VNG0713C	hypothetical protein VNG0713C [Halol	1.3	1.5	1.2
Cofactors and 2° Metabolite	VNG0715G	thiamine biosynthesis protein ThiC	1.2	2.2	1.1
Amino acid Metabolism	**VNG0723G**	**pepQ1; peptidase**	**1.3**	**1.6**	**1.3**
Energy metabolism	**VNG0732G**	**RNA 3'-terminal-phosphate cycla**	**1.4**	**1.5**	**1.1**
Cellular processes	VNG0743H	universal stress protein	1.4	1.6	1.3
Regulatory functions	VNG0748G	hypothetical protein VNG0748G [Halol	1.3	1.1	1.5
Regulatory functions	**VNG0749G**	**serine protein kinase [Halobacter**	**1.4**	**1.0**	**2.2**
Transcription and regula	**VNG0751C**	**hypothetical Transcriptional regu**	**1.3**	**1.7**	**1.0**
Energy metabolism	VNG0752G	galE1; UDP-glucose 4-epimerase	1.3	1.5	1.3
Transcription and regula	**VNG0757G**	**tfeA; transcription initiation facto**	**1.0**	**1.6**	**1.2**
Hypothetical proteins	VNG0769H	hypothetical protein VNG0769H [Halol	1.5	1.4	1.4
Energy metabolism	VNG0771G	aldY2; aldehyde dehydrogenase (NAD	1.4	2.1	1.5
Fatty acid/phospholipid met	VNG0775G	Acd2 [Halobacterium sp. NRC-1]	1.4	1.4	1.5
Central intermediary metab	VNG0777G	TaqD [Halobacterium sp. NRC-1]	1.2	1.4	1.5
DNA metabolism	VNG0779C	archaea-specific RecJ-like exonuclease	1.5	1.6	1.2
Unclassified	VNG0780H	hypothetical VNG0780H	1.6	1.8	1.3
Unknown function	VNG0782H	hypothetical VNG0782H	1.1	1.5	1.1
Energy metabolism	VNG0795G	hcpC; halocyanin-like protein	1.1	2.0	1.1
Amino acid Metabolism	**VNG0796G**	**cystathionine gamma synthase/l**	**1.2**	**1.7**	**1.3**
Cellular processes	**VNG0801C**	**hypothetical protein VNG0801C [**	**1.5**	**1.2**	**2.0**
Energy metabolism	VNG0808G	gabD; succinate-semialdehyde dehydr	1.4	1.6	1.2
Hypothetical proteins	**VNG0810H**	**hypothetical protein VNG0810H [**	**1.7**	**1.2**	**0.9**
Energy metabolism	VNG0815G	yfmJ; quinone oxidoreductase	1.7	1.3	1.5
Central intermediary metab	VNG0829G	dmsA; dimethylsulfoxide reductase; K	1.3	1.5	1.3
DNA metabolism	**VNG0838G**	**SsrA; integrase/recombinase**	**1.8**	**1.5**	**1.4**
Energy metabolism	**VNG0841G**	**icfA; IcfA; K01673 carbonic anhy**	**1.3**	**1.6**	**1.2**
Hypothetical proteins	VNG0851C	hypothetical VNG0851C; hydrolase act	1.4	1.9	1.4
Translation/ Protein synthes	VNG0854C	diphthamide synthase subunit DPH2	1.3	1.5	1.0
Translation/ Protein synthes	VNG0872G	gatA; aspartyl/glutamyl-tRNA amidotra	1.4	1.5	1.3
Regulatory functions	VNG0874G	traB; signaling protein	1.5	1.7	1.1
Unknown function	VNG0879C	hypothetical VNG0879C	1.5	1.8	1.3
Cellular processes	VNG0880G	psmA; proteasome subunit alpha;	1.4	1.5	1.3
DNA metabolism	VNG0884G	DNA topoisomerase VI subunit A [Hal	1.6	1.8	1.2
DNA metabolism	VNG0885G	DNA topoisomerase VI subunit B [Hal	1.4	1.5	1.1
DNA metabolism	VNG0887G	DNA gyrase subunit B [Halobacterium	1.5	1.5	1.1

DNA metabolism	VNG0889G	DNA gyrase subunit A [Halobacterium	1.5	1.5	1.1
Transcription and regulatior	VNG0890G	Imd2 [Halobacterium sp. NRC-1]	1.3	1.5	1.1
Energy metabolism	VNG0891G	NADH dehydrogenase [Halobacterium	1.4	1.5	1.2
Nucleotide metabolism	VNG0893G	udp2; uridine phosphorylase;	1.5	1.6	1.3
Transport and binding prote	VNG0903C	ABC-type transport system periplasmi	1.4	1.7	1.1
Energy metabolism	VNG0905G	Pmu2 [Halobacterium sp. NRC-1]	1.5	1.4	1.1
Transport and binding prote	VNG0924G	Ibp; iron(III) transport system substra	1.3	1.7	1.1
Energy metabolism	**VNG0930G**	**YvbT; alkanal monooxygenase ho**	**1.9**	**1.5**	**1.3**
Fatty acid/phospholipid met	VNG0931G	3-ketoacyl-CoA thiolase [Halobacteriur	1.3	1.6	1.2
Energy metabolism	**VNG0933G**	**NADH-dependent flavin oxidored**	**1.6**	**1.5**	**1.2**
Energy metabolism	**VNG0935G**	**NADH oxidase [Halobacterium sp**	**1.5**	**1.4**	**1.2**
Energy metabolism	VNG0940Gm	Acetyl-CoA synthetase [Halobacterium	1.5	1.6	1.1
DNA metabolism	VNG0954C	archaeal flagellar protein FlaE	1.4	1.5	1.2
Cellular processes	VNG0965C	hypothetical VNG0965C	1.2	1.5	1.1
Cellular processes	VNG0966G	hypothetical protein VNG0966G [Halol	1.6	1.4	1.4
Cellular processes	VNG0967Gm	chemotaxis protein [Halobacterium sp	1.3	1.5	1.1
Cellular processes	VNG0970G	cheC1; chemotaxis protein	1.7	1.6	1.3
Cellular processes	VNG0974G	two-component system, chemotaxis fa	1.2	1.5	1.1
Cellular processes	VNG0976G	CheW1 [Halobacterium sp. NRC-1]	1.5	1.6	1.2
Amino acid Metabolism	VNG0981C	Pyridoxal phosphate-dependent aminc	1.3	1.5	1.1
Transport and binding prote	VNG0983C	hypothetical K+ transport system, bin	1.8	1.6	1.3
Energy metabolism	**VNG0997G**	**Acs2 [Halobacterium sp. NRC-1]**	**1.5**	**1.4**	**1.3**
Central intermediary metabo	VNG0998G	YajO2 [Halobacterium sp. NRC-1]	1.7	1.4	1.4
Nucleotide metabolism	VNG1001G	guaB; IMP dehydrogenase	1.7	1.6	1.5
Cellular processes	VNG1008G	FlaA1a; archaeal flagellin FlaA	2.0	1.7	0.9
Cellular processes	VNG1009G	FlaA2 [Halobacterium sp. NRC-1]	1.5	1.4	0.7
Cellular processes	**VNG1013G**	**Htr13 [Halobacterium sp. NRC-1]**	**1.6**	**1.3**	**1.2**
Energy metabolism	VNG1027G	triosephosphate isomerase [Halobacte	1.5	1.6	1.2
Regulatory functions	VNG1029C	hypothetical protein VNG1029C [Halol	1.5	1.4	1.1
Cell envelope	VNG1048G	UDP-glucose dehydrogenase [Halobac	1.4	1.5	1.3
Hypothetical proteins	**VNG1052H**	**hypothetical protein VNG1052H [**	**1.6**	**1.4**	**1.3**
DNA metabolism	VNG1053G	Gtl [Halobacterium sp. NRC-1]	1.1	1.5	1.1
Nucleotide metabolism	VNG1055G	graD4; glucose-1-phosphate thymidyl	1.5	1.7	1.2
Unknown function	VNG1057C	hypothetical protein VNG1057C; Pfam	1.8	1.4	1.0
Hypothetical proteins	**VNG1063H**	**hypothetical protein VNG1063H [**	**0.8**	**1.4**	**1.7**
Fatty acid/phospholipid	**VNG1073G**	**lfl1; Lfl1; K01911 O-succinylbenz**	**1.6**	**1.7**	**1.3**
Cofactors and 2° Metabolite	VNG1079G	naphthoate synthase [Halobacterium s	1.4	1.5	1.1
Cofactors and 2° Metabo	**VNG1081G**	**menD; 2-succinyl-6-hydroxy-2,4-**	**1.7**	**1.5**	**1.3**
Unclassified	VNG1086C	hypothetical VNG1086C	1.3	1.5	1.2
Nucleotide metabolism	VNG1089G	adenylosuccinate synthetase [Halobac	1.5	1.5	1.1
Hypothetical proteins	VNG1092C	hypothetical protein VNG1092C [Halol	1.5	1.4	1.4
Translation/ Protein synthes	VNG1104G	acidic ribosomal protein P0 [Halobacte	1.4	1.5	1.1
Translation/ Protein synthes	VNG1105G	50S ribosomal protein L1P [Halobacter	1.4	1.6	1.1
Translation/ Protein synthes	VNG1108G	50S ribosomal protein L11P [Halobact	1.4	1.6	1.1
Energy metabolism	VNG1114G	glo1; glyoxalase; K01759 lactoylglutat	1.5	1.6	1.1
Energy metabolism	VNG1125G	korB; 2-ketoglutarate ferredoxin oxido	1.4	1.9	1.1
Energy metabolism	VNG1128G	korA; 2-ketoglutarate ferredoxin oxido	1.3	1.7	1.1
Cellular processes	VNG1131G	hypothetical protein VNG1131G [Halol	1.6	1.5	1.1
Translation/ Protein synthes	VNG1132G	30S ribosomal protein S13P [Halobact	1.4	1.5	1.1
Translation/ Protein synthes	VNG1134G	30S ribosomal protein S11P [Halobact	1.5	1.6	1.2
Translation/ Protein synthes	VNG1137G	50S ribosomal protein L18e [Halobact	1.4	1.6	1.1
Translation/ Protein synthes	VNG1138G	50S ribosomal protein L13P [Halobact	2.4	1.3	1.0

Translation/ Protein synthes	VNG1139Gm	30S ribosomal protein S9P [Halobacte	1.4	1.5	1.1
Transcription and regulatior	VNG1140G	DNA-directed RNA polymerase subuni	1.4	1.6	1.3
Energy metabolism	VNG1142G	phosphopyruvate hydratase [Halobact	1.6	1.6	1.2
Hypothetical proteins	**VNG1144H**	**hypothetical VNG1144H**	**1.6**	**1.5**	**1.1**
Central intermediary metab	VNG1145G	mevalonate kinase [Halobacterium sp.	1.3	1.5	1.1
Cellular processes	VNG1149Cm	metallo-beta-lactamase superfamily h	1.5	1.4	1.2
Fatty acid/phospholipid met	VNG1150G	idsA; IdsA; K13787 geranylgeranyl dip	1.5	1.7	1.2
Translation/ Protein synthes	VNG1157G	50S ribosomal protein L7Ae [Halobact	1.3	1.6	1.2
Nucleotide metabolism	VNG1160G	hypothetical protein VNG1160G [Halol	1.6	1.5	1.2
Translation/ Protein synthes	VNG1170G	50S ribosomal protein L21e [Halobact	1.4	1.5	1.0
Amino acid Metabolism	VNG1172G	metB; cystathionine alpha synthase	1.4	1.7	1.3
Translation/ Protein synthes	VNG1173G	elongation factor 1-beta [Halobacteriu	1.5	1.5	1.3
Cellular processes	**VNG1174G**	**RNA modification ribonucleoprot**	**1.4**	**1.6**	**1.2**
Transcription and regulatior	VNG1176G	fibrillarin; pre-RNA	1.4	2.0	1.3
Regulatory functions	VNG1179C	Cu-dependent activator of the Cu(II)-efflux ATPase YvgX.	1.3	1.7	1.5
Hypothetical proteins	VNG1182H	hypothetical protein VNG1182H [Halol	1.5	1.3	1.2
Hypothetical proteins	**VNG1183H**	**hypothetical VNG1183H**	**1.7**	**1.5**	**1.5**
Cofactors and 2° Metabolite	VNG1184Gm	Fe-S oxidoreductase involved in heme	1.6	1.4	1.4
Cell envelope	VNG1187G	Pan1; Cu-binding, membrane protein;	1.3	1.6	1.4
Cellular processes	VNG1190G	Sod1	1.5	1.9	1.6
Fatty acid/phospholipid	**VNG1191Gm**	**Acyl-CoA dehydrogenase [Haloba**	**1.5**	**1.4**	**2.0**
Transport and binding prote	VNG1197G	bcp; hypothetical protein; K03564 peroxiredoxin Q/BCP	1.2	1.6	1.4
Energy metabolism	VNG1198C	hypothetical protein VNG1198C [Halol	1.5	1.5	1.1
Amino acid Metabolism	VNG1204G	gdhA2; glutamate dehydrogenase (NA	1.9	1.5	1.2
Hypothetical proteins	VNG1214H	hypothetical protein VNG1214H [Halol	1.2	1.5	0.9
Energy metabolism	VNG1216G	phosphoglycerate kinase [Halobacteriu	1.5	1.8	1.3
Hypothetical proteins	VNG1220H	hypothetical VNG1220H	1.4	1.6	1.1
Unclassified	VNG1227H	hypothetical protein VNG1227H [Halol	1.5	1.7	1.2
Amino acid Metabolism	VNG1233G	PepQ2 [Halobacterium sp. NRC-1]	1.2	1.5	1.1
Regulatory functions	VNG1237C	hypothetical ptranscription regulation/	1.9	1.5	1.3
Central intermediary metab	VNG1241G	surE; hypothetical protein; K03787 5'-	1.7	1.6	1.2
Cell envelope	VNG1250H	hypothetical VNG1250H	1.2	2.0	1.0
Unclassified	VNG1253C	hypothetical protein VNG1253C	2.0	0.7	1.5
Energy metabolism	VNG1259G	hypothetical protein VNG1259G [Halol	1.3	1.5	1.1
Hypothetical proteins	**VNG1261H**	**hypothetical protein VNG1261H [**	**1.5**	**1.3**	**1.4**
Translation/ Protein synthes	VNG1262G	translation initiation factor IF-2 subuni	1.5	1.6	1.1
Regulatory functions	**VNG1285G**	**Trh2 [Halobacterium sp. NRC-1]**	**1.4**	**1.5**	**1.3**
Translation/ Protein synthes	VNG1287C	hypothetical Ribosomal_L5_domain.	1.6	1.7	1.2
Hypothetical proteins	VNG1291H	hypothetical VNG1291H	1.7	1.5	1.2
Cellular processes	VNG1294G	SlyD [Halobacterium sp. NRC-1]	1.4	1.5	1.3
Cellular processes	VNG1302H	hypothetical protein VNG1302H [Halol	1.5	1.3	1.2
Nucleotide metabolism	VNG1305G	hypothetical protein VNG1305G [Halol	1.5	1.1	1.2
Energy metabolism	VNG1306G	sdhA; succinate dehydrogenase flavo	1.4	1.7	1.2
Energy metabolism	VNG1308G	sdhB; hypothetical succinate dehydroc	1.4	2.0	1.1
Fatty acid/phospholipid met	VNG1313G	3-hydroxyacyl-CoA dehydrogenase [H	1.5	1.6	1.6
Hypothetical proteins	VNG1314H	hypothetical protein VNG1314H [Halol	1.5	1.0	1.4
Nucleotide metabolism	VNG1325C	thymidylate synthase (FAD)	1.3	1.5	1.1
Hypothetical proteins	**VNG1326H**	**hypothetical VNG1326H**	**1.5**	**2.1**	**1.6**
Cellular processes	**VNG1332G**	**Sod2**	**2.0**	**2.3**	**1.9**
DNA metabolism	**VNG1335G**	**phr2; photolyase/cryptochrome;**	**1.6**	**1.5**	**1.4**
Cofactors and 2° Metabolite	VNG1336C	Putative esterase	1.4	1.6	1.3

Unknown function	**VNG1337C**	**sulfuric ester hydrolase activity**	**1.1**	**1.6**	**1.5**
Fatty acid/phospholipid met	VNG1339C	long-chain acyl-CoA synthetase	2.0	1.4	1.8
Energy metabolism	**VNG1342Gm**	**mer; flavin-dependent oxidoredu**	**1.3**	**1.6**	**1.5**
Unclassified	VNG1343C	hypothetical protein VNG1343C [Halol	1.5	1.5	0.9
Cofactors and 2° Metabolite	VNG1344G	DchpS [Halobacterium sp. NRC-1]	1.6	1.4	1.1
Translation/ Protein synthes	VNG1347C	hypothetical RNA methyltransferase, T	1.4	1.5	1.2
Translation/ Protein synthes	VNG1352G	glutamyl-tRNA(Gln) amidotransferase	1.5	1.6	1.1
Energy metabolism	VNG1356G	fumC; fumarate hydratase	1.4	1.7	1.3
DNA metabolism	VNG1359G	rad2; flap endonuclease-1	1.4	1.9	1.3
Cellular processes	VNG1367G	srp19; signal recognition particle;	1.4	1.6	1.5
Regulatory functions	VNG1374G	kinA1; signal-transducing histidine kin	1.5	1.6	1.2
Unclassified	VNG1389C	hypothetical VNG1389C	1.6	1.5	1.2
Central intermediary metab	VNG1398C	hypothetical protein VNG1398C; N-ace	1.8	1.5	1.5
DNA metabolism	VNG1406Gm	helicase [Halobacterium sp. NRC-1]	1.4	1.5	0.9
Amino acid Metabolism	VNG1414G	glyA; serine hydroxymethyltransferase	1.4	1.7	1.4
Cofactors and 2° Metabolite	VNG1416G	folD; bifunctional 5,10-methylene-tetra	1.7	1.1	1.2
Unknown function	VNG1422H	hypothetical protein VNG1422H [Halol	1.6	1.3	1.5
Transcription and regula	**VNG1426H**	**hypothetical Transcriptional regu**	**1.2**	**1.7**	**1.0**
Translation/ Protein synthes	VNG1432G	putative deoxyhypusine synthase [Hal	1.6	1.3	1.2
Translation/ Protein synthes	VNG1433G	30S ribosomal protein S17e [Halobact	1.5	1.5	1.2
Amino acid Metabolism	**VNG1437G**	**serA2; phosphoglycerate dehydrc**	**1.5**	**1.8**	**1.3**
Translation/ Protein synthes	VNG1452G	eif2bd; translation initiation factor eIF	1.6	1.7	1.5
Energy metabolism	**VNG1463G**	**bacterio-opsin linked protein [Ha**	**1.6**	**1.3**	**2.4**
Cellular processes	VNG1472G	Cdc48b; cell division cycle protein	1.8	1.7	1.5
Fatty acid/phospholipid	**VNG1474G**	**est; carboxylesterase**	**1.4**	**1.5**	**1.3**
Fatty acid/phospholipid met	VNG1482G	acd5; acyl-CoA dehydrogenase;	1.5	1.9	1.2
Nucleotide metabolism	VNG1493G	hypothetical protein VNG1493G [Halol	1.5	1.1	0.9
DNA metabolism	VNG1496G	snp; snRNP-like protein; K04796 smal	1.4	1.6	1.6
Energy metabolism	VNG1498G	celM; endoglucanase;	1.3	1.5	1.2
Translation/ Protein synthes	VNG1506G	pelA; cell division protein pelota;	1.5	1.8	1.3
Transcription and regulatior	VNG1508C	hypothetical protein VNG1508C [Halol	1.5	1.4	1.4
DNA metabolism	VNG1511C	hypothetical protein VNG1511C [Halol	1.4	1.6	1.0
Nucleotide metabolism	VNG1515G	hypothetical protein VNG1515G [Halol	1.4	1.5	1.1
Central intermediary metab	VNG1524C	hypothetical 4-aminobutyrate aminotra	1.8	1.7	1.2
Central intermediary metab	VNG1529G	mmdA; methylmalonyl-CoA decarboxy	1.3	1.5	1.3
Fatty acid/phospholipid met	VNG1532G	acc; carbamoyl phosphate synthase su	1.5	1.5	1.3
Cellular processes	**VNG1536C**	**Universal stress protein UspA-like**	**1.2**	**1.6**	**1.2**
Regulatory functions	VNG1537C	Metal dependent phosphohydrolase	1.3	1.6	1.0
Cell envelope	VNG1538H	hypothetical protein VNG1538H [Halol	1.5	1.4	1.2
Energy metabolism	VNG1541G	hypothetical protein VNG1541G [Halol	1.5	1.4	1.2
Energy metabolism	VNG1542G	hypothetical protein VNG1542G [Halol	1.5	1.4	1.4
Energy metabolism	**VNG1547C**	**hypothetical ATP/cobalamin ader**	**1.5**	**1.7**	**1.4**
Cofactors and 2° Metabolite	VNG1573G	CbiA [Halobacterium sp. NRC-1]	1.5	1.4	1.4
Hypothetical proteins	VNG1591H	hypothetical VNG1591H	1.7	1.7	1.3
Energy metabolism	VNG1605G	gdcH; glycine cleavage system proteir	1.3	1.6	1.5
Hypothetical proteins	**VNG1609C**	**hypothetical VNG1609C**	**1.3**	**1.6**	**1.1**
Fatty acid/phospholipid met	VNG1615G	mvaB; 3-hydroxy-3-methylglutaryl-coe	1.4	1.6	1.0
Unclassified	VNG1618H	NADH-dependent FMN reductase	1.4	1.5	1.2
Energy metabolism	VNG1624G	mdh; malic enzyme (EC:1.1.1.40); K0	1.3	1.6	1.2
Hypothetical proteins	VNG1638H	hypothetical VNG1638H	1.4	1.5	1.2
Nucleotide metabolism	VNG1644G	nrdB2; ribonucleoside reductase large	1.3	1.7	1.1
Cellular processes	**VNG1658C**	**hypothetical pUniversal_stress_U**	**1.3**	**1.5**	**1.1**

Translation/ Protein syn	**VNG1663C**	**hypothetical VNG1663C; Riboson**	**1.6**	**1.8**	**1.3**
DNA metabolism	VNG1665G	radB; DNA repair and recombination p	1.4	1.6	1.3
Cellular processes	VNG1667G	Cdc48c [Halobacterium sp. NRC-1]	1.4	1.5	1.2
Translation/ Protein synthes	VNG1668G	30S ribosomal protein S8e [Halobacte	1.5	1.6	1.0
Hypothetical proteins	VNG1679H	hypothetical VNG1679H; ribosomal 30	1.6	2.0	1.4
Central intermediary me	**VNG1680G**	**CrtB2 [Halobacterium sp. NRC-1]**	**1.5**	**1.3**	**1.2**
Cofactors and 2° Metabolite	VNG1686G	N(5),N(10)-methenyltetrahydrometha	1.3	1.5	1.2
Translation/ Protein synthes	VNG1689G	50S ribosomal protein L3P [Halobacte	1.4	1.5	1.1
Translation/ Protein synthes	VNG1690G	50S ribosomal protein L4P [Halobacte	1.4	1.6	1.1
Translation/ Protein synthes	VNG1691G	50S ribosomal protein L23 [Halobacte	1.4	1.5	1.1
Translation/ Protein synthes	VNG1693G	30S ribosomal protein S19P [Halobact	1.5	1.7	1.2
Translation/ Protein synthes	VNG1695G	50S ribosomal protein L22P [Halobact	1.5	1.7	1.2
Translation/ Protein synthes	VNG1697G	30S ribosomal protein S3P [Halobacte	1.4	1.5	1.2
Translation/ Protein synthes	VNG1700G	30S ribosomal protein S17P [Halobact	1.5	1.6	1.2
Translation/ Protein synthes	VNG1701G	50S ribosomal protein L14P [Halobact	1.3	1.5	1.0
Translation/ Protein synthes	VNG1702G	50S ribosomal protein L24P [Halobact	1.4	1.5	1.1
Translation/ Protein synthes	VNG1706G	30S ribosomal protein S14P [Halobact	1.9	1.8	1.1
Translation/ Protein synthes	VNG1707G	30S ribosomal protein S8P [Halobacte	1.4	1.6	1.2
Translation/ Protein synthes	VNG1709G	50S ribosomal protein L6P [Halobacte	1.4	1.7	1.2
Translation/ Protein synthes	VNG1713G	50S ribosomal protein L19e [Halobact	1.4	1.5	1.1
Translation/ Protein synthes	VNG1714G	50S ribosomal protein L18P [Halobact	1.3	1.5	1.2
Translation/ Protein synthes	VNG1715G	30S ribosomal protein S5P [Halobacte	1.6	1.8	1.3
Nucleotide metabolism	VNG1727G	cytidylate kinase [Halobacterium sp. N	1.5	1.4	1.2
Hypothetical proteins	**VNG1746C**	**hypothetical protein VNG1746C [**	**1.4**	**1.4**	**2.0**
DNA metabolism	**VNG1754G**	**Phr1 [Halobacterium sp. NRC-1]**	**1.5**	**1.4**	**1.8**
Central intermediary me	**VNG1755G**	**CrtI2 [Halobacterium sp. NRC-1]**	**1.4**	**1.3**	**1.7**
Cellular processes	**VNG1760G**	**Htr5 [Halobacterium sp. NRC-1]**	**1.2**	**1.6**	**1.0**
Hypothetical proteins	VNG1766C	hypothetical protein VNG1766C [Halol	1.5	1.4	1.1
Unclassified	VNG1769Cm	putative amidase [Halobacterium sp. N	1.5	1.3	1.3
Cofactors and 2° Metabolite	VNG1776G	NirH; heme biosynthesis protein	1.5	1.7	1.4
Cofactors and 2° Metabolite	VNG1795C	Amine oxidase	1.3	1.6	1.2
Hypothetical proteins	VNG1802H	hypothetical protein VNG1802H [Halol	0.9	1.5	0.8
Energy metabolism	VNG1804G	noxA; NADH oxidase;	1.5	1.6	1.2
Hypothetical proteins	VNG1807H	hypothetical protein VNG1807H [Halol	1.4	1.5	1.1
Hypothetical proteins	VNG1809H	hypothetical VNG1809H	1.4	1.8	1.2
Cofactors and 2° Metabo	**VNG1823C**	**hypothetical 5-formyltetrahydrof**	**1.1**	**1.6**	**1.0**
Energy metabolism	VNG1829G	GMP synthase subunit B [Halobacteriu	1.5	1.6	1.1
Nucleotide metabolism	VNG1830G	CTP synthetase [Halobacterium sp. NF	1.3	1.6	1.1
Translation/ Protein synthes	VNG1835G	thrS; threonyl-tRNA synthetase	1.5	1.7	1.1
Translation/ Protein synthes	VNG1844G	glutamyl-tRNA(Gln) amidotransferase	1.4	1.5	1.0
Transcription and regulatior	VNG1845C	hypothetical GCN5-related N-acetyltra	1.7	1.7	1.3
Regulatory functions	VNG1864G	Hit2; Histidine triad protein	1.4	1.9	1.3
Amino acid Metabolism	VNG1866G	methionine aminopeptidase [Halobact	1.4	1.6	1.2
Energy metabolism	VNG1873G	icd; isocitrate dehydrogenase	1.5	1.8	1.2
Hypothetical proteins	VNG1877C	hypothetical protein VNG1877C [Halol	1.1	1.5	1.2
Cofactors and 2° Metabolite	VNG1882G	nadA; quinolinate synthetase [Haloba	5.0	1.2	0.8
Cofactors and 2° Metabolite	VNG1883G	nadB; L-aspartate oxidase [Halobacte	6.9	1.5	1.0
Cofactors and 2° Metabolite	VNG1884G	nadC; nicotinate-nucleotide pyrophosp	3.2	1.1	0.8
Energy metabolism	VNG1887G	phosphoglyceromutase	1.6	1.7	1.1
Energy metabolism	VNG1900C	hypothetical NAD+ kinase	1.3	1.6	1.0
Cofactors and 2° Metabolite	VNG1901C	GTP cyclohydrolase; cofacter biosynth	1.5	2.0	1.2
Nucleotide metabolism	VNG1912G	trpD2; phosphoribosyl transferase	1.5	1.9	1.6

Cellular processes	VNG1914G	ppiA; peptidyl-prolyl isomerase	1.4	1.5	1.2
Unknown function	VNG1918C	geranylgeranylglyceryl phosphate synt	1.6	1.5	1.3
Regulatory functions	**VNG1922G**	**Trh5 [Halobacterium sp. NRC-1]**	**1.4**	**1.2**	**1.9**
Transport and binding p	**VNG1924G**	**TRK potassium uptake system pr**	**1.2**	**1.1**	**1.8**
Energy metabolism	VNG1926G	pdhA1; pyruvate dehydrogenase alpha	1.4	1.6	1.2
Nucleotide metabolism	VNG1929G	thymidylate kinase [Halobacterium sp.	1.6	1.8	1.2
Energy metabolism	**VNG1932G**	**NADH dehydrogenase/oxidoredu**	**1.5**	**1.4**	**1.5**
Cellular processes	VNG1933G	FtsZ3	1.6	1.8	1.3
Hypothetical proteins	VNG1941C	hypothetical Radical SAM domain prot	1.4	1.6	1.2
Hypothetical proteins	**VNG1977H**	**hypothetical VNG1977H**	**1.3**	**1.6**	**1.1**
Translation/ Protein synthes	VNG1982C	tRNA pseudouridine synthase	1.3	1.5	1.1
Unclassified	VNG1995C	hypothetical PRC-barrel domain prote	1.5	1.6	1.2
Translation/ Protein synthes	VNG1997G	translation initiation factor IF-2 [Halob	1.5	1.6	1.2
Cellular processes	VNG2000G	prrIV1; proteasome-activating nucleot	1.8	1.4	1.6
Amino acid Metabolism	**VNG2001G**	**yjbG; oligopeptidase; K08602 olig**	**1.4**	**1.6**	**1.3**
Translation/ Protein synthes	VNG2005G	histidyl-tRNA synthetase [Halobacteriu	1.3	1.5	1.1
Transcription and regula	**VNG2008H**	**hypothetical protein; K06875 pro**	**1.4**	**1.5**	**1.3**
Translation/ Protein synthes	VNG2010G	30S ribosomal protein S19e [Halobact	1.5	1.4	1.1
Translation/ Protein synthes	VNG2017G	hypothetical protein VNG2017G [Halol	1.5	1.4	1.2
Cellular processes	VNG2021C	hypothetical VNG2021C	1.4	1.5	1.2
Cellular processes	VNG2023G	gsp; general stress protein 69	1.5	1.5	1.5
Cofactors and 2° Metabo	**VNG2031G**	**nadE; NAD synthetase;**	**1.5**	**1.5**	**1.3**
DNA metabolism	VNG2043G	ham1; dITP/XTP pyrophosphatase	1.3	1.6	1.2
Transcription and regulatior	VNG2051G	rpoE; DNA-directed RNA polymerase s	1.7	1.6	1.2
Translation/ Protein synthes	VNG2056G	translation initiation factor IF-2 subuni	1.6	1.5	1.2
Cellular processes	VNG2062G	atp; ATPase AAA	1.3	1.6	1.0
Unclassified	VNG2063G	acetyl-CoA acetyltransferaseACA [Halc	1.5	1.6	1.8
Translation/ Protein synthes	VNG2072G	seryl-tRNA synthetase [Halobacterium	1.4	1.6	1.2
Energy metabolism	VNG2086G	hbp; phosphonate transport system su	1.3	1.8	1.2
Amino acid Metabolism	**VNG2087G**	**imidazole glycerol phosphate syn**	**1.4**	**1.6**	**1.2**
Amino acid Metabolism	VNG2093G	hypothetical protein VNG2093G [Halol	1.7	1.4	1.1
Transcription and regulatior	VNG2099C	hypothetical Ribonuclease, PSP-type	1.5	1.6	1.3
Amino acid Metabolism	VNG2100G	threonine dehydratase [Halobacterium	0.9	1.6	1.1
Energy metabolism	VNG2102G	CitZ [Halobacterium sp. NRC-1]	1.4	1.8	1.4
Energy metabolism	VNG2106G	sdh; succinate dehydrogenase subunit	1.2	1.6	1.2
Nucleotide metabolism	VNG2117C	adenine phosphoribosyltransferase [H	1.6	1.8	1.0
Energy metabolism	VNG2120G	yusM; proline dehydrogenase	1.5	1.9	1.3
Amino acid Metabolism	VNG2122G	branched-chain amino acid aminotran	1.3	1.7	1.1
Energy metabolism	VNG2138G	V-type ATP synthase subunit B [Halob	1.4	1.6	1.3
Energy metabolism	VNG2139G	V-type ATP synthase subunit A [Halob	1.5	1.7	1.3
Energy metabolism	VNG2142G	V-type ATP synthase subunit E [Halob	3.4	3.3	2.3
Energy metabolism	VNG2143G	atpK; H+-transporting ATP synthase s	1.1	1.9	1.3
Energy metabolism	VNG2144G	atpI; H+-transporting ATP synthase su	1.4	1.5	1.2
Cofactors and 2° Metabolite	VNG2147G	hmp; Hmp; K03183 ubiquinone/mena	1.6	1.4	1.1
Energy metabolism	VNG2151G	etfA; electron transfer flavoprotein sul	1.6	1.5	1.3
DNA metabolism	VNG2160C	rfa3	2.5	3.4	2.3
DNA metabolism	**VNG2162C**	**rfa8**	**4.0**	**5.0**	**3.2**
DNA metabolism	**VNG2173G**	**rad24a; DNA repair protein; K037**	**1.7**	**1.9**	**1.0**
Regulatory functions	VNG2186G	Hit1 [Halobacterium sp. NRC-1]	1.1	1.5	1.3
Translation/ Protein synthes	VNG2190G	isoleucyl-tRNA synthetase [Halobacter	1.3	1.7	1.2
Energy metabolism	VNG2193Gm	cytochrome c oxidase subunit I [Halol	1.2	1.6	1.0
Energy metabolism	VNG2195G	coxB2; cytochrome c oxidase subunit	1.3	1.9	1.1

Nucleotide metabolism	VNG2203G	prsA; ribose-phosphate pyrophosphok	1.5	1.9	1.3
Translation/ Protein synthes	VNG2208G	tryptophanyl-tRNA synthetase [Haloba	1.3	1.5	1.1
Energy metabolism	VNG2217G	pdhA2; pyruvate dehydrogenase alpha	1.6	1.8	1.3
Energy metabolism	VNG2218G	pdhB; pyruvate dehydrogenase E1	1.7	2.0	1.4
Energy metabolism	VNG2219G	dsa; branched-chain alpha-keto acid d	1.5	1.5	1.2
Energy metabolism	VNG2220G	lpdA; LpdA; K00382 dihydrolipoamide	1.6	1.7	1.2
Amino acid Metabolism	VNG2224G	ocd1; ornithine cyclodeaminase;	1.5	1.7	1.2
Transcription and regulatior	VNG2227C	putative RNA-processing protein [Halc	1.4	2.0	1.2
Translation/ Protein synthes	VNG2237G	tyrosyl-tRNA synthetase [Halobacteriu	1.3	1.8	1.2
Amino acid Metabolism	VNG2247G	ATP phosphoribosyltransferase [Halob	1.2	1.6	1.1
Cellular processes	VNG2249G	N-ethylammeline chlorohydrolase [Hal	1.3	1.5	1.1
Cofactors and 2° Metabolite	VNG2251G	achY; S-adenosyl-L-homocysteine hyd	1.2	1.6	1.2
Hypothetical proteins	VNG2260H	hypothetical VNG2260H	1.5	1.6	1.4
Hypothetical proteins	VNG2268H	hypothetical regulation of transcriptior	1.3	1.5	1.0
Energy metabolism	VNG2276G	pmm; phosphoglucomutase	1.3	2.0	1.3
DNA metabolism	VNG2280G	replication factor C small subunit [Halc	1.4	1.5	1.1
Central intermediary me	**VNG2281C**	**putative glutathione S-transferas**	**1.2**	**1.8**	**1.5**
Energy metabolism	VNG2293G	fer2; ferredoxin	1.4	1.7	1.5
Transcription and regula	**VNG2296C**	**hypothetical Amino acid-binding**	**1.2**	**1.6**	**1.0**
Amino acid Metabolism	VNG2302G	yuxL; acylaminoacyl peptidase	1.5	1.5	1.6
Nucleotide metabolism	VNG2305C	upp; uracil phosphoribosyltransferase	1.4	1.9	1.4
Cellular processes	**VNG2308G**	**hlp; Hlp; K03699 putative hemoly**	**1.2**	**1.7**	**1.1**
Translation/ Protein synthes	VNG2312C	tRNA threonylcarbamoyladenosine bio	2.2	1.9	1.6
Cofactors and 2° Metabolite	VNG2322G	hem2; delta-aminolevulinic acid dehyc	1.3	1.6	1.1
Cofactors and 2° Metabolite	VNG2326G	hemL; glutamate-1-semialdehyde ami	1.4	1.6	1.1
Cofactors and 2° Metabolite	VNG2330G	hem3; porphobilinogen deaminase	1.2	1.5	1.0
Cofactors and 2° Metabolite	VNG2331G	uroM; S-adenosyl-L-methionine:uropo	1.2	1.7	1.2
Transport and binding prote	VNG2344G	OppD2; peptide/nickel transport syste	1.4	1.5	1.1
Transport and binding prote	VNG2349G	dppA; peptide/nickel transport system	1.3	2.0	1.3
Unclassified	VNG2351C	hypothetical cystathionine-beta-synth	1.4	1.7	1.1
Translation/ Protein synthes	VNG2352G	glycyl-tRNA synthetase [Halobacteriun	1.4	1.6	1.2
Transport and binding p	**VNG2358G**	**AppA; peptide/nickel transport sy**	**1.1**	**2.1**	**1.5**
Energy metabolism	VNG2367G	malate dehydrogenase [Halobacterium	1.5	1.5	1.4
DNA metabolism	VNG2368G	ski2-like helicase [Halobacterium sp. N	1.5	1.5	1.2
Nucleotide metabolism	VNG2372G	rad24c; DNA repair protein	1.1	1.7	1.0
Energy metabolism	**VNG2373G**	**tnaA; tryptophanase**	**1.3**	**1.7**	**1.2**
DNA metabolism	VNG2390G	uvrB; excinuclease ABC subunit B [Hal	1.6	1.5	1.2
Central intermediary metabc	VNG2394G	TssB [Halobacterium sp. NRC-1]	1.3	1.5	1.0
Transport and binding prote	VNG2395C	hypothetical thiamine transport systen	1.2	1.5	0.9
Cofactors and 2° Metabolite	VNG2398G	scm; 24-sterol C-methyltransferase	1.6	1.7	1.3
Hypothetical proteins	VNG2400H	hypothetical VNG2400H	1.4	1.8	1.5
Cellular processes	VNG2410G	gbp3; GTP-binding protein	1.5	1.7	1.2
Amino acid Metabolism	**VNG2418G**	**AspC1 [Halobacterium sp. NRC-1]**	**1.5**	**1.4**	**1.3**
Central intermediary me	**VNG2422G**	**Glycolate oxidase subunit**	**1.2**	**1.7**	**1.1**
Amino acid Metabolism	**VNG2423G**	**serB; phosphoserine phosphatase**	**1.9**	**1.6**	**1.4**
Translation/ Protein syn	**VNG2430G**	**threonine synthase**	**1.6**	**1.7**	**1.6**
Unclassified	VNG2432C	UPF0145 protein VNG_2432C	1.1	1.5	1.1
Cellular processes	**VNG2443G**	**DpsA**	**1.3**	**1.6**	**1.4**
Amino acid Metabolism	VNG2449G	pepB2; aminopeptidase;	1.3	1.7	1.2
Cellular processes	VNG2459G	Srp54 [Halobacterium sp. NRC-1]	1.4	1.5	1.3
Cellular processes	VNG2462G	dpa; signal recognition particle recept	1.2	1.8	1.0
Cellular processes	VNG2465C	hypothetical protein VNG2465C [Halob	1.7	1.5	1.5

Unclassified	VNG2468C	hypothetical VNG2468C	1.6	1.7	1.2
Translation/ Protein synthes	VNG2469G	50S ribosomal protein L39e [Halobact	1.6	1.8	1.2
Amino acid Metabolism	VNG2471G	nifS; cysteine desulfurase / selenocyst	1.4	1.6	1.2
DNA metabolism	VNG2473G	radA; DNA repair and recombination p	1.1	1.8	1.0
Energy metabolism	VNG2499G	gcdH; glutaryl-CoA dehydrogenase	1.4	1.9	1.2
Nucleotide metabolism	VNG2501C	hypothetical protein VNG2501C	1.8	1.7	1.4
Translation/ Protein synthes	VNG2505G	phenylalanyl-tRNA synthetase subunit	1.3	1.8	1.1
Nucleotide metabolism	VNG2507G	pyrD; dihydroorotate dehydrogenase 1	1.1	1.6	1.1
Energy metabolism	VNG2513G	AldY1 [Halobacterium sp. NRC-1]	1.4	1.4	1.7
Translation/ Protein synthes	VNG2514G	30S ribosomal protein S6e [Halobacte	1.5	1.5	1.1
Hypothetical proteins	VNG2519H	hypothetical VNG2519H	1.4	1.5	1.1
Cellular processes	**VNG2520C**	**hypothetical Universal_stress_Us**	**1.2**	**1.6**	**1.1**
Cellular processes	**VNG2521H**	**hypothetical VNG2521H; universa**	**1.4**	**1.9**	**1.4**
Cellular processes	VNG2523H	hypothetical VNG2523H; universal stre	1.4	1.9	1.3
Nucleotide metabolism	VNG2533G	pyrC; dihydroorotase	1.2	1.5	1.2
Cofactors and 2° Metabolite	VNG2537G	EntB [Halobacterium sp. NRC-1]	1.5	1.5	1.5
Hypothetical proteins	VNG2539H	hypothetical protein VNG2539H [Halol	1.1	1.2	1.5
Amino acid Metabolism	VNG2546G	pepB3; aminopeptidase	1.3	1.5	1.2
Translation/ Protein synthes	VNG2547G	valyl-tRNA synthetase [Halobacterium	1.4	1.6	1.1
Transport and binding prote	VNG2552G	yfmF; ferrichrome ABC transporter AT	1.2	1.4	0.9
Unclassified	VNG2554H	hypothetical VNG2554H	1.4	1.8	1.2
Energy metabolism	VNG2574G	can; aconitate hydratase	1.3	1.5	1.1
Cellular processes	VNG2587C	GTP-binding protein; possible cell cycl	1.7	1.8	1.2
Cellular processes	VNG2595G	gbp4; GTP-binding protein; K06943 n	1.7	1.3	0.7
Unclassified	VNG2597C	hypothetical DNase-RNase. 1 hit.	1.3	1.5	1.4
Energy metabolism	VNG2600G	hypothetical protein VNG2600G [Halol	1.3	1.5	1.4
Cofactors and 2° Metabolite	VNG2604Gm	ribulose-1,5-biphosphate synthetase	1.3	2.2	1.3
Cofactors and 2° Metabolite	VNG2606G	thiD; hypothetical protein; K00941 hy	1.2	1.6	1.1
Unclassified	VNG2612G	rli; ATPase RIL; K06174 ATP-binding	1.4	1.8	1.2
Unclassified	VNG2615C	ATPase [Halobacterium sp. NRC-1]	1.5	1.5	1.1
Energy metabolism	VNG2616G	cxp; carboxypeptidase	1.7	1.9	1.5
Energy metabolism	**VNG2617G**	**adh2; alcohol dehydrogenase**	**1.4**	**1.5**	**1.5**
DNA metabolism	VNG2620G	uvrD	1.5	1.3	1.1
Translation/ Protein synthes	VNG2627C	hypothetical protein VNG2627C [Halol	1.3	1.5	1.1
DNA metabolism	VNG2636G	uvrA	1.5	1.3	1.6
Cell envelope	VNG2639G	UDP-N-acetylglucosamine 2-epimerase	1.4	1.8	1.2
Unclassified	VNG2644C	hypothetical VNG2644C; barrier septu	1.1	2.0	1.1
Transcription and regula	**VNG2647G**	**vacB; hypothetical protein;ribonu**	**1.3**	**1.6**	**1.3**
Translation/ Protein synthes	VNG2648G	30S ribosomal protein S10P [Halobact	1.3	1.5	1.1
Translation/ Protein synthes	VNG2649G	elongation factor 1-alpha [Halobacteri	1.6	1.5	1.2
DNA metabolism	VNG2652H	hypothetical VNG2652H; putative tran	1.5	1.9	1.2
Translation/ Protein synthes	VNG2654Gm	elongation factor EF-2 [Halobacterium	1.4	1.5	1.1
Translation/ Protein synthes	VNG2658G	30S ribosomal protein S12P [Halobact	1.4	1.5	1.2
Transcription and regulatior	VNG2662G	DNA-directed RNA polymerase subunit	1.5	1.5	1.1
Transcription and regulatior	VNG2664Gm	rpoA1; DNA-directed RNA polymerase	1.7	1.5	1.2
Transcription and regulatior	VNG2665G	rpoB; DNA-directed RNA polymerase s	1.7	1.8	1.3
Regulatory functions	VNG2675C	Transcription regulator homolog	1.4	1.5	1.2
Cell envelope	VNG2679G	cell surface glycoprotein [Halobacteriu	1.2	1.7	1.1
Unclassified	VNG6126H	hypothetical protein VNG6126H	2.2	0.3	1.3
Unclassified	VNG6171H	hypothetical protein VNG6171H	2.2	1.3	1.0
Transport and binding p	**VNG6179G**	**Cat3; cationic amino acid transpo**	**2.5**	**1.3**	**0.9**
Unclassified	**VNG6225C**	**hypothetical protein VNG6225C [**	**1.6**	**1.4**	**1.1**

Unclassified	VNG6226H	hypothetical protein VNG6226H [Halol	1.7	1.2	1.2
Transport and binding prote	VNG6247G	TRK potassium uptake system protein	1.5	1.4	1.1
Central intermediary metab	VNG6270G	glycerol dehydrogenase [Halobacteriu	1.5	1.4	1.1
Unclassified	VNG6296C	hypothetical protein VNG6296C [Halol	1.5	1.4	1.3
Nucleotide metabolism	VNG6309G	aspartate carbamoyltransferase cataly	1.5	1.3	1.1
Translation/ Protein synthes	VNG6312G	hypothetical protein VNG6312G [Halol	1.6	1.1	1.2
Transport and binding p	**VNG6313G**	**arcD; arginine/ornithine antiport**	**0.5**	**1.8**	**1.2**
Amino acid Metabolism	VNG6315G	hypothetical protein VNG6315G [Halol	1.4	1.5	1.5
Energy metabolism	VNG6317G	arcA; arginine deiminase	1.3	1.5	1.3
Regulatory functions	VNG6318G	ArcR [Halobacterium sp. NRC-1]	0.4	1.5	1.1
Unclassified	VNG6320C	hypothetical protein VNG6320C [Halol	1.5	1.3	0.8
Regulatory functions	VNG6337G	SojE [Halobacterium sp. NRC-1]	1.6	0.6	0.6
Unclassified	VNG6379C	hypothetical VNG6379C; Fe-S binding,	0.6	5.5	0.7
Cofactors and 2° Metabolite	VNG6445G	crt_2; isopentenyl pyrophosphate ison	0.7	1.7	0.6
Hypothetical proteins	VNG7086	hypothetical protein VNG7086	2.1	0.3	1.2
Hypothetical proteins	VNG7090	VNG5131H, VNG6127H	1.9	1.5	1.3
Hypothetical proteins	VNG7091	hypothetical protein VNG7091 [Haloba	1.7	1.4	1.1
Hypothetical proteins	VNG7092	VNG5133C, VNG6129C	1.6	1.7	0.9
Hypothetical proteins	VNG7102	hypothetical protein VNG7102 [Haloba	1.5	0.2	1.1
Regulatory functions	VNG7114	transcription factor [Halobacterium sp	0.4	0.4	1.5
Hypothetical proteins	VNG7115	hypothetical protein VNG7115 [Haloba	0.6	0.6	1.5

Appendix C – Additional Figures

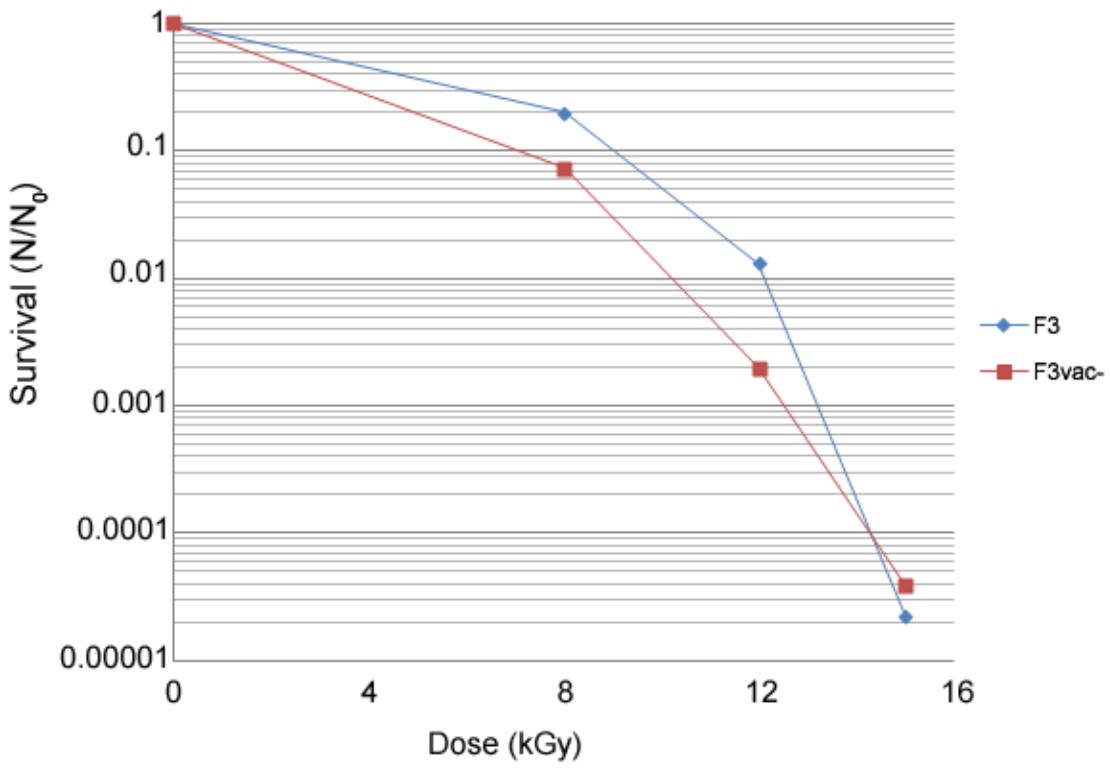

Figure 1. Survival curves of *H. salinarum* founder strain F3 and F3 vac- strain exposed to 0, 8, 12 and 15 kGy of IR. Survival was calculated as the average ratio (N/N_0) of cfu/ml from irradiated (N) compared to un-irradiated (N_0) cultures, with 3 replicates used for each calculation.

Appendix D

Table 1. Estimation of intracellular concentration of compatible solutes

EtOH extracts (µmol/mg prot)

Trehalose

	µmol/mg protein	total mg prot	total tre µmol	total cells	total vol (µl)*	tre (µmol/µl)	tre (mM)
Rrad	1.7	0.6	1.0	7.7E+09	51.7	0.0	20.0
Rxyl	1.5	0.9	1.4	7.5E+09	50.4	0.0	27.0

Mannosylglycerate (MG)

	µmol/mg protein	total mg prot	total MG umol	total cells	total vol (µl)*	MG (µmol/µl)	MG (mM)
Rrad	2.4	0.6	1.5	7.7E+09	51.7	0.0	28.1
Rxyl	3.0	0.9	2.7	7.5E+09	50.4	0.1	54.2

Di-*myo* -inositol phosphate (DIP)

	µmol/mg protein	total mg prot	total DIP µmol	total cells	total vol (µl)*	DIP (µmol/µl)	DIP (mM)
Rxyl	0.7	0.9	0.7	7.5E+09	50.4	0.0	13.2

*6.76ul per 10E9 cells

EtOH extracts (µmol/mg prot)

	MG	MG (mM)	DIP	DIP (mM)
Tgam	0.1	20.8	0.1	11.1
Pfur	0.2	49.0	0.0	9.6

*calculated from Martins paper, cell volume in text : 4.5 µl/mg of protein

References

1. Cavicchioli R, Amils R, Wagner D, McGenity T. (2011) Life and applications of extremophiles. Environ Microbiol 13(8): 1903-1907.

2. Canganella F, Wiegel J. (2011) Extremophiles: From abyssal to terrestrial ecosystems and possibly beyond. Naturwissenschaften 98(4): 253-279.

3. MacElroy RD. (1974) Some comments on the evolution of extremophiles. Biosystems 6: 74-75.

4. Gladyshev E, Meselson M. (2008) Extreme resistance of *Bdelloid rotifers* to ionizing radiation. Proc Natl Acad Sci U S A 105(13): 5139-5144.

5. Holliday R. (2004) Early studies on recombination and DNA repair in *Ustilago maydis*. DNA Repair (Amst) 3(6): 671-682.

6. Atomi H, Sato T, Kanai T. (2011) Application of hyperthermophiles and their enzymes. Curr Opin Biotechnol 22(5): 618-626.

7. Chien A, Edgar DB, Trela JM. (1976) Deoxyribonucleic acid polymerase from the extreme thermophile *Thermus aquaticus*. J Bacteriol 127(3): 1550-1557.

8. Petsko GA. (2001) Structural basis of thermostability in hyperthermophilic proteins, or "there's more than one way to skin a cat". Methods Enzymol 334: 469-478.

9. Guyer RL, Koshland DE,Jr. (1989) The molecule of the year. Science 246(4937): 1543-1546.

10. Kish A, Griffin PL, Rogers KL, Fogel ML, Hemley RJ, et al. (2012) High-pressure tolerance in *Halobacterium salinarum* NRC-1 and other non-piezophilic prokaryotes. Extremophiles 16(2):355-61. Epub 2012 Jan 3.

11. Robinson CK, Webb K, Kaur A, Jaruga P, Dizdaroglu M, et al. (2011) A major role for nonenzymatic antioxidant processes in the radioresistance of *Halobacterium salinarum*. J Bacteriol 193(7): 1653-1662.

12. Kottemann M, Kish A, Iloanusi C, Bjork S, DiRuggiero J. (2005) Physiological responses of the halophilic archaeon *Halobacterium* sp. strain NRC1 to desiccation and gamma irradiation. Extremophiles 9(3): 219-227.

13. Trigui H, Masmoudi S, Brochier-Armanet C, Maalej S, Dukan S. (2011) Survival of extremely and moderately halophilic isolates of tunisian solar salterns after UV-B or oxidative stress. Can J Microbiol 57(11): 923-933.

14. Daly MJ, Gaidamakova EK, Matrosova VY, Kiang JG, Fukumoto R, et al. (2010) Small-molecule antioxidant proteome-shields in *Deinococcus radiodurans*. PLoS One 5(9): e12570.

15. Slade D, Radman M. (2011) Oxidative stress resistance in *Deinococcus radiodurans*. Microbiol Mol Biol Rev 75(1): 133-191.

16. Daly MJ. (2011) Death by protein damage in irradiated cells. DNA Repair (Amst) 11(1):12-21. doi: 10.1016/j.dnarep.2011.10.024. Epub 2011 Nov 23.

17. Mattimore V, Battista JR. (1996) Radioresistance of *Deinococcus radiodurans*: Functions necessary to survive ionizing radiation are also necessary to survive prolonged desiccation. J Bacteriol 178(3): 633-637.

18. Fredrickson JK, Li SM, Gaidamakova EK, Matrosova VY, Zhai M, et al. (2008) Protein oxidation: Key to bacterial desiccation resistance? ISME J 2(4): 393-403.

19. Riley PA. (1994) Free radicals in biology: Oxidative stress and the effects of ionizing radiation. Int J Radiat Biol 65(1): 27-33.

20. Imlay JA. (2003) Pathways of oxidative damage. Annu Rev Microbiol 57: 395-418.

21. Imlay JA. (2008) Cellular defenses against superoxide and hydrogen peroxide. Annu Rev Biochem 77: 755-776.

22. Daly MJ. (2009) A new perspective on radiation resistance based on *Deinococcus radiodurans*. Nat Rev Microbiol 7(3): 237-245.

23. Robb FT, Hauman JH, Peak MJ. (1978) Similar spectra for the inactivation by monochromatic light of two distinct leucine transport systems in *Escherichia coli*. Photochem. Photobiol. 27: 465-469.

24. Hutchinson F. (1966) The molecular basis for radiation effects on cells. Cancer Res 26(9): 2045-2052.

25. Gerard E, Jolivet E, Prieur D, Forterre P. (2001) DNA protection mechanisms are not involved in the radioresistance of the hyperthermophilic archaea *Pyrococcus abyssi* and *P. furiosus*. Mol Genet Genomics 266(1): 72-78.

26. DiRuggiero J, Brown J, Bogert AP, Robb FT. (1999) DNA Repair Systems in Archaea: Mementos from the Last Universal Common Ancestor? J Mol Evol 49:474–484

27. Whitehead K, Kish A, Pan M, Kaur A, Reiss DJ, et al. (2006) An integrated systems approach for understanding cellular responses to gamma radiation. Mol Syst Biol 2: 47.

28. Makarova KS, Aravind L, Wolf YI, Tatusov RL, Minton KW, et al. (2001) Genome of the extremely radiation-resistant bacterium *Deinococcus radiodurans* viewed from the perspective of comparative genomics. Microbiol Mol Biol Rev 65(1): 44-79.

29. Blasius M, Sommer S, Hubscher U. (2008) *Deinococcus radiodurans*: What belongs to the survival kit? Crit Rev Biochem Mol Biol 43(3): 221-238.

30. Bentchikou E, Servant P, Coste G, Sommer S. (2010) A major role of the RecFOR pathway in DNA double-strand-break repair through ESDSA in *Deinococcus radiodurans*. PLoS Genet 6(1): e1000774.

31. Confalonieri F, Sommer S. (2011) Bacterial and archaeal resistance to ionizing radiation. Journal of Physics 261: 012005.

32. Weller GR, Kysela B, Roy R, Tonkin LM, Scanlan E, et al. (2002) Identification of a DNA nonhomologous end-joining complex in bacteria. Science 297(5587): 1686-1689.

33. Tanaka M, Earl AM, Howell HA, Park MJ, Eisen JA, et al. (2004) Analysis of *Deinococcus radiodurans*'s transcriptional response to ionizing radiation and desiccation reveals novel proteins that contribute to extreme radioresistance. Genetics 168(1): 21-33.

34. Daly, MJ ,Minton KW. (1996) An alternative pathway for recombination of chromosomal fragments precedes *recA*-dependent recombination in the radioresistant bacterium *Deinococcus radiodurans*. J. Bacteriol. 178: 4461-4471.

35. Kish A, DiRuggiero J. (2008) Rad50 is not essential for the Mre11-dependent repair of DNA double-strand breaks in *Halobacterium* sp. strain NRC-1. J Bacteriol 190(15): 5210-5216.

36. Dale WM. (1940) The effect of X-rays on enzymes. Biochem J 34(10-11): 1367-1373.

37. Dale WM. (1942) The effect of X-rays on the conjugated protein d-amino-acid oxidase. Biochem J 36(1-2): 80-85.

38. Du J, Gebicki JM. (2004) Proteins are major initial cell targets of hydroxyl free radicals. Int J Biochem Cell Biol 36(11): 2334-2343.

39. Krisko A, Radman M. (2010) Protein damage and death by radiation in *Escherichia coli* and *Deinococcus radiodurans*. Proc Natl Acad Sci U S A 107(32): 14373-14377.

40. Krisko A, Leroy M, Radman M, Meselson M. (2012) Extreme anti-oxidant protection against ionizing radiation in *Bdelloid rotifers*. Proc Natl Acad Sci U S A 109(7): 2354-2357.

41. Fridovich I. (1997) Superoxide anion radical (O2-.), superoxide dismutases, and related matters. J Biol Chem 272(30): 18515-18517.

42. Archibald FS, Fridovich I. (1982) The scavenging of superoxide radical by manganous complexes: In vitro. Arch Biochem Biophys 214(2): 452-463.

43. Archibald FS, Fridovich I. (1981) Manganese, superoxide dismutase, and oxygen tolerance in some lactic acid bacteria. J Bacteriol 146(3): 928-936.

44. Chang EC, Kosman DJ. (1989) Intracellular Mn (II)-associated superoxide scavenging activity protects cu,zn superoxide dismutase-deficient *Saccharomyces cerevisiae* against dioxygen stress. J Biol Chem 264(21): 12172-12178.

45. Al-Maghrebi M, Fridovich I, Benov L. (2002) Manganese supplementation relieves the phenotypic deficits seen in superoxide-dismutase-null *Escherichia coli*. Arch Biochem Biophys 402(1): 104-109.

46. Barnese K, Gralla EB, Cabelli DE, Valentine JS. (2008) Manganous phosphate acts as a superoxide dismutase. J Am Chem Soc 130(14): 4604-4606.

47. Berlett BS, Chock PB, Yim MB, Stadtman ER. (1990) Manganese(II) catalyzes the bicarbonate-dependent oxidation of amino acids by hydrogen peroxide and the amino acid-facilitated dismutation of hydrogen peroxide. Proc Natl Acad Sci U S A 87(1): 389-393.

48. Daly MJ, Gaidamakova EK, Matrosova VY, Vasilenko A, Zhai M, et al. (2007) Protein oxidation implicated as the primary determinant of bacterial radioresistance. PLoS Biol 5(4): e92.

49. Daly, MJ, Gaidamakova EK, Matrosova, VY, Vasilenko, A., et al. (2004) Accumulation of Mn(II) in *Deinococcus radiodurans* Facilitates Gamma-Radiation Resistance. Science 306: 925-1084.

50. Barnese, K, Gralla, EB, Valentine, JS, Cabelli, DE. (2012). Biologically relevant mechanism for catalytic superoxide removal by simple manganese compounds. Proc Natl Acad Sci U S A 109(18): 6892-6897.

51. Ghosh S, Ramirez-Peralta A, Gaidamakova E, Zhang P, Li YQ, et al. (2011) Effects of Mn levels on resistance of *Bacillus megaterium* spores to heat, radiation and hydrogen peroxide. J Appl Microbiol 111(3): 663-670.

52. Granger AC, Gaidamakova EK, Matrosova VY, Daly MJ, Setlow P. (2011) Effects of levels of Mn and Fe on *Bacillus subtilis* spore resistance, and effects of Mn^{2+}, other divalent cations, orthophosphate, and dipicolinic acid on resistance of a protein to ionizing radiation. Appl. Environ. Microbiol. 77(1): 32-40.

53. Rastogi RP, Richa, Sinha RP, Singh SP, Hader DP. (2010) Photoprotective compounds from marine organisms. J Ind Microbiol Biotechnol 37(6): 537-558.

54. Oren A, Gunde-Cimerman N. (2007) Mycosporines and mycosporine-like amino acids: UV protectants or multipurpose secondary metabolites? FEMS Microbiol Lett 269(1): 1-10.

55. Beblo K, Douki T, Schmalz G, Rachel R, Wirth R, et al. (2011) Survival of thermophilic and hyperthermophilic microorganisms after exposure to UV-C, ionizing radiation and desiccation. Arch Microbiol 193(11): 797-809.

56. DiRuggiero J, Santangelo N, Nackerdien Z, Ravel J, Robb FT. (1997) Repair of extensive ionizing-radiation DNA damage at 95 degrees C in the hyperthermophilic archaeon *Pyrococcus furiosus*. J Bacteriol 179(14): 4643-4645.

57. Jolivet E, L'Haridon S, Corre E, Forterre P, Prieur D. (2003) *Thermococcus gammatolerans* sp. nov., a hyperthermophilic archaeon from a deep-sea hydrothermal vent that resists ionizing radiation. Int J Syst Evol Microbiol 53(Pt 3): 847-851.

58. Suzuki K, Collins MD, Iijima E, Komagata K. (1988) Chemotaxonomic characterization of a radiotolerant bacterium, *Arthrobacter radiotolerans*: Description of *Rubrobacter radiotolerans* gen. nov., comb. nov. FEMS Microbiol.Lett. 52(33-40).

59. Carreto L, Moore E, Nobre MF, Wait R, Riley PW, et al. (1996) *Rubrobacter xylanophilus* sp. nov., a new thermophilic species isolated from a thermally polluted efluent. Int J Syst Bacteriol 46(2): 460-465.

60. Rolfsmeier ML, Laughery MF, Haseltine CA. (2011) Repair of DNA double-strand breaks induced by ionizing radiation damage correlates with upregulation of homologous recombination genes in *Sulfolobus solfataricus*. J Mol Biol 414(4): 485-498.

61. Johnson TE, Hartman PS. (1988) Radiation effects on life span in *Caenorhabditis elegans*. J Gerontol 43: B137-B141.

62. Yoshinaka T, Yano K, Yamaguchi H. (1973) Isolation of highly radioresistant bacterium, *Arthrobacter radiotolerans* nov. sp. Agr. Bio 37(10): 2269-2275.

63. Laiz L, Miller AZ, Jurado V, Akatova E, Sanchez-Moral S, et al. (2009) Isolation of five *Rubrobacter* strains from biodeteriorated monuments. Naturwissenschaften 96(1): 71-79.

64. The Genome Portal of the Department of Energy Joint Genome Institute. Grigoriev, IV, Nordberg, H, Shabalov, I, Aerts, A, Cantor, M., et al. (2011) Nucleic Acids Res 0: gkr947v1-gkr947

65. Empadinhas N, Mendes V, Simoes C, Santos MS, Mingote A, et al. (2007) Organic solutes in *Rubrobacter xylanophilus*: The first example of di-*myo*-inositol-phosphate in a thermophile. Extremophiles 11(5): 667-673.

66. Martins LO, Santos H. (1995) Accumulation of mannosylglycerate and di-myo-inositol-phosphate by *Pyrococcus furiosus* in response to salinity and temperature. Appl Environ Microbiol 61(9): 3299-3303.

67. Elbein AD, Pan YT, Pastuszak I, Carroll D. (2003) New insights on trehalose: A multifunctional molecule. Glycobiology 13(4): 17R-27R.

68. Hengherr S, Schill RO, Clegg JS. (2011) Mechanisms associated with cellular desiccation tolerance in the animal extremophile *Artemia*. Physiol Biochem Zool 84(3): 249-257.

69. Empadinhas N, da Costa MS. (2008) Osmoadaptation mechanisms in prokaryotes: Distribution of compatible solutes. Int Microbiol 11(3): 151-161.

70. Higashiyama T. (2002) Novel functions and applications of trehalose*. Pure Appl Chem 74: 1263–1269.

71. Nobre A, Alarico S, Fernandes C, Empadinhas N, da Costa MS. (2008) A unique combination of genetic systems for the synthesis of trehalose in *Rubrobacter xylanophilus*: Properties of a rare actinobacterial TreT. J Bacteriol 190(24): 7939-7946.

72. Fiala G, Stetter KO. (1986) *Pyrococcus furiosus* sp. nov. represents a novel genus of marine heterotrophic archaebacteria growing optimally at 100C. Arch.Microbiol. 145: 56-61.

73. Williams E, Lowe TM, Savas J, DiRuggiero J. (2007) Microarray analysis of the hyperthermophilic archaeon *Pyrococcus furiosus* exposed to gamma irradiation. Extremophiles 11(1): 19-29.

74. Robb FT, Maeder DL, Brown JR, DiRuggiero J, Stump MD, et al. (2001) Genomic sequence of hyperthermophile, *Pyrococcus furiosus*: Implications for physiology and enzymology. Methods Enzymol 330: 134-157.

75. Kletzin A, Adams MW. (1996) Tungsten in biological systems. FEMS Microbiol Rev 18(1): 5-63.

76. Cvetkovic A, Menon AL, Thorgersen MP, Scott JW, Poole FL,2nd, et al. (2010) Microbial metalloproteomes are largely uncharacterized. Nature 466(7307): 779-782.

77. Strand KR, Sun C, Li T, Jenney FE,Jr, Schut GJ, et al. (2010) Oxidative stress protection and the repair response to hydrogen peroxide in the hyperthermophilic archaeon *Pyrococcus furiosus* and in related species. Arch Microbiol 192(6): 447-459.

78. Jenney FE,Jr, Verhagen MF, Cui X, Adams MW. (1999) Anaerobic microbes: Oxygen detoxification without superoxide dismutase. Science 286(5438): 306-309.

79. Ramsay B, Wiedenheft B, Allen M, Gauss GH, Lawrence CM, et al. (2006) Dps-like protein from the hyperthermophilic archaeon *Pyrococcus furiosus*. J Inorg Biochem 100(5-6): 1061-1068.

80. Molina-Heredia FP, Houee-Levin C, Berthomieu C, Touati D, Tremey E, et al. (2006) Detoxification of superoxide without production of H2O2: Antioxidant activity of superoxide reductase complexed with ferrocyanide. Proc Natl Acad Sci U S A 103(40): 14750-14755.

81. Zivanovic Y, Armengaud J, Lagorce A, Leplat C, Guerin P, et al. (2009) Genome analysis and genome-wide proteomics of *Thermococcus gammatolerans*, the most radioresistant organism known amongst the archaea. Genome Biol 10(6): R70.

82. Engel MB, Catchpole HR. (2005) A microprobe analysis of inorganic elements in *Halobacterium salinarum*. Cell Biol Int 29(8): 616-622.

83. Baliga NS, Bjork SJ, Bonneau R, Pan M, Iloanusi C, et al. (2004) Systems level insights into the stress response to UV radiation in the halophilic archaeon *Halobacterium* NRC-1. Genome Res 14(6): 1025-1035.

84. Ng WV, Kennedy SP, Mahairas GG, Berquist B, Pan M, et al. (2000) Genome sequence of *Halobacterium* species NRC-1. Proc Natl Acad Sci U S A 97(22): 12176-12181.

85. Peck RF, DasSarma S, Krebs MP. (2000) Homologous gene knockout in the archaeon *Halobacterium salinarum* with *ura3* as a counterselectable marker. Mol Microbiol 35(3): 667-676.

86. Kaur A, Pan M, Meislin M, Facciotti MT, El-Gewely R, et al. (2006) A systems view of haloarchaeal strategies to withstand stress from transition metals. Genome Res 16(7): 841-854.

87. Kish A, Kirkali G, Robinson C, Rosenblatt R, Jaruga P, et al. (2009) Salt shield: Intracellular salts provide cellular protection against ionizing radiation in the halophilic archaeon, *Halobacterium salinarum* NRC-1. Environ Microbiol 11(5): 1066-1078.

88. Kaur A, Van PT, Busch CR, Robinson CK, Pan M, et al. (2010) Coordination of frontline defense mechanisms under severe oxidative stress. Mol Syst Biol 6: 393.

89. DeVeaux LC, Muller JA, Smith J, Petrisko J, Wells DP, et al. (2007) Extremely radiation-resistant mutants of a halophilic archaeon with increased single-stranded DNA-binding protein (RPA) gene expression. Radiat Res 168(4): 507-514.

90. Harris DR, Pollock SV, Wood EA, Goiffon RJ, Klingele AJ, et al. (2009) Directed evolution of ionizing radiation resistance in *Escherichia coli*. J Bacteriol 191(16): 5240-5252.

91. Davies R, Sinskey AJ. (1973) Radiation-resistant mutants of *Salmonella typhimurium* LT2: Development and characterization. J Bacteriol 113(1): 133-144.

92. McCready S, Muller JA, Boubriak I, Berquist BR, Ng WL, et al. (2005) UV irradiation induces homologous recombination genes in the model archaeon, *Halobacterium* sp. NRC-1. Saline Systems 1: 3.

93. Gostincar C, Grube M, de Hoog S, Zalar P, Gunde-Cimerman N. (2010) Extremotolerance in fungi: Evolution on the edge. FEMS Microbiol Ecol 71(1): 2-11.

94. Kogej T, Ramos J, Plemenitas A, Gunde-Cimerman N. (2005) The halophilic fungus *Hortaea werneckii* and the halotolerant fungus *Aureobasidium pullulans* maintain low intracellular cation concentrations in hypersaline environments. Appl Environ Microbiol. 71(11):6600-5.

95. Stadtman ER, Levine RL. (2003) Free radical-mediated oxidation of free amino acids and amino acid residues in proteins. Amino Acids 25(3-4): 207-218.

96. Markillie LM, Varnum SM, Hradecky P, Wong KK. (1999) Targeted mutagenesis by duplication insertion in the radioresistant bacterium *Deinococcus radiodurans*: Radiation sensitivities of catalase (*katA*) and superoxide dismutase (*sodA*) mutants. J Bacteriol 181(2): 666-669.

97. Clark JM. (1964) Experimental biochemistry. New York: W. H. Freeman and Co.

98. Yu J. (2011) Molecular basis for Radiation Resistance in Highly Resistant Mutants of the Archaeon, *Halobacterium salinarum.* Masters thesis. Johns Hopkins University.

99. Kennedy SP, Ng WV, Salzberg SL, Hood L, DasSarma S. (2001) Understanding the adaptation of *Halobacterium* species NRC-1 to its extreme environment through computational analysis of its genome sequence. Genome Res 11(10): 1641-1650.

100. Van PT, Schmid AK, King NL, Kaur A, Pan M, et al. (2008) *Halobacterium salinarum* NRC-1 PeptideAtlas: Toward strategies for targeted proteomics and improved proteome coverage. J Proteome Res 7(9): 3755-3764.

101. Chu LJ, Chen MC, Setter J, Tsai YS, Yang H, et al. (2011) New structural proteins of *Halobacterium salinarum* gas vesicle revealed by comparative proteomics analysis. J Proteome Res 10(3): 1170-1178.

102. Yao AI, Facciotti MT. (2011) Regulatory multidimensionality of gas vesicle biogenesis *in Halobacterium salinarum* NRC-1. Archaea 2011: 716456.

103. Dassarma S, Halladay JT, Jones JG, Donovan JW, Giannasca PJ, de Marsac NT. (1988) High-frequency mutations in a plasmid-encoded gas vesicle gene in *Halobacterium halobium*. Proc Natl Acad Sci U S A. 85(18):6861-5.

104. Skowyra A, MacNeill SA. (2012) Identification of essential and non-essential single-stranded DNA-binding proteins in a model archaeal organism. Nucleic Acids Res. 40(3):1077-90. Epub 2011 Oct 5.

105. Stroud A, Liddell S, Allers T. (2012) Genetic and Biochemical Identification of a Novel Single-Stranded DNA-Binding Complex in *Haloferax volcanii*. Front Microbiol. 3:224. Epub 2012 Jun 18.

106. Facciotti MT, Pang WL, Lo FY, Whitehead K, Koide T, et al. (2010) Large scale physiological readjustment during growth enables rapid, comprehensive and inexpensive systems analysis. BMC Syst Biol 4: 64.

107. Nystrom T. (2004) Stationary-phase physiology. Annu Rev Microbiol 58: 161-181.

108. Kehres DG, Maguire ME. (2003) Emerging themes in manganese transport, biochemistry and pathogenesis in bacteria. FEMS Microbiol Rev 27(2-3): 263-290.

109. Ogunniyi AD, Mahdi LK, Jennings MP, McEwan AG, McDevitt CA, et al. (2010) Central role of manganese in regulation of stress responses, physiology, and metabolism in *Streptococcus pneumoniae*. J Bacteriol 192(17): 4489-4497.

110. Gonzalez O, Gronau S, Falb M, Pfeiffer F, Mendoza E, et al. (2008) Reconstruction, modeling & analysis of *Halobacterium salinarum* R-1 metabolism. Mol Biosyst 4(2): 148-159.

111. Bonneau, R, Reiss, DJ, Shannon, P, Facciotti, M, Hood, L., et, al. (2006. The Inferelator: An algorithm for learning parsimonious regulatory networks from systems-biology data sets de novo. Genome Biol. **7:** R36.

112. Reddi AR, Culotta VC. (2011) Regulation of manganese antioxidants by nutrient sensing pathways in *Saccharomyces cerevisiae*. Genetics 189(4): 1261-1270.

113. Puri S, Hohle TH, O'Brian MR. (2010) Control of bacterial iron homeostasis by manganese. Proc Natl Acad Sci U S A 107(23): 10691-10695.

114. Swinnen, E, Wanke, V, Roosen, J, Smets, B, Dubouloz, F., et al. (2006) Rim15 and the crossroads of nutrient signalling pathways in *Saccharomyces cerevisiae*. Cell Division 1:3 doi:10.1186/1747-1028-1-3

115. Potts M. (2001) Desiccation tolerance: A simple process? Trends Microbiol 9(11): 553-559.

116. Santos H, da Costa MS. (2002) Compatible solutes of organisms that live in hot saline environments. Environ Microbiol 4(9): 501-509.

117. Santos H, Lamosa P, Faria TQ, Borges N, Neves C. (2007) The physiological role, biosynthesis, and mode of action of compatible solutes from (hyper)thermophiles. In: Gerday C, Glansdorff N, editors. Physiology and Biochemistry of Extremophiles. Washington D.C.: ASM Press. pp. 86.

118. Empadinhas N, da Costa MS. (2006) Diversity and biosynthesis of compatible solutes in hyper/thermophiles. Int Microbiol 9(3): 199-206.

119. Borges N, Ramos A, Raven ND, Sharp RJ, Santos H. (2002) Comparative study of the thermostabilizing properties of mannosylglycerate and other compatible solutes on model enzymes. Extremophiles 6(3): 209-216.

120. Ramos A, Raven N, Sharp RJ, Bartolucci S, Rossi M, et al. (1997) Stabilization of enzymes against thermal stress and freeze-drying by mannosylglycerate. Appl Environ Microbiol 63(10): 4020-4025.

121. Lentzen G, Schwarz T. (2006) Extremolytes: Natural compounds from extremophiles for versatile applications. Appl Microbiol Biotechnol 72(4): 623-634.

122. Longo CM, Wei Y, Roberts MF, Miller SJ. (2009) Asymmetric syntheses of L,L- and L,D-di-*myo*-inositol-1,1'-phosphate and their behavior as stabilizers of enzyme activity at extreme temperatures. Angew Chem Int Ed Engl 48(23): 4158-4161.

123. Ferreira AC, Nobre MF, Moore E, Rainey FA, Battista JR, et al. (1999) Characterization and radiation resistance of new isolates of *Rubrobacter radiotolerans* and *Rubrobacter xylanophilus*. Extremophiles 3(4): 235-238.

124. Tapias A, Leplat C, Confalonieri F. (2009) Recovery of ionizing-radiation damage after high doses of gamma ray in the hyperthermophilic archaeon *Thermococcus gammatolerans*. Extremophiles 13(2): 333-343.

125. Gonçalves LG, Borges N, Serra F, Fernandes PL, Dopazo H, et al.(2012) Evolution of the biosynthesis of di-*myo*-inositol phosphate, a marker of adaptation to hot marine environments. Environ Microbiol. 14(3):691-701. doi: 10.1111/j.1462-2920.2011.02621.x. Epub 2011 Oct 26.

126. Gonzalez JM, Masuchi Y, Robb FT, Ammerman JW, Maeder DL, et al. (1998) *Pyrococcus horikoshii* sp. nov., a hyperthermophilic archaeon isolated from a hydrothermal vent at the okinawa trough. Extremophiles 2(2): 123-130.

127. Billi D, Friedmann EI, Hofer KG, Caiola MG, Ocampo-Friedmann R. (2000) Ionizing-radiation resistance in the desiccation-tolerant cyanobacterium *Chroococcidiopsis*. Appl Environ Microbiol 66(4): 1489-1492.

128. Hershkovitz N, Oren A, Cohen Y. (1991) Accumulation of trehalose and sucrose in cyanobacteria exposed to matric water stress. Appl Environ Microbiol 57(3): 645-648.

129. Jenney FE,Jr, Adams MW. (2008) Hydrogenases of the model hyperthermophiles. Ann N Y Acad Sci 1125: 252-266.

130. Schut GJ, Nixon WJ, Lipscomb GL, Scott RA, Adams MW. (2012) Mutational analyses of the enzymes involved in the metabolism of hydrogen by the hyperthermophilic archaeon *Pyrococcus furiosus*. Front Microbiol 3: 163.

131. Lancaster WA, Praissman JL, Poole FL,2nd, Cvetkovic A, Menon AL, et al. (2011) A computational framework for proteome-wide pursuit and prediction of metalloproteins using ICP-MS and MS/MS data. BMC Bioinformatics 12: 64.

132. Lin LH, Slater GF, Lollar BS, Lacrampe-Couloume G, Onstott TC. (2005) The yield and isotopic composition of radiolytic H2, a potential energy source for the deep subsurface biosphere. Geochimica Et Cosmochimica Acta 69: 893–903.

133. von Sonntag C. (1987) The chemical basis of radiation biology. London: Taylor & Francis.